UNIVERSITA' DEGLI STUDI DI PADOVA

Sede Amministrativa: Università degli Studi di Padova

Dipartimento di GEOSCIENZE

SCUOLA DI DOTTORATO DI RICERCA IN : SCIENZE DELLA TERRA
CICLO XXI

SEDIMENTOLOGY OF UPPER TRIASSIC HEMIPELAGIC MICRITES (LAGONEGRO AND SICANI BASINS)

Direttore della Scuola : Ch.mo Prof. Gilberto Artioli
Supervisore : Dr. Nereo Preto

Dottorando : Chiara Guaiumi

to my sister Valentina

to my little ones love Diego and Mattia.

I love you!!!

AKNOWLEDGEMENTS

First of all I thank my supervisor, Nereo Preto, for giving me this work opportunity and for continuous discussions.

A BIG THANK to my working group for friendship and encouragement: Paolo, Guido, Anna, Manuel, Marco, Matteo, Jacopo, Alessandro, Lisa and Renata.

Stefano, Rachele, Letizia, Nicola, Claudia, Edoardo, Michele and Marco, thank for your friendship!!!

Piero Gianolla and Alda Nicora: thank for discussions and support.

I would like to Thank Dr. Hildegard Westphal for her help and her patience with my English.

Thank to technicians (Maui, Stefano, Micola, Lorenzo, Leonardo and Elena) and all peoples of Geoscience department.

Thanks to FBK and ENI peoples, for introducing me to the 3d world.

Thanks to the IAS for partially supporting the Pizzo Mondello project.

A special thank to my friends: Jul, Laura(ina), Alice, Laura, Sabina, Melissa, Ele, Fava, France, Moro, "gli Amici da Mare", Lagonegro's friends (Nicola, Andrea, Luca, Jack, and Sara) and all the friends I forgot to mention.

Finally, I thank my parents, my sister and my brother and all my grand family; without you this experience wouldn't have been possible! To my grandfather: I love you!!

INDEX

ABSTRACT

The sedimentology and stratigraphy of the Calcari con Selce formation (Cherty Limestones) have been studied. The Calcari con Selce are an Upper Triassic hemipelagic formation consisting of thin-bedded limestones with chert nodules and beds, marl interlayers and containing thin-shelled bivalves (halobids), radiolarians, ammonoids, foraminifers and calcispheres (Scandone, 1967; Di Stefano, 1990). In Italy, this formation outcrops in the Lagonegro (Southern Apennines) and Sicani (Sicily) basins. These two basins are considered part of the same branch of Tethys during the Triassic.

The Calcari con Selce formation is organized in sedimentary cycles given by limestone-marl alternations, the limestone being mostly fine grained carbonate (micrite). The origin of such sedimentary cycles can be understood only if the origin and composition of micrite and lateral continuity of limestone beds are known to some degree.

The components of the Upper Triassic hemipelagites have been known for long, but a quantitative and provenance study is still missing. The Triassic is considered a time of "Aragonite Sea" (Stanley & Hardie, 1998), the mineralogy of micrite precursor, which is still unknown, should thus be aragonite or high-Mg calcite. Moreover, the calcareous nannofossils, originated during the Triassic time (Di Nocera & Scandone, 1977), is considered insufficient to build up hundred-meters-thick successions as those of the Calcari con Selce (Bellanca et alii, 1995). Thus, many Authors suggest that this hemipelagic formation is constituted mostly by carbonate from adjacent platforms (e.g., Bellanca et alii, 1995; Rigo et alii, 2007). Several samples of carbonate micrite have been analyzed at SEM. In order to discriminate the main micrite precursor, morphological parameters (average crystal dimension and presence/absence of elongated pits) were considered; micrite with aragonite-dominated precursor has large crystals (microspar), relict aragonite needles and pits, while micrite with calcite-dominated precursor has small crystals (2-5 μm) and lack of aragonite needles and pits. The fine carbonate fraction from Sicani Basin (Pizzo Mondello section) indicates a mainly calcite-precursor. The quantitative analyses of the carbonate micrite at the optical microscope show that the calcareous nannofossils provided a significant contribution (18% of total volume) to carbonate sedimentation. Furthermore, some 50% of the total volume consists of pelagic components, while the 45% is fine micrite, probably mainly coming from adjacent platforms by density cascading.

The carbonate micrite from Lagonegro Basin is often diagenetically altered, thus the morphological analysis of precursor mineralogy is difficult to carry out. In this area, I studied the lateral continuity of limestone beds because correlative sections of the Calcari con Selce outcrop in many sites. It is important to understand whether sedimentary cycles are related to

allocyclic, autocyclic or diagenetic phenomena (Westphal, 2006). Allocyclic origin of sedimentary cycles may be indicated by basin-scale continuity of beds. Two stratigraphic markers have been used as reference levels, and the lateral continuity of adjacent limestone beds has been evaluated. The first marker is the Carnian Green clay-radiolaritic horizon ("livello argilloso ad *Halobia superba*" in Scandone, 1967; Rigo et alii, 2007), recognized in four sections within distances of up to 50 km. In this horizon, in all sections, two ash beds and a distinctive calciturbidite are present, that can be used as chronostratigraphic markers. Above the Green clay-radiolaritic horizon, the same sequence of limestone banks or beds is present and recognizable in all sections. The second marker is a "red shale" (Scandone, 1967) dated Upper Norian (Rigo et alii, 2005). This horizon consists of 3-6 m of red shales and was studied with the Laserscanner technique in two sections separated by 7 km. Below the "red shale", the sequence of limestone banks and shale interlayers is identical. The thickness of each meter-scale sedimentary cycle (limestone bed and shale interlayer) is identical within instrumental resolution. In conclusion, limestone beds of Calcari con Selce formation are continuous at basinal scale and their allocyclic origin is demonstrated. This suggests that future studies should be aimed at the identification of a Milankovitch signal in the stratal patterns of the Upper Triassic Calcari con Selce.

RIASSUNTO

La formazione dei Calcari con Selce è stata studiata dal punto di vista sedimentologico e stratigrafico. I Calcari con Selce sono una unità carbonatica emipelagica del Triassico superiore che in Italia affiora nel Bacino di Lagonegro (Appennino Meridionale) e nel Bacino Sicano (Sicilia) (Scandone, 1967; Di Stefano, 1990). Questi due bacini sono considerati una parte dello stesso ramo della Tetide durante il Triassico. La formazione è costituita da calcari micritici in strati più o meno nodulari, con liste e noduli di selce e con interstrati marnosi. Il contenuto paleontologico è dato da bivalvi dal guscio sottile (genere *Halobia*), radiolari, ammonoidi, foraminiferi e calcisfere (Scandone, 1967; Di Stefano, 1990). Gli strati calcarei hanno spessori da decimetrici a metrici e sono separati da giunti stilolitici o interstrati marnosi millimetrici-centimetrici. I Calcari con Selce rientrano pertanto nella categoria delle "*limestone-marl alternations*" (Einsele, 1982; Westphal, 2006). Stabilire l'origine di questa alternanza è un passo necessario se si vuole affrontare lo studio ciclostratigrafico di queste successioni. A questo scopo sono state studiate la provenienza e la mineralogia originaria della micrite e la continuità laterale degli strati calcarei.

La sedimentazione carbonatica nei bacini triassici è poco chiara ed è ancora oggetto di studio. Sono, infatti, numerosi gli studi qualitativi su queste formazioni emipelagiche, ma mancano completamente analisi di tipo quantitativo. Il carbonato dei Calcari con Selce, secondo il modello di Stanley & Hardie (1998), dovrebbe essere aragonite e calcite alto magnesiaca, in quanto il Triassico è considerato un periodo di "Mare Aragonitico", come quello attuale. Inoltre, i nannofossili calcarei anche se già presenti nel Triassico (Di Nocera & Scandone, 1977), non hanno abbondanze tali da contribuire significativamente all'accumulo di spesse successioni come i Calcari con Selce (Bellanca et alii,1995). Molti Autori sostengono quindi che questa formazione sia costituita da carbonato trasportato dalle adiacenti piattaforme (Bellanca et alii, 1995).

L'analisi microstrutturale di frammenti di calcare al Microscopio Elettronico a Scansione (SEM) permette di discriminare il principale precursore della micrite carbonatica. Analizzando, infatti, le dimensioni dei cristalli, la presenza/assenza di aghi di aragonite o di *pits* sulla superficie dei cristalli è possibile distinguere tra due tipi di principali precursori: precursore prevalentemente calcitico e precursore prevalentemente aragonitico. I campioni di micrite provenienti dalla sezione di Pizzo Mondello (Bacino Sicano) analizzati al SEM sono caratterizzati da cristalli di calcite di piccole dimensioni (2-5 μm) e dall'assenza di aghi e *pits* di aragonite. Quindi la frazione fine dei Calcari con Selce aveva un precursore prevalentemente calcitico. L'analisi quantitativa (conteggi) effettutata al microscopio ottico di numerosi cam-

pioni di calcare provenienti sempre dalla sezione di Pizzo Mondello, ha messo in evidenza un significativo contributo da parte dei nannofossili calcarei (18% del volume totale) nella sedimentazione carbonatica. Nel complesso, circa il 50% del volume totale del sedimento è costituito da elementi di origine pelagica, il restante 45% è dato da micrite fine, che probabilmente proviene, in massima parte, dalle piattaforme circostanti.

Lo studio sulla continuità laterale degli strati calcarei della formazione dei Calcari con Selce è stato effettuato nel Bacino di Lagonegro, in quanto in quest'area affiorano diverse sezioni correlabili, mentre la micrite carbonatica è alterata diageneticamente e quindi non si presta per uno studio microstrutturale. È importante comprendere se i cicli sedimentari (alternanza marna-calcare) che caratterizzano i Calcari con Selce sono il risultato di fenomeni allociclici, autociclici o l'effetto di una auto-organizzazione in ambiente diagenetico (Westphal, 2006). L'origine allociclica viene dimostrata se gli strati sono continui a scala chilometrica. Sono stati individuati due marker stratigrafici all'interno dei Calcari con Selce e si è analizzato il comportamento degli strati adiacenti a tali marker. Il primo marker è il "livello argilloso ad *Halobia superba*" già segnalato in Scandone (1967), e studiato in dettaglio da Rigo et alii (2007). L'intervallo è datato al Carnico ed è stato studiato in quattro sezioni che distano in linea d'aria circa 48 km. All'interno del livello marker in tutte le sezioni sono presenti alcune cineriti primarie (depositi di caduta) che costituiscono marker cronostratigrafici e una calcitorbidite grossolana che rimaneggia elementi dei Calcari con Selce sottostanti. Al di sopra del livello marker, è sempre presente una sequenza di banchi o strati carbonatici riconoscibili per la loro posizione stratigrafica ed alcune caratteristiche comuni, come lo spessore degli interstrati marnosi o la presenza di letti di selce. Il secondo marker è il cosiddetto "livello rosso", anch'esso identificato da Scandone (1967) e successivamente datato da Rigo et alii (2005) al Sevatico (Norico superiore). Il "livello rosso" è costituito da 3-6 m di prevalenti argilliti rosse e si trova alla base dell'intervallo di transizione tra Calcari con Selce e Scisti Silicei. L'intervallo adiacente al "livello rosso" è stato analizzato con il supporto della tecnica Laserscanner in due sezioni che distano tra loro circa 7 km in linea d'aria. Al di sotto del "livello rosso" si osserva, nelle due sezioni, una sequenza regolare di cicli sedimentari (strati calcarei con interstrati argillitici) con spessori identici entro i limiti strumentali di risoluzione. Quindi, gli strati calcarei della formazione dei Calcari con Selce sono continui alla scala bacinale ed è dimostrata la loro origine allociclica.

Questo suggerisce un possibile studio futuro sulla identificazione del segnale milankoviano che caratterizza i cicli sedimentari dei Calcari con Selce.

CHAPTER 1
Introduction

1.1 Aims of the work

The main aim of this work is the sedimentological and stratigraphic study of the Upper Triassic Calcari con Selce formation, to understand the origin of its prominent sedimentary cyclicity.
The work is subdivided into two parts; the first is focused on the lateral continuity of limestone beds of the Calcari con Selce formation, and is aimed at understanding if the sedimentary cycles are related to allocyclic phenomena. The studied area is Lagonegro Basin, where the Calcari con Selce formation crops out in many sites.
The second part is focused on the origin and mineralogy of the carbonate constituting the Calcari con Selce formation. The studied area is the Sicani Basin. In particular, Pizzo Mondello section is perhaps the best outcrop of the Calcari con Selce in Italy.
The present results suggest that future research should be addressed at the identification of a Milankovitch signal in the sedimentary cycles of the Upper Triassic Calcari con Selce.

1.2 Geological setting

1.2.1 Late Triassic paleogeography

During the whole Triassic, the continents were merged together in a supercontinent called Pangea. Pangea was surrounded by Panthalassa, a single, vast superocean. In the western margin of Pangea, there was a deep gulf, named Tethys, arranged along the equator (Fig. 1.1). The Lagonegro (Southern Apennines) and Sicani (Sicily) basins are considered part of the same branch of Tethys during the Triassic (Fig. 1.2).

1.2.2 Late Triassic paleoclimate

The Triassic was considered warm and arid. There is no evidence of glaciation at or near either pole; in fact, the Polar Regions were apparently moist and temperate (Ziegler et alii, 1994; Price, 1999). The atmospheric circulation was a consequence of the extreme landmass distribution. The Tethys region was characterized by monsoonal atmospheric circulation with enhanced seasonal variability (Kutzbach & Gallimore, 1989), in the framework of an overall arid climate.
During the Carnian, and precisely at the boundary between the lower and upper Carnian, the climate conditions suddenly changed. This change, known as Carnian Pluvial Event (Simms &

RUFFELL, 1989), is a humid climate pulse that provoked an increase in rainfall and siliciclastic input, oceanographic changes and a biotic crisis.

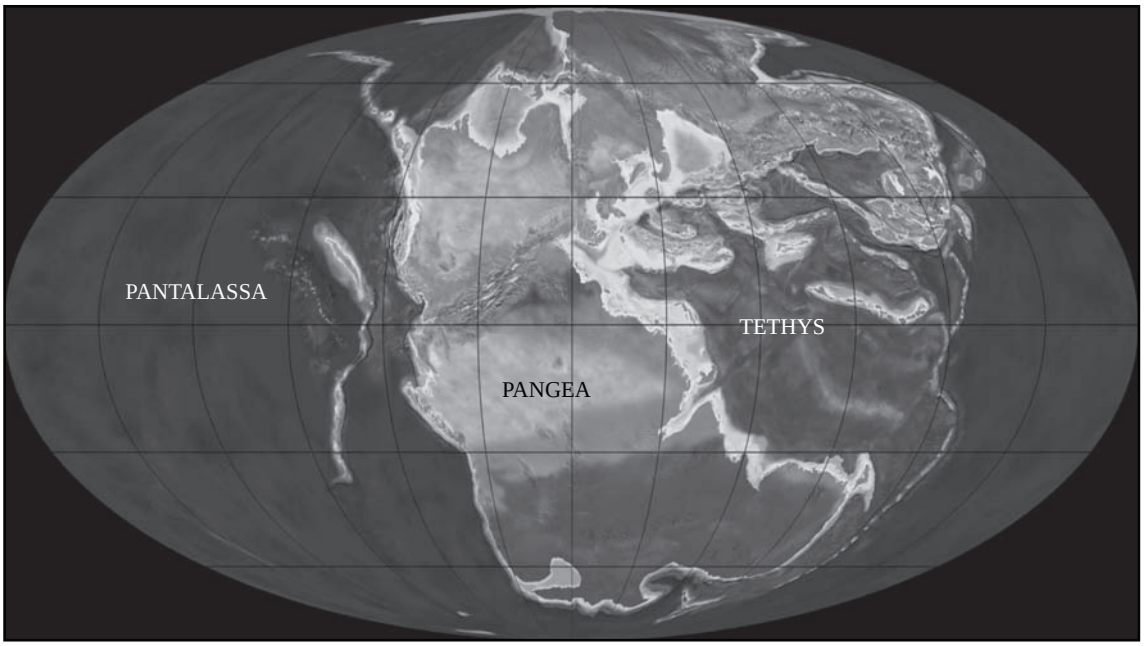

Figure 1.1 - Global paleogeography in the Upper Triassic time (www.earthscienceworld.org).

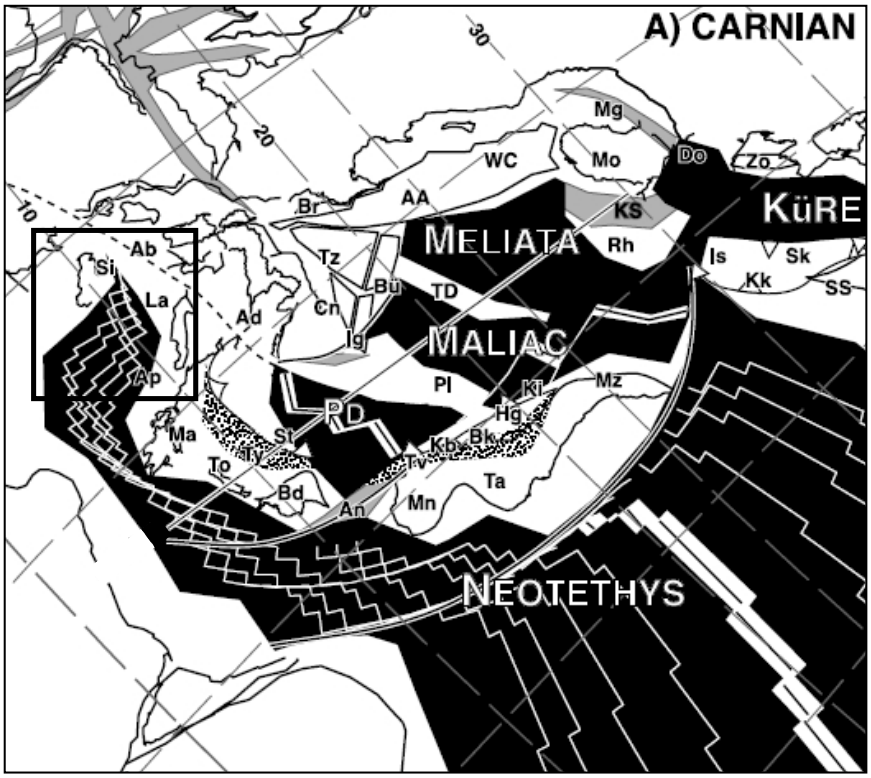

Figure 1.2 - Carnian reconstructions of the western Tethyan region (STAMPLI et alii, 2002). Black box: probable position of Lagonegro (La) and Sicani basins (Si).

1.2.3 Lagonegro Basin

The Lagonegro successions crop out in Southern Apennines (southern Italy) (Fig. 1.3) and the Lagonegro Basin is considered a branch of the Mesozoic western Tethys Ocean (Finetti, 1982, 1985; Sengör et alii, 1984; Stampfli et alii, 1991; Catalano et alii, 1991; Stampfli & Marchant, 1995; Stampfli et alii, 1998; Ciarapica & Passeri, 1998, 2002; Stampfli et alii, 2003). The Lagonegro succession is formed by basinal stratigraphic units of Permian to Tortonian ages (Miocene) (Fig. 1.4). The Upper Triassic in the Lagonegro Basin is represented by two formations: Calcari con Selce (Cherty Limestones) and Scisti Silicei (Siliceous Shales). In the distal and some intermediate Lagonegro successions the boundary between the Calcari con Selce and Scisti Silicei Formations is gradational. It was informally called "Transitional Interval" and was included within the Calcari con Selce formation (Scandone, 1967; Miconnet, 1983; Amodeo & Baumgartner, 1994; Amodeo, 1999; Bertinelli, 2003). The "Transitional Interval" starts with a 3-6 m thick horizon of Sevatian Red shale (Bertinelli, 2003; Reggiani et alii, 2005; Rigo et alii, 2005) used in literature as a lithologic marker throughout the Lagonegro Basin (Scandone, 1967; Miconnet, 1983; Amodeo & Baumgartner, 1994; Amodeo, 1999; Bertinelli, 2003; Rigo et alii, 2005). The Mesozoic Lagonegro successions were subdivided into three facies: distal, intermediate and proximal. They differ in the sedimentation rate and in the amount of resedimented calcarenites from adjacent carbonate platforms (Bertinelli et alii, 2005; Passeri et alii, 2005).

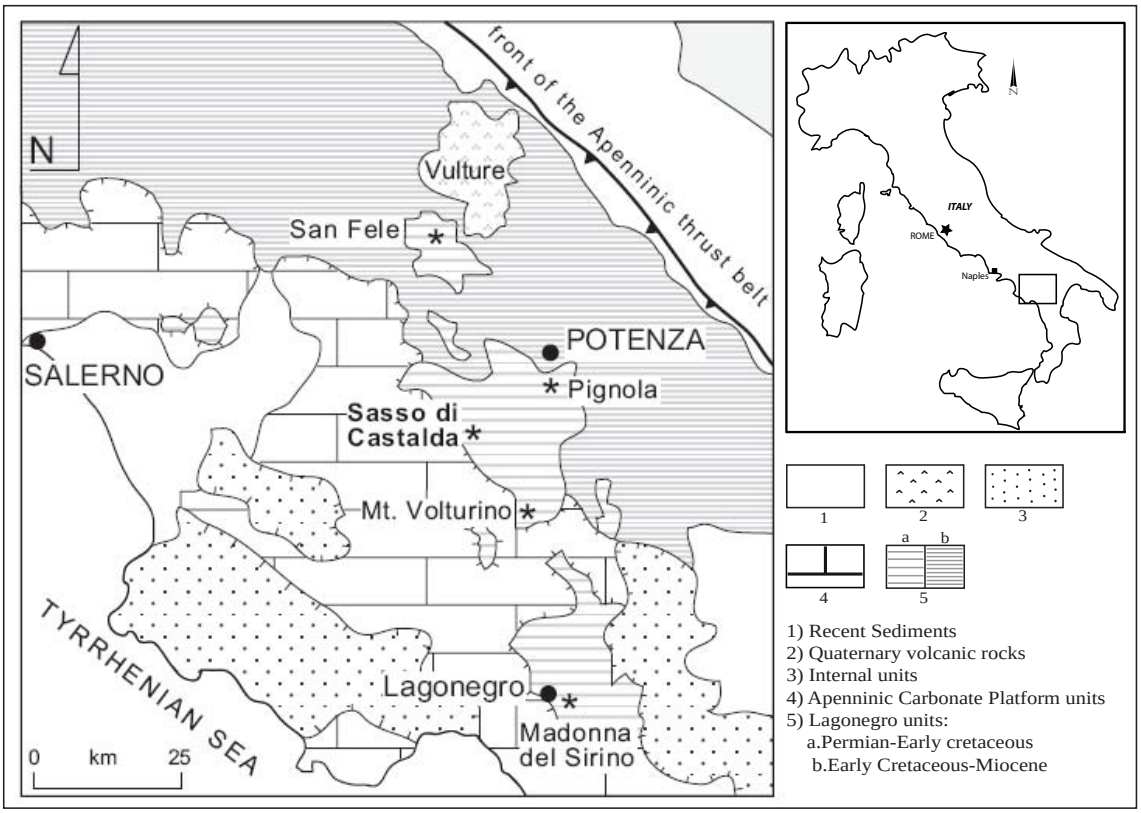

Figure 1.3 – Geological map of the Lagonegro Basin, Southern Apennines (modified from Bertinelli et alii, 2005).

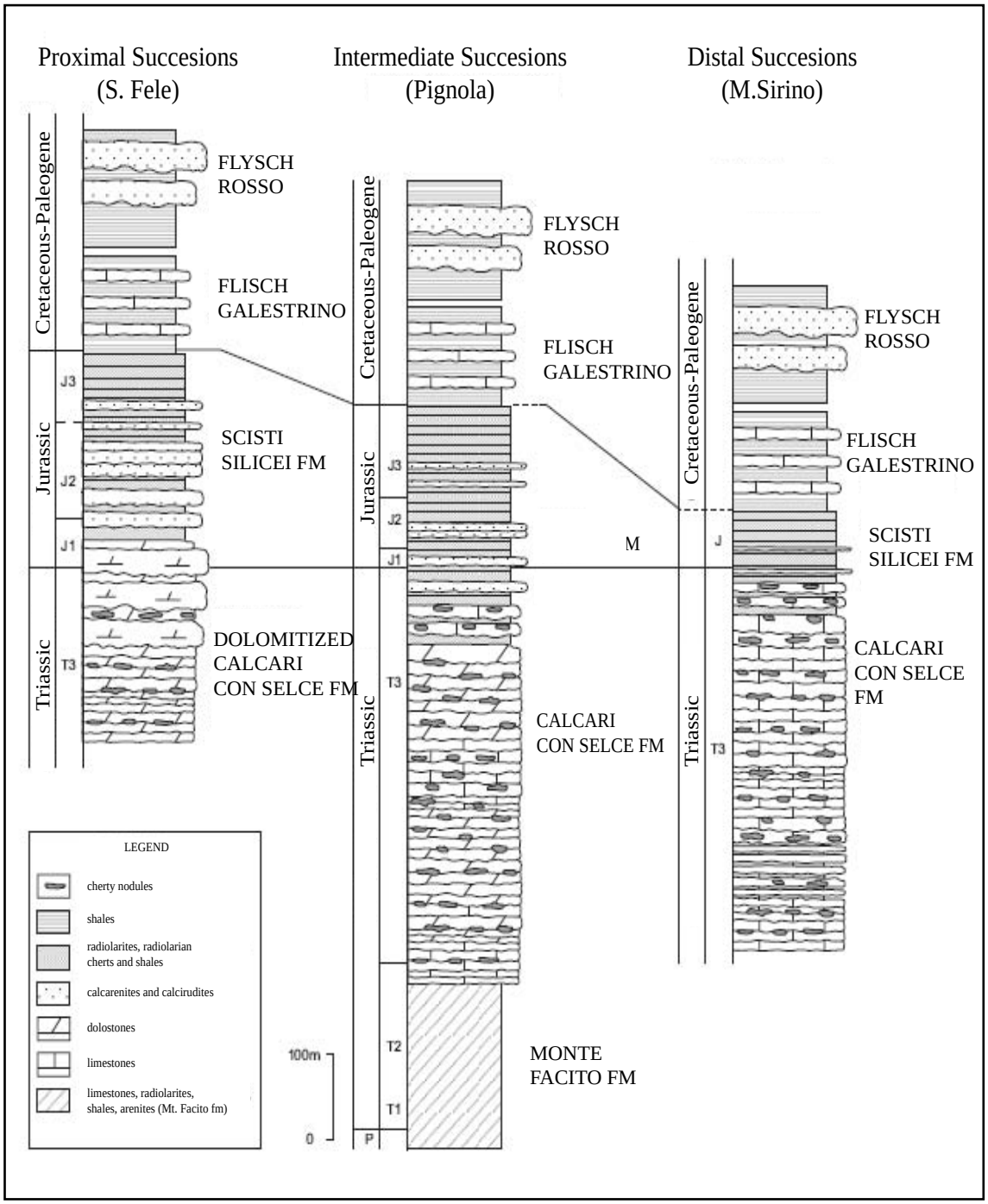

Figure 1.4 – Schematic Lagonegro stratigraphic successions (PASSERI et alii, 2005).
I have studied the sedimentological characteristics of the Calcari con Selce formation, with particular attention on Late Carnian and Sevatian intervals.

1.2.4 Sicani Basin

The Pizzo Mondello section is located in the Sicani Mountains in the western Sicily (Fig. 1.5). The Sicani Mountains consist of pelagic sediments of Permian to Cenozoic age deposited in a Tethyan ocean with African affinity (Di Stefano, 1990). They are segment of the Maghrebian thrust and fold belt. The Pizzo Mondello unit is characterized by ca. 1200 m of hemipelagic carbonates, radiolarites and marls of Mesozoic to Cenozoic age and overthrusts a thick allochthonous complex of Neogene clays and evaporites attributed to the Gela Nappe (Bellanca et alii, 1993, 1995, and references therein). The Pizzo Mondello section (Fig. 1.6) starts with a few meters of marls and marly limestones of late Carnian attributed to the Mufara Formation (Di Stefano & Gullo, 1997; Buratti & Carrillat, 2002). This formation is overlain by 450 m of evenly-bedded to nodular *Halobia*-bearing cherty calcilutites (Calcari con Selce or Cherty Limestones). Above this unit, 20 meters of Lower to Middle Rhaetian calcilutites and marls (Portella Gebbia Formation), follow (Gullo, 1996).

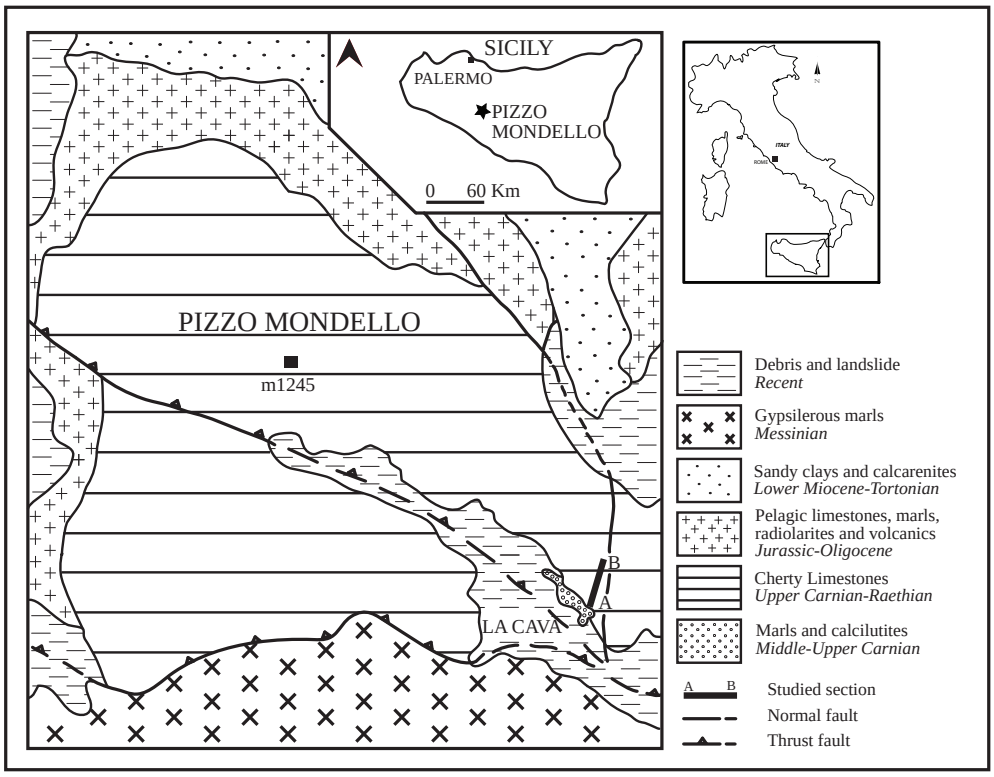

Figure 1.5 – Geological setting of the Pizzo Mondello area, Sicani Mountains, Sicily (after Bellanca et alii, 1993). Pizzo Mondello is the exposed part of a large thrust sheet that overthrusts Upper Tortonian-Messinian clays. The black line shows the studied section within the Calcari con Selce formation.

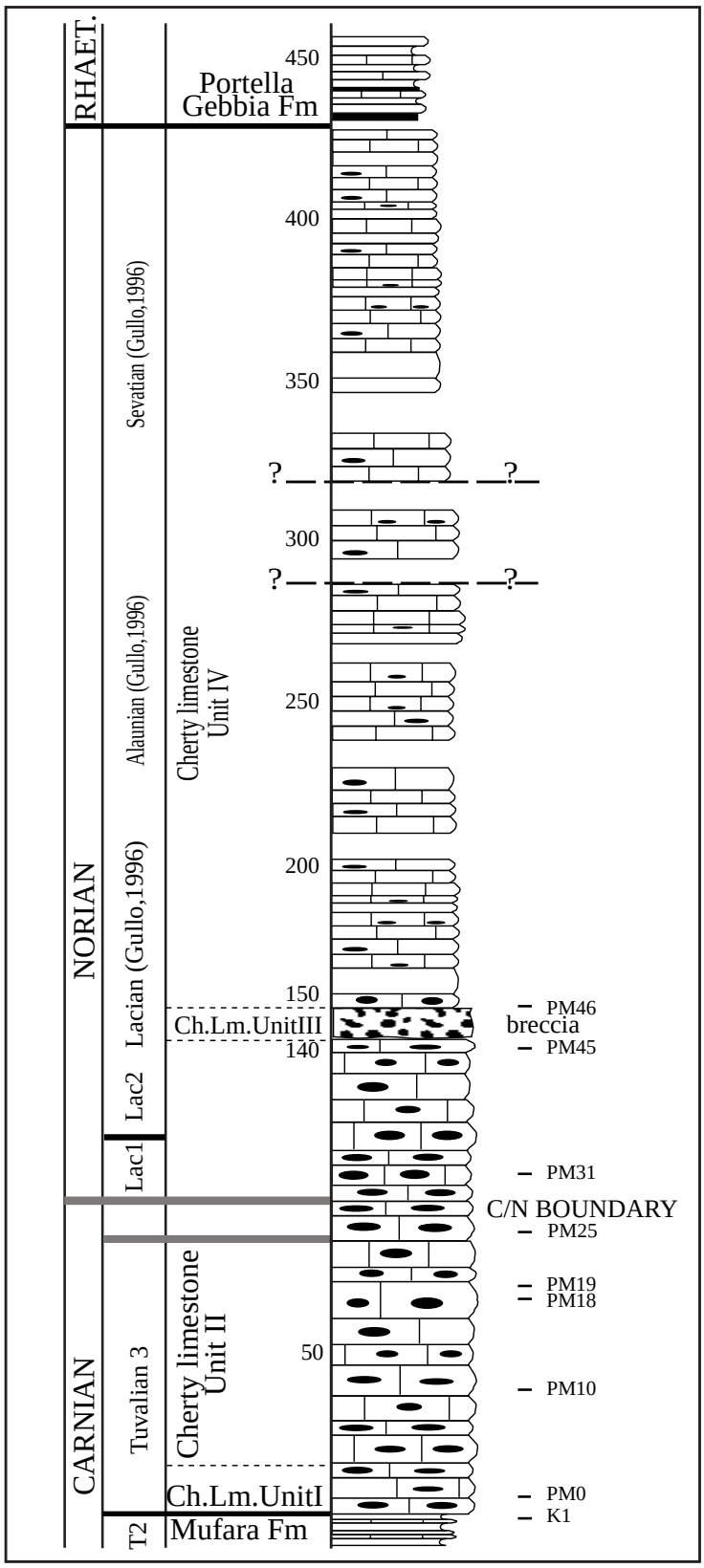

Figure 1.6 – Pizzo Mondello schematic succession (modified from MUTTONI et alii, 2004).

1.3 Calcari con Selce formation

The Calcari con Selce (Cherty Limestones) are an Upper Triassic hemipelagic formation consisting of thin-bedded limestones with chert nodules and beds, marl interlayers (Fig. 1.7 and 1.8) and containing thin-shelled bivalves (Halobids), radiolarians, ammonoids, foraminifers and calcispheres (Scandone, 1967; Di Stefano, 1990). In Italy, this formation outcrops in the Lagonegro (Southern Apennines) and Sicani (Sicily) basins. The typical microfacies are mainly mudstones and wackestones with thin–shelled bivalves and calcified radiolarians (Fig. 1.9). In this formation, scattered calcarenitic beds, with distal characteristics (Tb and Tc of Bouma sequences) are present. Some levels are very rich in *Halobia* to form coquina beds. This is a typical fossil of the Calcari con Selce formation, which provided the first data about its age (Scandone, 1967, 1972; De Capoa Bonardi, 1970, 1984). Due to the presence of these bivalves, the Calcari con Selce formation is known in literature also as «*Halobia* limestones» (Scandone, 1975).

Figure 1.7 – Calcari con Selce formation in the Lagonegro Basin (Southern Italy).

Figure 1.8 – Calcari con Selce formation in the Sicani basin (Sicily).

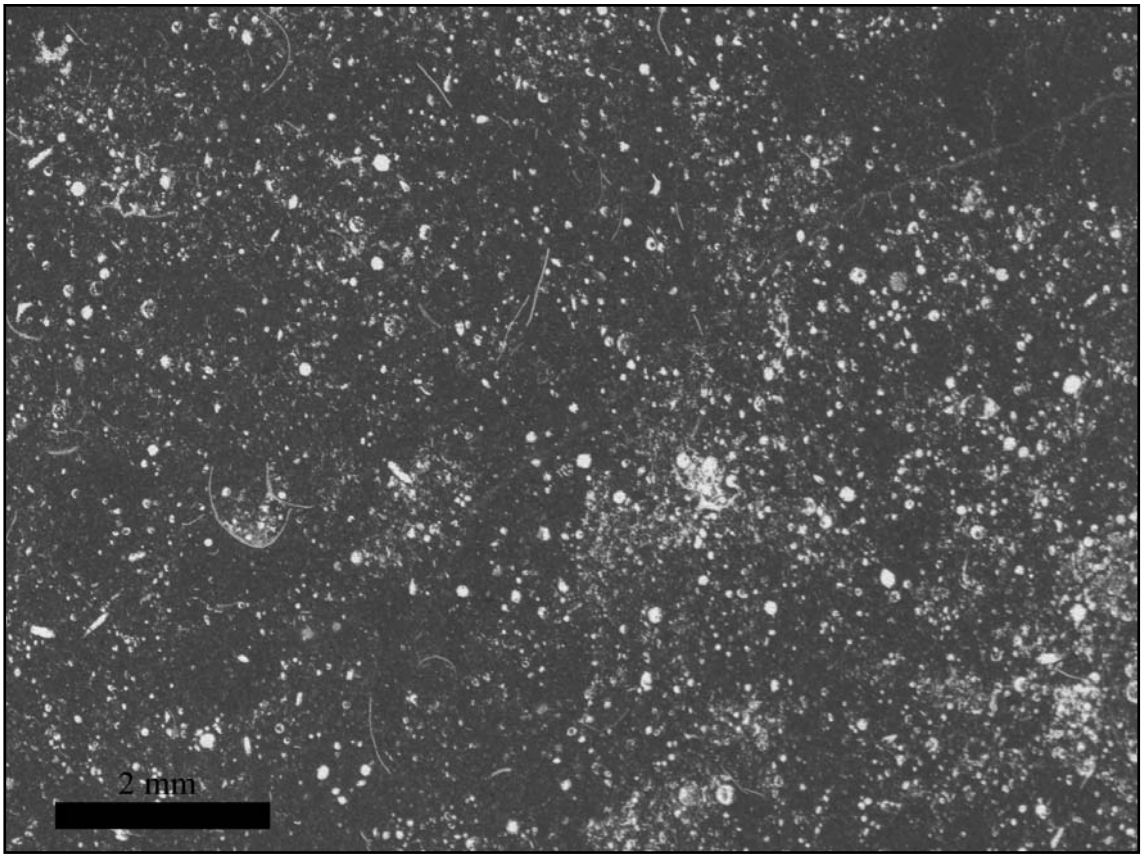

Figure 1.9 – Typical microfacies of the Calcari con Selce formation. Mudstone and wackestones with thin–shelled bivalves and calcified radiolarians.

CHAPTER 2
Continuity of beds in Upper Triassic carbonate hemipelagites (Lagonegro Basin, Southern Apennines)

2.1 Introduction

The Calcari con Selce formation is organized in sedimentary cycles given by limestone-marl alternations (Einsele, 1982). If this sedimentary cyclicity are driven by external (allocyclic) factors, and in particular by oscillations of Earth's orbital parameters at Milankovitch frequencies, limestone-marl alternations can be used as powerful paleoclimatic and chronologic archives (e.g. Grippo et alii, 2004); however, their allocyclic nature needs to be demonstrated first, e.g., by evaluating the continuity of cycles at the basinal scale. Limestone-marl alternations indeed can be generated, in principle, by a variety of causes, including allocyclic, autocyclic or diagenetic processes (Westphal, 2006). Two stratigraphic markers have been used as reference levels, to study the lateral continuity of adjacent limestone beds.

The first marker is the Green clay-radiolaritic horizon (Rigo et alii, 2007) also known as "livello argilloso and *Halobia superba*" (Scandone, 1967) that documents the Carnian Pluvial Event in the Lagonegro Basin. The Carnian Pluvial Event is interpreted as an increase in rainfall in the tropics, that resulted in coarse siliciclastic input in marginal seas, oceanographic changes and biotic crisis (Simms & Ruffell, 1989, 1990; Simms et alii, 1995; Gianolla et alii, 1998; Hornung et alii, 2007; Rigo et alii, 2007). In the Lagonegro Basin, the carbonate hemipelagic sedimentation typical of the Calcari con Selce formation was temporarily replaced by silstones, shales and radiolarites in this interval. Outside the Lagonegro Basin, the Carnian Pluvial Event has so far never been recognized in such a deep-water, distal setting. The Green clay-radiolaritic horizon has been studied in four stratigraphic sections: San Michele, Pezza la Quagliara, Pignola 2 and Monte Armizzone (Fig. 2.1).

The second marker is a 3-6 m thick horizon of red shale of Late Norian (Sevatian) age (Scandone, 1967; Miconnet, 1983; Amodeo & Baumgartner, 1994; Amodeo, 1999; Bertinelli, 2003; Reggiani et alii, 2005; Rigo et alii, 2005) marking the base of the Transitional interval between Calcari con Selce and Scisti Silicei formations. The Red shale horizon has been studied in two sections of the Lagonegro Basin: Monte Buccaglione and Monte Cugnone (Fig. 2.1).

In the Calcari con Selce formation many calcareous turbidite beds are observed. They consist of fine sand to silt-grained carbonate sediment exported from adjacent platforms and are characterized by a incomplete Bouma sequence (Bertinelli et alii, 2005; Passeri et alii, 2005); they can thus be interpreted as distal turbidites. Above the Green clay-radiolaritic horizon, all over the Lagonegro basin, a calciturbidite with proximal features (horizon "A" of the Bouma sequence) is found. This calciturbidite mostly consists of sand to pebble-sized clasts of pelagic

sediment. This turbidite bed constituted an exception within the Calcari con Selce formation, and was thus analysed with more detail. Its triggering mechanism is then discussed.

2.2 Sections

We have analysed six sections of the Calcari con Selce formation (Fig. 2.1).
Four sections were logged in the upper Carnian interval and include the Green clay-radiolaritic horizon. In these four sections we have analysed the sedimentological features of the Green clay-radiolaritic horizon (Fig. 2.2). The sections were then correlated in order to assess the continuity of adjacent limestone beds.
The Monte Armizzone section (Scandone, 1967) is located near the town of Castelsaraceno, on the western side of the Monte Armizzone (latitude 40° 8'51. 24"N longitude 15°58'41. 80"E). We have measured in detail the 11 m interval encompassing the Green clay-radiolaritic horizon, which is here 2 m-thick (Fig. 2.3).
The 6,50 m long Pezza la Quagliara section is located along the road connecting Sasso di Castalda to Pignola (Potenza Province), (latitude 40°30'17. 60"N, longitude 15°42'36. 48"E). The section is interrupted by a fault in the last part of the Green clay-radiolaritic horizon (Fig. 2.4).
The San Michele section is located near to the village of Sasso di Castalda (Potenza Province) along a trail (Latitude 40°29'58. 82"N, Longitude 15°42'56. 92"E). We have measured the 10 m that encompass the Green clay-radiolaritic horizon, which is here 4.50 m-thick (Fig. 2.5).
The Pignola2 section is a road cut near the village of Pignola, along the road connecting Pignola to Abriola (Latitude 40°32'53. 59"N, longitude 15°47'12. 02"E). (Rigo et alii, 2007; Preto et alii, in press). The Green clay-radiolaritic horizon in the Pignola2 section measures ca. 5 m (Fig. 2.6).
Two sections represent the Norian – Hettangian interval of Calcari con Selce and Scisti Silicei formations and the Red shale horizon is present. These sections were measured and correlated with a remote sensing approach with the use of terrestrial laser scanner (TLS) in order to objectively evaluate the continuity and thickness persistence of limestone beds (Fig. 2.2).
Monte Buccaglione section (Bertinelli et alii, 2005) outcrops near the village of Sasso di Castalda (Potenza Province) (Latitude 40°29'29.47"N, Longitude 15°40'33.78"E).
Monte Cugnone section is within an old quarry near Marsico Nuovo (Latitude 40°26'10.74"N, Longitude15°43'34.01"E).

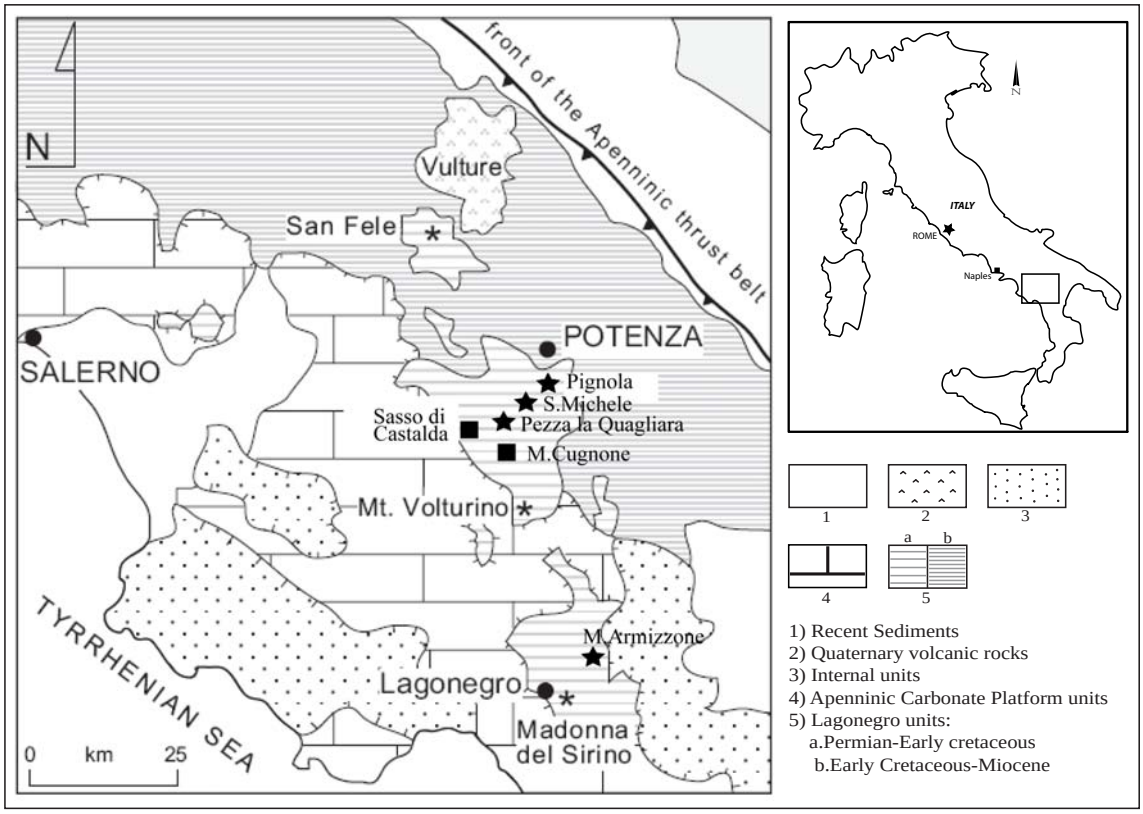

Figure 2.1 – Geological map of Southern Apennines and location of the studied sections (modified from BERTINELLI et alii, 2005). The stars show the sections encompassing the Green-clay radiolaritic horizon, while squares show sections including the Red shale horizon.

2.3 Methods

Thirty samples of limestone, shale, siliceous shale, radiolarite, tuff and calcareous turbidite were collected in the four sections encompassing the Green clay-radiolaritic horizon. All samples were prepared as thin sections and were examined at high magnification using a Leica DM-EP petrographic microscope.

In order to determinate the composition of the proximal calciturbidites that is always found above the Green clay-radiolaritic horizon, thin sections from bottom and top of the calciturbidite bed were collected in each of the studied sections and point-counted. For each thin section more than 500 points were counted. The maximum standard deviation amounts thus to 4% (VAN DER PLAS & TOBI, 1965). In all sections the grains have roughly constant dimensions and in the counting analyses the grain size is smaller than the step of the measure. Counting was performed along lines normal to the bedding plane.

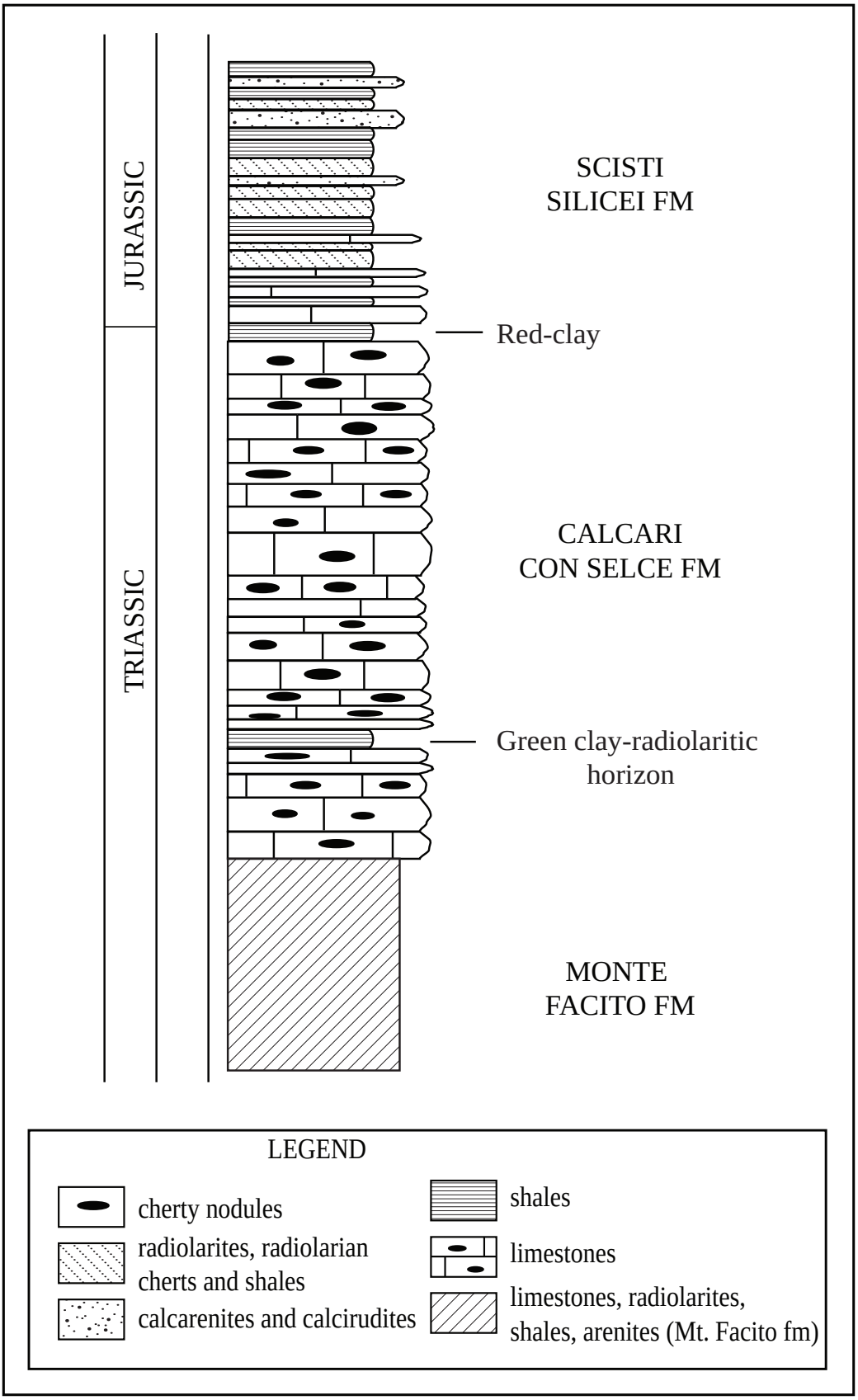

Figure 2.2 – Schematic log of the Calcari con Selce formation and position of Green clay-radiolaritic horizon and Red shale.

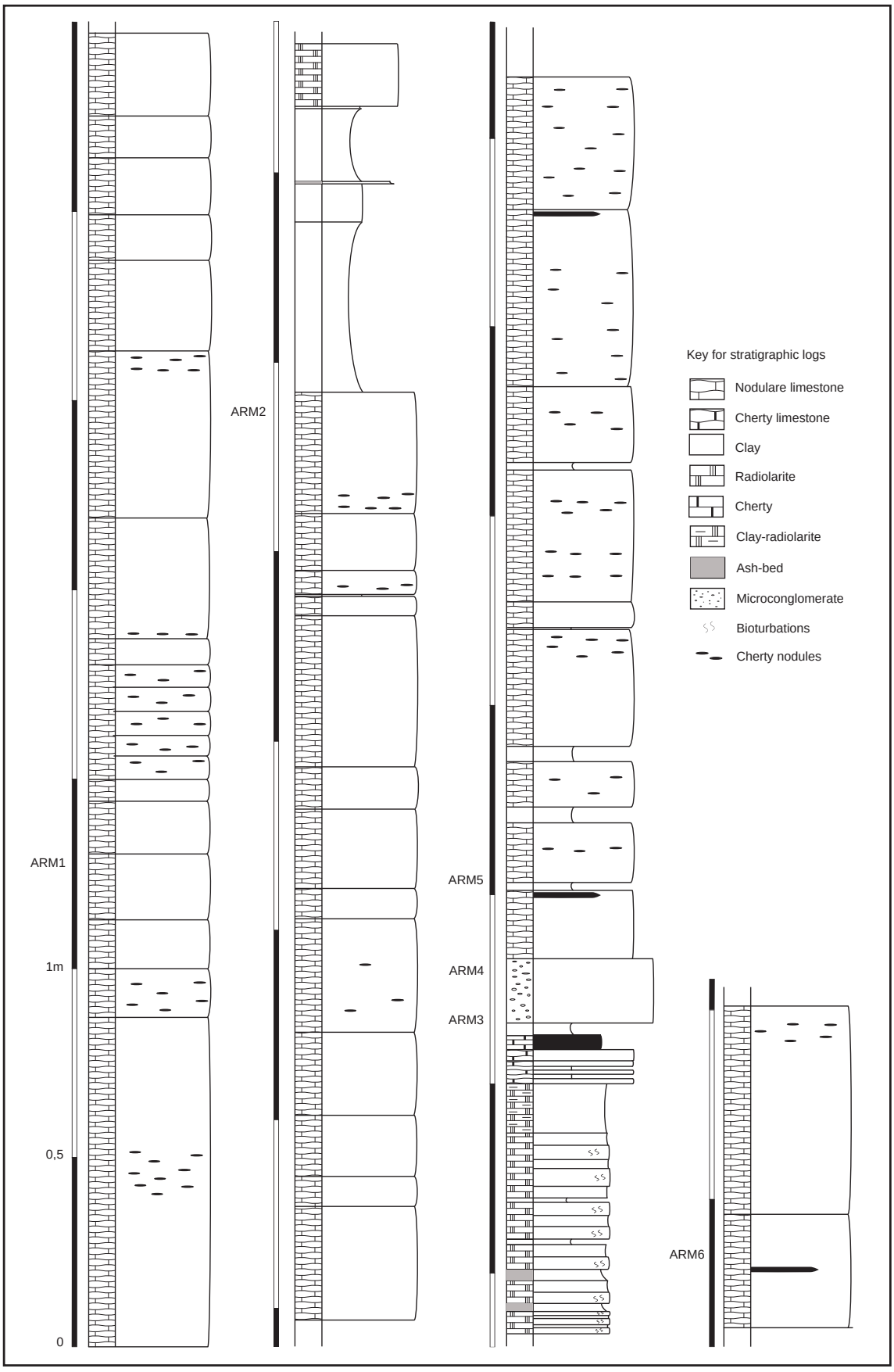

Figure 2.3 – Stratigraphic log of the Monte Armizzone section.

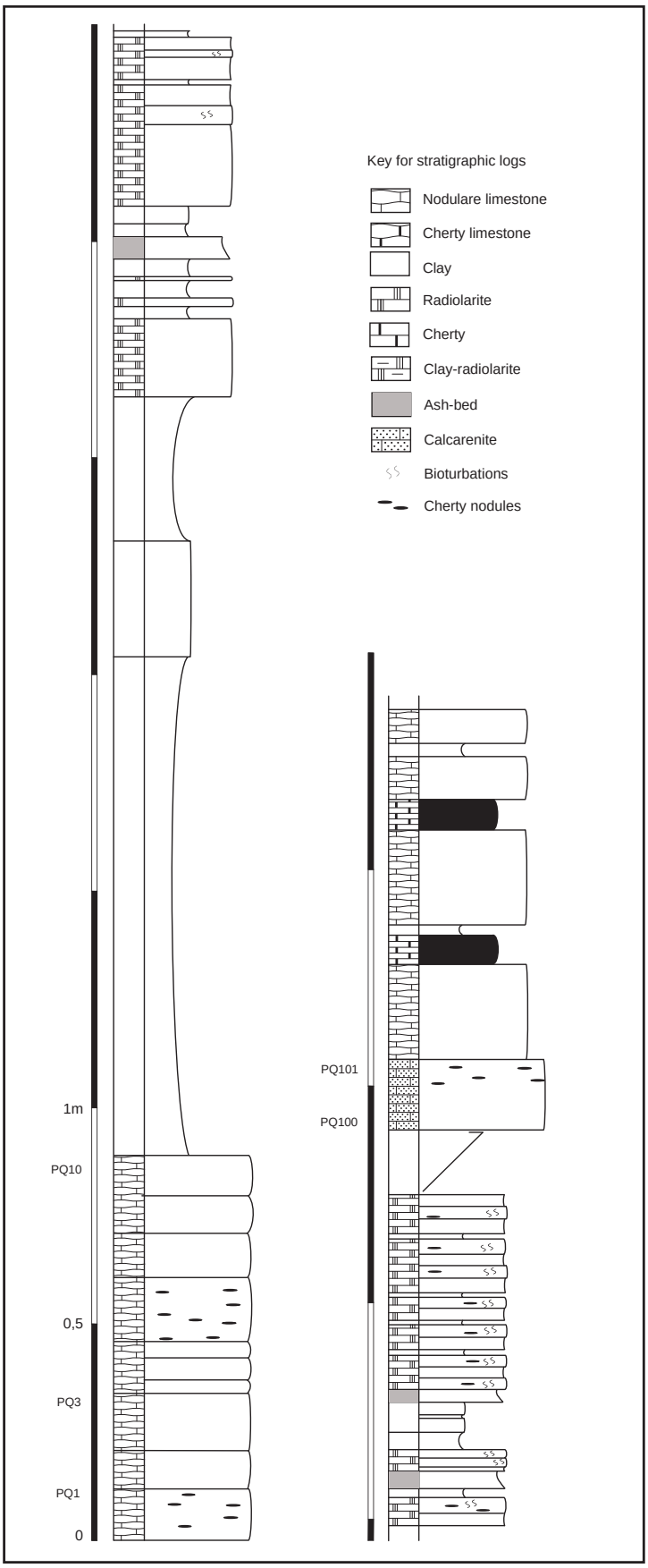

Figure 2.4 – Stratigraphic log of the Pezza la Quagliara section.

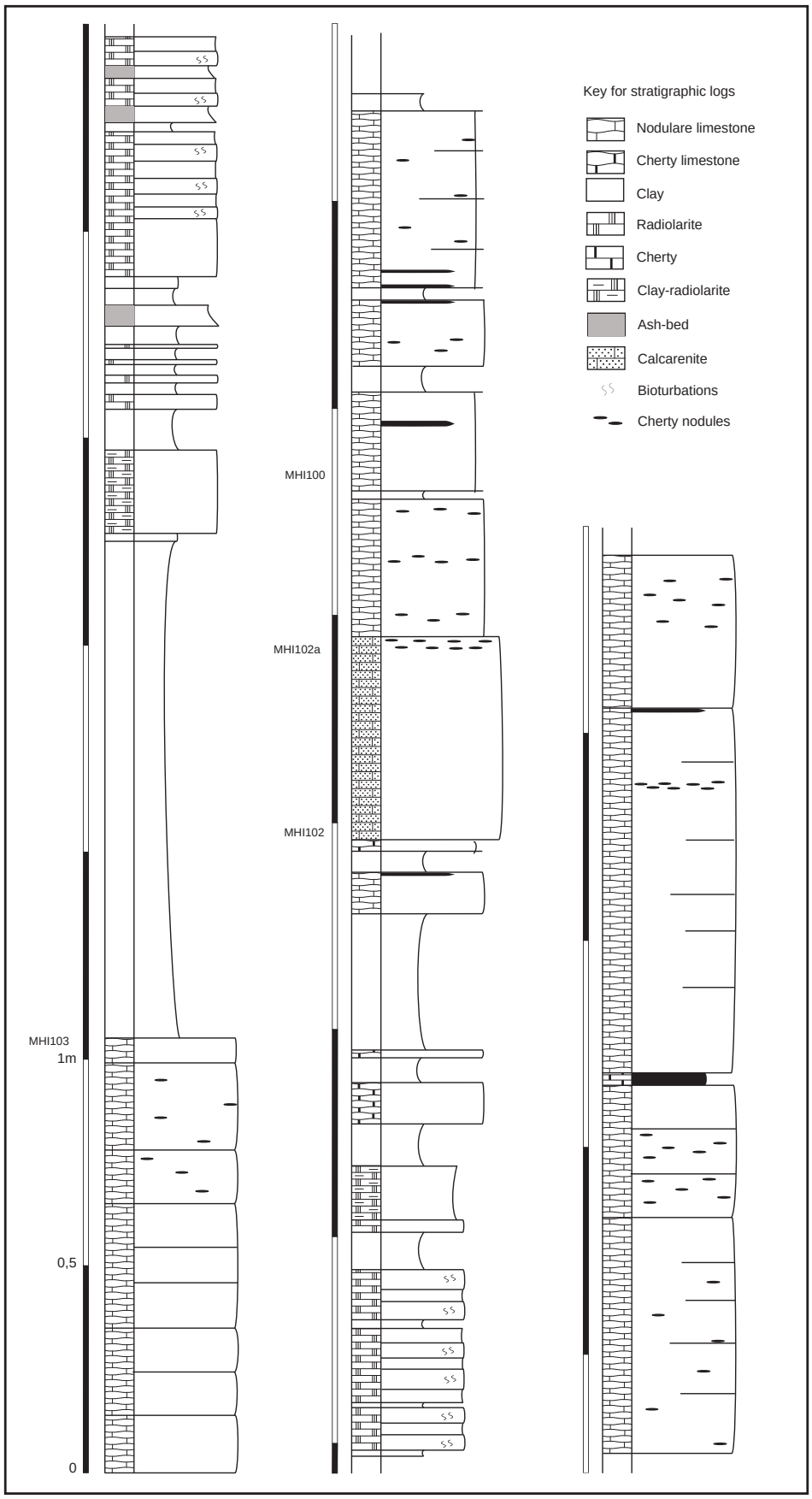

Figure 2.5 – Stratigraphic log of the San Michele section.

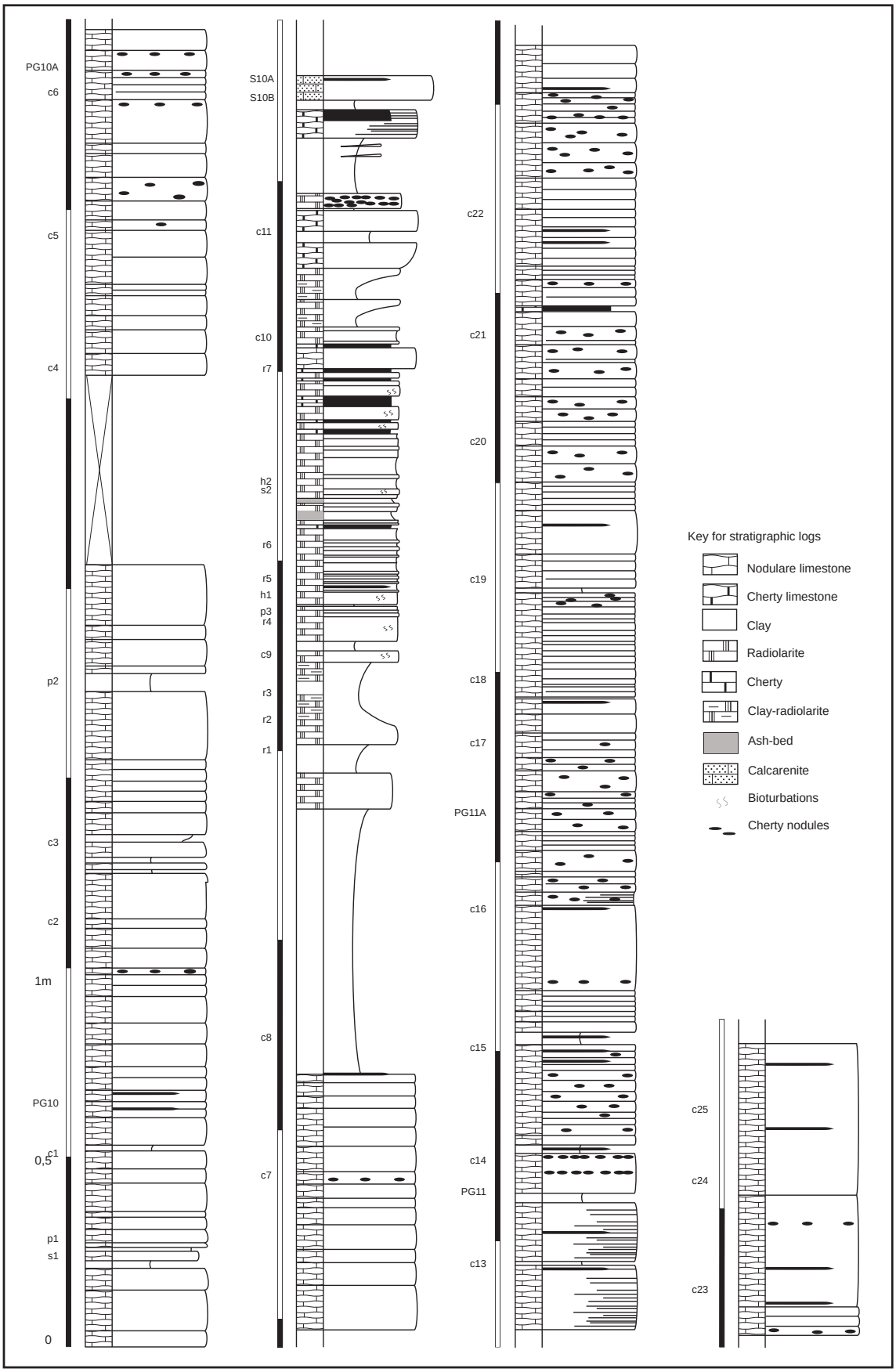

Figure 2.6 – Stratigraphic log of the Pignola2 section (modified from RIGO et alii, 2007).

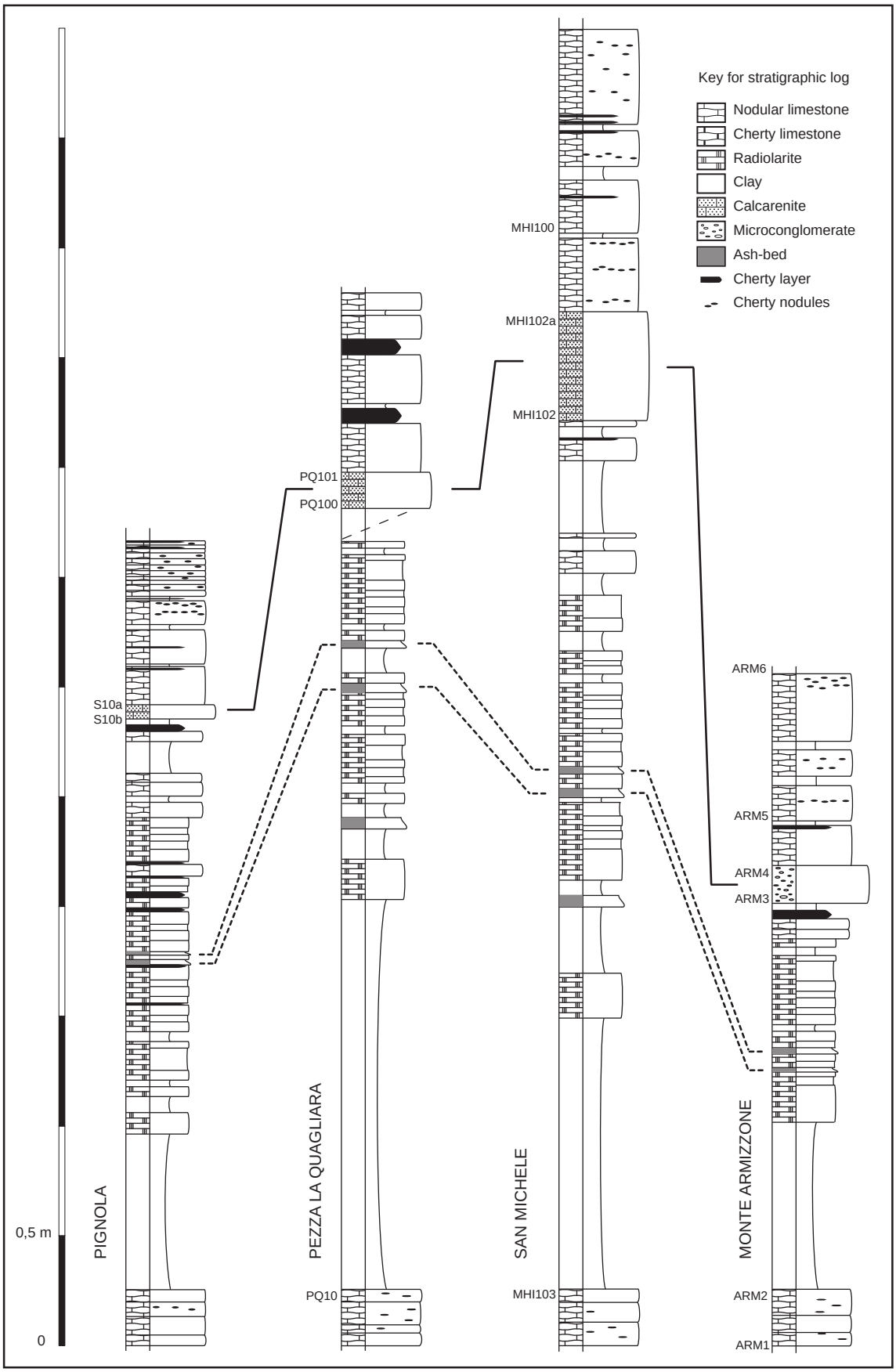

Figure 2.7 – Stratigraphic logs of the studied sections. The black lines show a calciturbidite bed, while the dash lines show the Aglianico volcanic ash-beds, dated 230.91+/-0.33 Ma (FURIN et alii, 2006, 2007).

2.3.1 Conodont Biostratigraphy

Conodont samples have been collected from Pezza la Quagliara (PQ), San Michele (MHI) and Armizzone (ARM) sections for biostratigraphic investigations. Conodont biostratigraphy of Pignola2 (PIG2) section has already been illustrated in Rigo et alii (2007) and it is here compared to those of the other three sections in order to better constrain the age of the Green clay-radiolaritic horizon. Each sample has an average weight of 5 kg (of limestones), with a content in conodonts of ca. 100 specimens (both ramiform and pectiniform conodont elements) per kg for Pignola2 and San Michele sections and ca. 30 specimens per kg for Pezza la Quagliara and Armizzone sections.

2.3.2 Terrestrial Laser Scanner

A terrestrial laser scanner (TLS) was employed to measure the thickness of limestone beds in the Monte Cugnone and Buccaglione sections. TLS is an instrument capable of producing a detailed 3D model of the surface of an object in the form of a point-cloud in which each point is characterized by spatial coordinates and intensity value. The main characteristics of TLS are: long range, high precision and accuracy, automatic data acquisition and short acquisition time. If an outcrop is acquired, on the resulting point-cloud is possible to perform measurement with a remote sensing approach also in the case of inaccessible and long sections. In the geometrical measurements perspective deformations are absent because of the 3D nature of the dataset.
The Monte Cugnone section has been scanned with a point to point spacing of 6 cm, from a distance of approximately 170 m, while Monte Buccaglione section has been scanned with 8 cm resolution at a distance of 400 m.

2.4 Stratigraphy and Lithology of the Green clay-radiolaritic horizon

2.4.1 Green clay-radiolaritic horizon

All sections consist of nodular limestones (wackestones) with cherty nodules and beds, radiolarians and thin-shelled bivalves (Calcari con Selce formation), interrupted with sharp contact by the deposition of the 3-6 m thick Green clay-radiolaritic horizon (Fig. 2.7) in which carbonate sediment is lacking. The horizon starts with 30-200 cm thick polychromous and laminated shales alternated with clay radiolarite beds. The succession continues with green and white radiolarites alternated with thin shale interlayers. The white radiolarites are bioturbated, while green radiolarites are laminated and more erodible. At least three thin (3-5 cm) crystal tuffs are present (Aglianico volcanic ash-beds). The last meters of the Green clay-radiolaritic horizon are composed of thin, polychromous radiolarites and shales, siliceous coquina beds and a black cherty layer. At Pezza la Quagliara, the section is truncated by a fault above green-white radiolarites, and, after a non-documented interval, the section continues with a calciturbidite (Fig. 2.4). The Green clay-radiolaritic horizon finishes with this 16-49 cm-thick

calciturbidite. Above the calciturbidite, carbonate sedimentation starts again with the typical facies of the Calcari con Selce formation, but the limestone beds are more nodular and thicker (40 cm-thick) and rich in cherty nodules and beds compared to the interval below the Green clay-radiolaritic horizon. Shale interlayers are initially abundant and thick but decrease rapidly upward.

2.4.2 Calciturbidite

In all the sections, the Green clay-radiolaritic horizon ends with a calciturbidite bed (Fig. 2.7) characterized by strong thickness variations, irregular and erosional base with a basal intraformational conglomerate (horizon "A" of the Bouma sequence), and black chert nodules in the upper part. The calciturbidite bed is present in Pezza la Quagliara, San Michele and Pignola2 sections and it is constituted of echinoderm fragments, isolated thin-shelled bivalves and reworked, partially lithified intraclasts of the Calcari con Selce formation (Fig. 2.8A-C). In the Monte Armizzone section, the calciturbidite is a microconglomerate bed (Fig. 2.8D1), with similar composition. Bioturbation is absent in all samples. In all the sections studied the top of the calciturbidite is characterized by laminations, absent in the Monte Armizzone section.

The calciturbidite shows the same lithological characteristics in all localities, being mostly composed of carbonate grains with little siliciclastic grains (volcanic lithics, feldspar, biotite and chlorite). There are two types of carbonate intraclasts. The first consists of wackestones and mudstones with thin–shelled bivalves and calcified radiolarians (partially lithified grains of Calcari con Selce formation). The second is a calcisphere wackestone-packstones. Micrite sediment is absent, but a non-carbonate, red-brown, interstitial component is present. This non-carbonate component is probably constituted by clay and oxide minerals that derive from the erosion of the Green clay-radiolaritic horizon. Foraminifers, radiolarians, thin-shelled bivalves and echinoderm fragments are also present. Other carbonates grains that might suggest a provenance from platform facies are absent.

In all the studied thin sections the top of the calciturbidite is characterized by parallel-laminations, reduction of grains size and increase of thin-shelled bivalves. In the calciturbidite samples of the Monte Armizzone section, the size of grains is very coarse (microconglomerate) also at the top, but there is normal gradation; in the upper part of the calciturbidite thin-shelled bivalves are not as abundant as below.

Thus, the typical constituents of calciturbidites were summarised in 9 categories: intraclasts A (wackestones and mudstones with thin–shelled bivalves and calcified radiolarians), intraclasts B (wackestone and packstone with calcispheres), thin-shelled bivalves and their fragments, echinoderm fragments, foraminifers, non-carbonate grains (feldspar, biotite, chlorite crystals), non-identifiable carbonate grains (dolomitized and indeterminate skeletal grains), sparite and interstitial sediment (red-brown non-carbonate sediment).

The composition of the calciturbidite is summarized in Table 2.1.

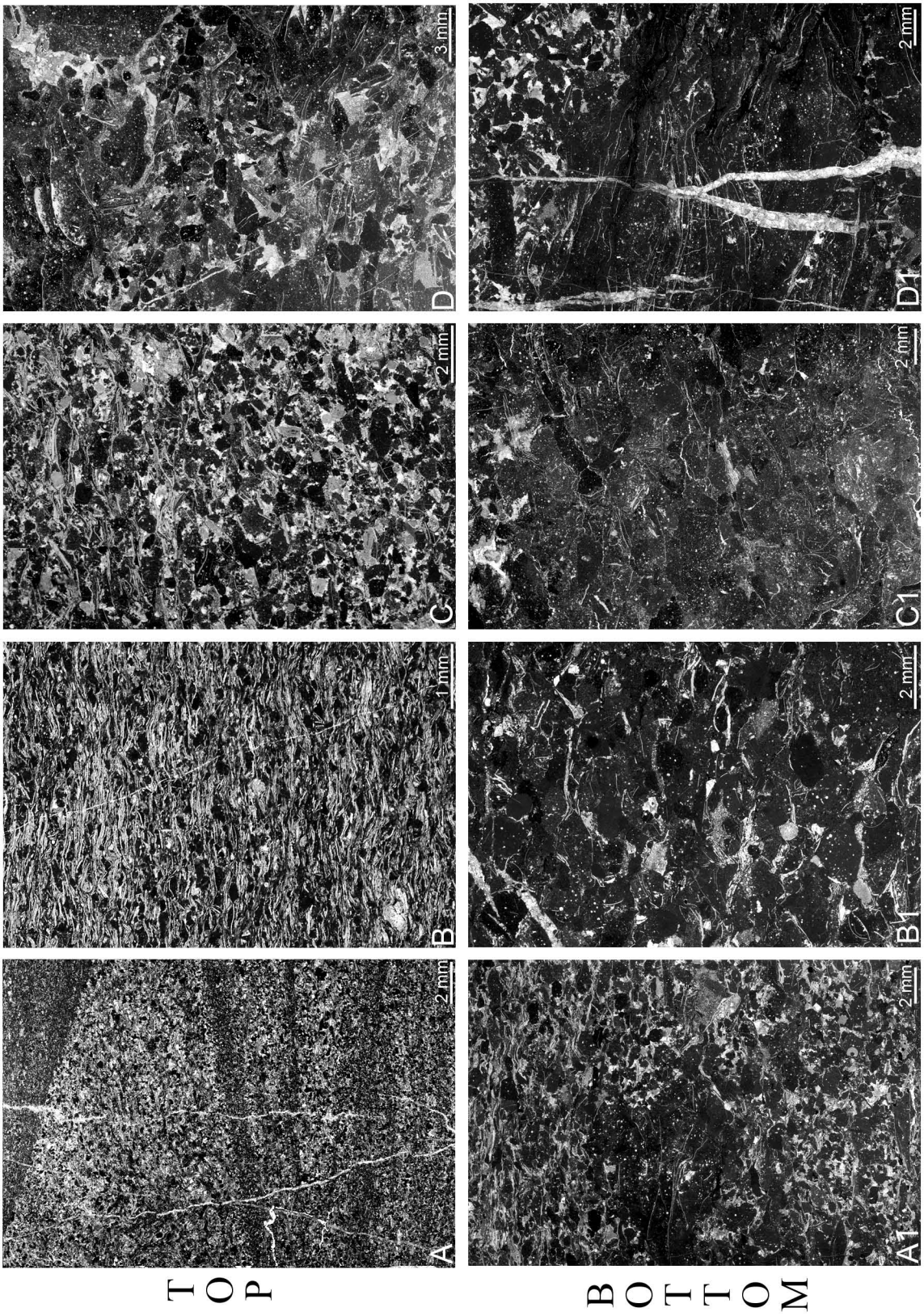

Figure 2.8 – Plate showing the thin sections of calciturbidite in the different section. A-A1: Pezza la Quagliara section; B-B1: San Michele section; C-C1: Monte Armizzone section; D-D1: Pignola2 section.

Point count group	Intracl. A	Intracl. B	Bivalves	Echinoderm Fragments	Non carbonate	Foraminifers	Sparite	Interstitials	Indeterminable
PQ 100 P.Quagliara Bottom	50.41	19.12	12.32	2.92	1.13	0.65	7.94	4.54	0.97
PQ 101 P.Quagliara Top	44.62	2.92	22.31	6.62	0.92	1.08	19.54	1.08	0.92
SMI 102 S.Michele Bottom	56.55	21.19	7.47	2.74	0.76	0	5.03	5.49	0.76
SMI 102A S.Michele Top	36.32	3.10	38.38	5.51	0.52	0.86	10.84	4.13	0.34
ARM 3 Armizzone Bottom	66.13	8.91	6.32	3.40	0.81	0	10.21	3.89	0.32
ARM 4 Armizzone Top	55.64	15.52	5.02	3.45	1.88	0	10.19	7.68	0.63
S 10B Pignola2 Bottom	56.42	25.37	3.74	1.46	0.49	0	5.04	7.15	0.33
S10A Pignola2 Top	42.63	16.16	12.84	7.61	0.48	0.48	15.06	4.12	0.63
mean value	51.09	14.04	13.55	4.21	0.87	0.38	10.48	4.76	0.61

Table 2.1 – Summary of the nine point count groups analysed in 8 thin-sections.

The intraclasts A are the most common constituent with a mean value of 51.09% per thin section, followed by intraclasts B with 14.04%. Intraclasts are thus by far the main constituent of the calciturbidite. Thin-shelled bivalves are the second most common constituent with an average abundance of 13.55%. They consist of disarticulated valves and small fragments and complete shells are very rare. Non-carbonate grains are rare with a mean value of 0.87%. They consist of volcanic lithics, feldspar, biotite and chlorite which are also found in the Green clay-radiolaritic horizon. Echinoderms are relatively common (4.21%) and occur as fragments. Benthic hyaline foraminifers have the lowest abundance with 0.38%. Interstitial sediment is scarce, 4.76%. Figure 2.9 summarizes the calciturbidites constituents.

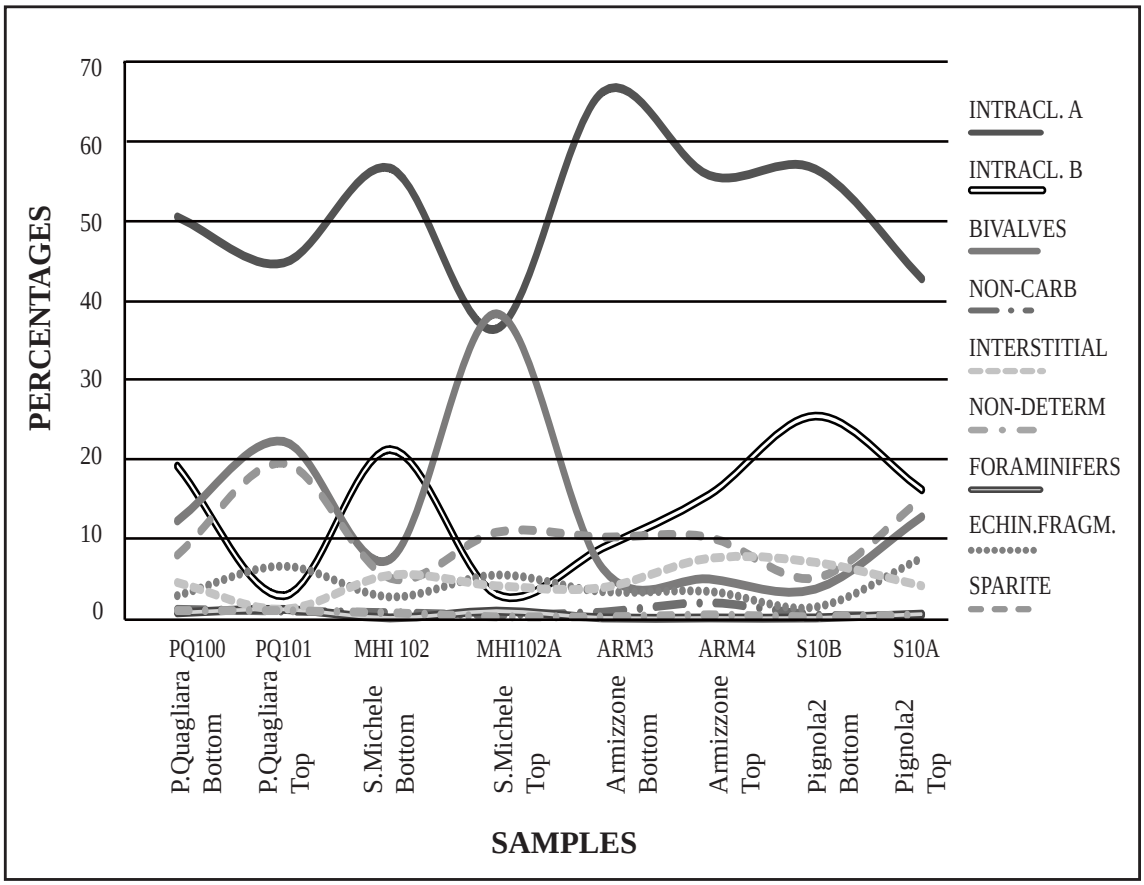

Figure 2.9 – Plots showing the variation in composition of 8 thin sections.

2.5 Continuity of Limestone Beds

The Calcari con Selce formation shows clear and regular lithological repetitions of micritic limestones and thin marl or shale interbeds. It is important to understand if these sedimentary cycles are produced by autocyclic or diagenetic processes, rather than recording an external (allocyclic) forcing. In fact, only if sedimentary cycles are continuous their origin can be related to external forcing. Thus, two stratigraphic markers have been used as reference levels to study the lateral continuity of limestone beds. These two markers are within the Calcari con Selce formation and we have analysed the continuity of contiguous limestone beds (Fig. 2.2). The first marker is the Green clay-radiolaritic horizon described in this chapter (Fig. 2.7). The horizon was recognized in four sections, presently up to 50 Km apart. Their original distance, however, might reveal substantially greater if tectonic restoration could be performed. This horizon is considered a chronostratigraphic marker in the Lagonegro Basin because it includes correlatable ash-beds (Aglianico volcanic ash-bed), and a calciturbidite, and because of conodont biostratigraphy. Above the horizon, the limestone beds are more nodular and thicker than in the lower part of the section. Furthermore, single carbonate beds or banks with the

same stratigraphic position and common characteristics are present and recognizable in all sections (Fig. 2.10). The thickness of these limestone beds is different, but the shale interlayers and cherty beds occur in an identical sequence: about the Green clay-radiolaritic horizon, the succession has the same limestone banks or beds throughout the basin.

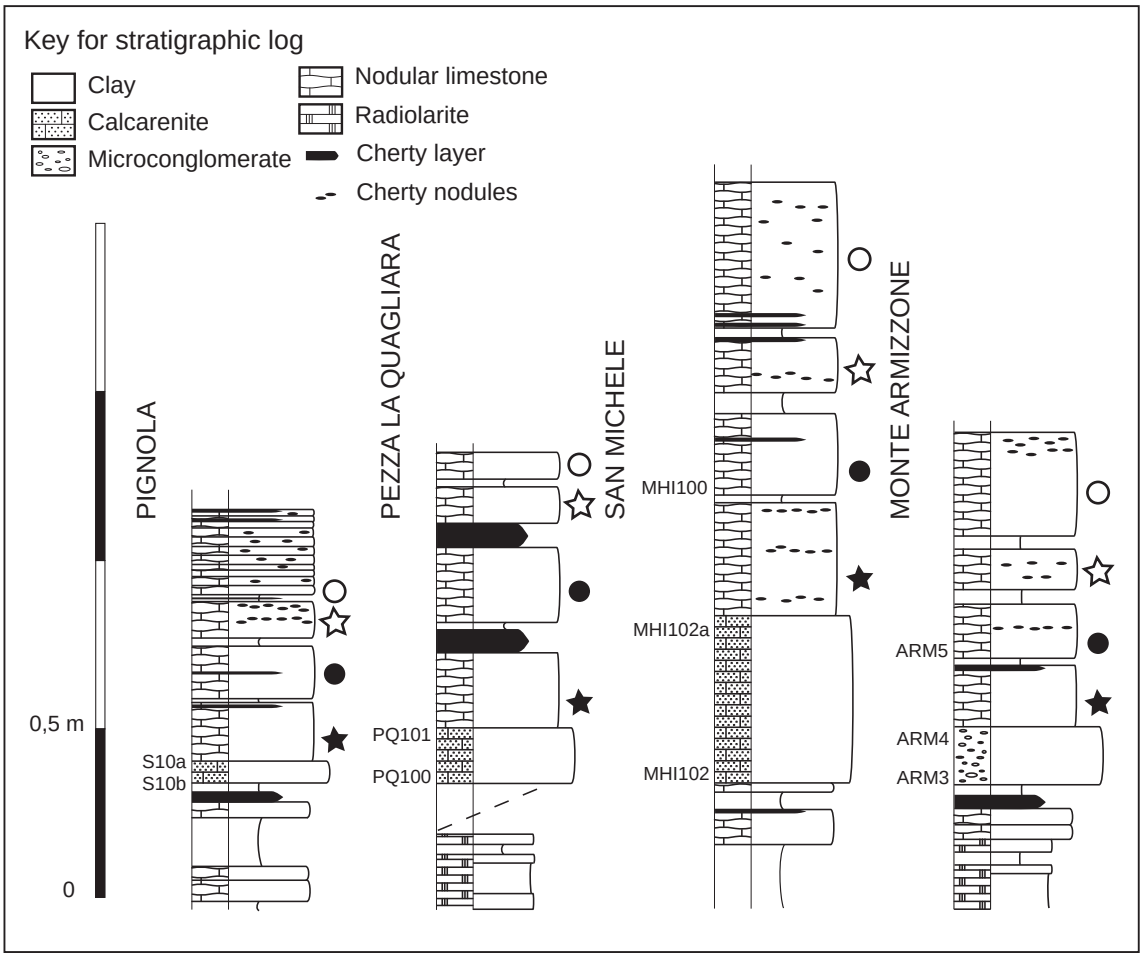

Figure 2.10 - Carbonate beds and banks above the Green clay-radiolaritic horizon. The same symbols indicate the limestone beds or banks with same sedimentological characteristics.

The second marker is the Red shale horizon, a lithologic marker throughout the Lagonegro Basin (Scandone, 1967; Miconnet, 1983; Amodeo & Baumgartner, 1994; Amodeo, 1999; Bertinelli, 2003; Reggiani et alii, 2005; Rigo et alii, 2005). This horizon marks the base of the «Transitional interval» and consists of 3-m-thick red shale dated to the Sevatian (upper Norian) (Fig. 2.11) (Rigo et alii, 2005). We have measured the limestone beds and shale interlayers below the Red shale horizon in two sections separated by 7 Km, Monte Buccaglione and Monte Cugnone sections. The sections were measured with laser scanner technique. Furthermore, a measurement carried out with traditional techniques was already available for Monte Buccaglione section (Bertinelli et alii, 2005). We have scanned the succession from three different view-points. In the case of the Monte Cugnone section measurements has been carried out only on laser acquisitions because of the inaccessibility of the outcrop.

Two digital outcrop models (DOMs) have been realized from the TLS-generated point-clouds and the limestone and marl beds thicknesses have been obtained directly from them. Below the Red shale horizon, a regular sequence of limestone beds and shale interlayers is present. The thickness of carbonate banks is identical between the two sections, within the limits of instrumental resolution (Table 2.2).

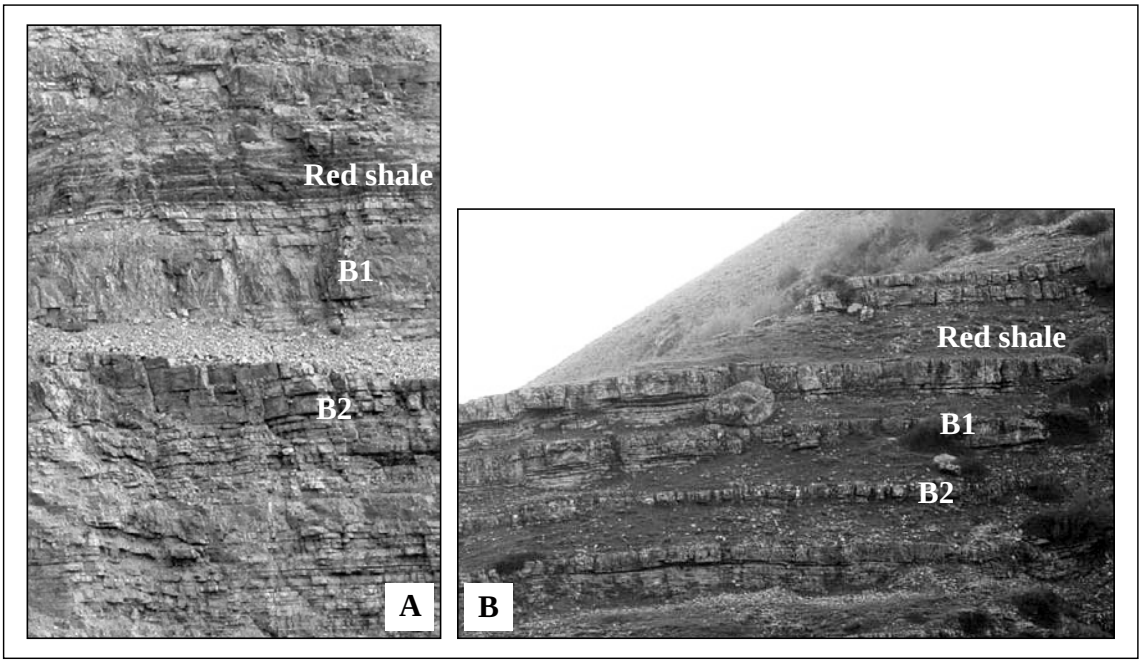

Figure 2.11 – The Red shale horizon in the Monte Buccaglione (B) and Monte Cugnone (A) sections.

	M. Buccaglione section	M. Cugnone section
Red shale	5.47 m	4.28 m
Bed 1	4.46 m	4.34 m
Bed 2	4.44 m	4.44 m

Table 2.2 – Thickness of limestone beds in Monte Cugnone and Monte Buccaglione sections measured with laser scanner technique.

2.6 Conodont Biostratigraphy

The CAI (Conodont Alteration Index, EPSTEIN et alii, 1977) of conodonts is 1.5 for Pignola 2 (PIG) and San Michele (MHI); 2 for Pezza la Quagliara (PQ) and 4 for Armizzone (ARM) sections.

A typical Julian conodont fauna (Table 2.3) occurs in the lower part of the section, just below the Green clay-radiolaritic horizon. It consists of *Paragondolella polygnathiformis*

noah (MHI103, ARM1,2, PIG), *P. praelindae* (PQ10, MHI103, ARM1,2, PIG), P. *inclinata* (ARM1,2, PIG2), *P. tadpole* (PQ10, ARM1,2, PIG 2), *Paragondolella n. sp. A aff. P. foliata* (MHI103, PIG2), *Nicoraella postkockeli* (PQ10, ARM1,2, PIG2) and *Gladigondolella ssp.* (PQ10, MHI103, PIG2).

A Tuvalian conodont assemblage (Table 2.3) has been recorded from the calcareous layers above the Green clay-radiolaritic horizon in San Michele, Armizzone e Pignola 2 section. Pezza la Quagliara lacks the Tuvalian portion of the succession. This fauna includes *P. polygnathiformis noah* (MHI100, ARM6, PIG2), *Metapolygnathus carpathicus* (ARM6, PIG2), *Carnepigondolella zoae* (=*Metapolygnathus nodosus*) (MHI100, PIG2) and *M. communisti* (MHI100, PIG2).

	Conodonts	*Gladigondolella* ssp.	*Gladigondolella tethydis*	*Nicoraella postkockeli*	*Paragondolella praelindae*	*Paragondolella inclinata*	*Paragondolella tadpole*	*Paragondolella* n. sp. A aff. *P. foliata*	*Paragondolella polygnathiformis noah*	*Carnepigondolella zoae*	*Metapolygnathus carpathicus*	*Metapolygnathus communisti*
Tuvalian	ARM6								X		X	
	MHI100								X	X		X
Julian	ARM2			X	X				X			
	ARM1	X			X	X	X		X			
	MHI103		X		X			X	X			
	PQ10	X		X	X		X					

Table 2.3 – Simplified distribution of the most important conodont bioevents of studied sections. For Pignola2 conodonts distribution, see Rigo et alii (2007). ARM: Monte Armizzone section; MHI: San Michele section; PQ: Pezza la Quagliara section.

2.7 Discussion

2.7.1 Green clay-radiolaritic horizon as a stratigraphic marker

The Green clay-radiolaritic horizon represents an anomalous event within the Upper Triassic hemipelagic carbonate sedimentation of the Lagonegro Basin. During the deposition of this horizon, carbonates are absent and substituted by shales, siliceous shales and radiolarites. This event of anomalous sedimentation has the same age of a Carnian humid pulse recognized in shallow-water and continental environments of Eurasia and Tethys (Simms & Ruffell, 1989, 1990; Simms et alii, 1995). Rigo et alii (2007) suggest that the green clay-radiolaritic horizon represents a temporary rise of the Carbonate Compensation Depth above the sea floor.

The Green clay-radiolaritic horizon was recognized in the four sections studied, for distances up to 50 Km, thus, it can be considered a marker of the Carnian Pluvial Event throughout the Lagonegro Basin, as suggest already by Scandone (1967).

However, as the Green clay-radiolaritic horizon is the response of this hemipelagic setting to a climate shift recognized globally, at least at tropical latitudes (see discussion in Rigo et alii, 2007), it might be present also in other deep-water settings of the western Tethys. Nodular cherty limestones as those of the Calcari con Selce are a common facies for the upper Triassic of Tethys, being common in the southern Apennines and Dinarids as well (Preto et alii, 2005, and references therein), and are found as far as Japan and Timor (Martini et alii, 2000; Onoue & Sano, 2007). It is suggested that this stratigraphic interval should be investigated in these settings, and the equivalent of the Green clay-radiolaritic horizon recognized, if not for the presence of ash beds, at least for a temporary halt of the carbonate sedimentation.

2.7.2 Origin of the calciturbidite bed

Calcarenite beds within the Calcari con Selce formation are documented in proximal to distal portions of the Lagonegro Basin (Passeri et alii, 2005). These calcarenite beds often display erosional lower surface and normal gradation, with incomplete Bouma sequences, including B and C horizons only. The calcarenites consist of small grains exported from adjacent carbonate platforms and contain benthic foraminifers and fragments of other benthic organisms (Bertinelli et alii, 2005; Passeri et alii, 2005).

The calciturbidite bed above the Green clay-radiolaritic horizon is unique because it has proximal characteristics in all the sections studied, as highlighted by complete Bouma sequence and coarse sand to pebble sized grains. It consists of lithoclasts of hemipelagic-pelagic wackestone-packstones and it has irregular and erosional base and a basal intraformational conglomerate. The thickness of this calciturbidite changes from section to section, but even more within each locality, as in the case of Pignola2, where the calciturbidite bed thickness varies between 0 and 40 cm. These differences are probably due to a peculiar provenance and depositional process.

The main components of this calciturbidite are semilithified intraclasts of the Calcari con

Selce formation. During the deposition of the Green clay-radiolaritic horizon, the Carbonate Compensation Depth temporary rose (Rigo et alii, 2007) and the carbonate sedimentation was present probably only on the flanks of the basin. Thus, the source of lithoclasts cannot be the basin floor and must rather lie on the basin slopes. The platform contribution, in the form of echinoderm fragments and perhaps foraminifers, is 4.5%. Non-carbonate grains and siliciclastic interstitial sediment are instead interpreted as the result of erosion of the underlying Green clay-radiolaritic horizon by the turbidity current. Indeed, the calciturbidite bed lies directly on the Green clay-radiolaritic horizon. The shortage of platform-derived elements as echinoderm fragments and foraminifers, the abundance of thin-shelled bivalves and lithoclasts of pelagic-hemipelagic origin indicate that the provenance of sediment is mostly from a deep water slope setting.

The reason why this particular calciturbidite emplaced right at the top of the Green clay-radiolaritic horizon is unclear. The trigger mechanisms of turbidity currents are several and can include earthquakes, storm surges, river discharge during a flood (Mulder et alii, 1995), mass failures on deltaic and basin slopes (Normark & Piper, 1991). The criteria for distinguishing the origin of different turbidites are also not unambiguous, even if in the last years some progress has been made. Nakaijama & Kanai (2000) suggest the sedimentary features to distinguish between seismoturbidites (i.e., turbidites triggered by earthquakes) and other type of turbidites. The seismoturbidites are characterized by amalgamated beds, irregular and incomplete Bouma sequence, multiple or line sources, variable composition and normal and inverse grading of grains. Other turbidites are instead single beds with regular Bouma sequence, and have uniform composition, normal grading and derive from a single source. The calciturbidite of the Green clay-radiolaritic horizon hardly fits into the model of seismoturbidites of Nakaijama & Kanai (2000). However, river discharge and storm surges are not possible trigger mechanisms either, because the calciturbidite is mainly composed of hemipelagic-pelagic reworked lithoclasts and riverine or terrigenous sediments are only a subordinate component.

Then, the probable mechanism is slope instabilities, but, again, the possible causes of instability are different: sea-level changes, dissociation of gas hydrates, seismic activity and storm waves. Storm waves are restricted on a shallow marine environment and in the calciturbidite, platform sediments are scarce. During the Carnian age in the Lagonegro Basin there are not evidences of dissociation of gas hydrates and seismicity and, in any event, it would be difficult to envisage a single seismic event producing a turbidite without companion events being registered in a record of millions of years. Furthermore, the calciturbidite lacks the characteristics of seismoturbidites, exhibiting instead normal grading, a complete Bouma sequence, uniform composition (mainly hemipelagic-pelagic sediments). Thus, this calciturbidite is not believed to be generated by an earthquake.

Sea-level change is identified as the most probable trigger mechanism of slope instability and turbidite deposition. During the Tuvalian, a major transgressive phase (3rd and 2nd order

cycle) is documented in the Tethyan realm (Gianolla & Jacquin, 1998), that is well-calibrated with conodont fauna by Hirsch (1991; 1994) to the lower Tuvalian. In the Southern Alps, this transgressive phase corresponds to the regional shift from the continental-paralic facies of the Travenanzes Formation to the platform interior facies of the epicontinental rimmed carbonate platform of the Dolomia Principale (Breda et alii, 2006; Neri et alii, 2007). The rise of the sea-level probably produced, along the slope, sediment instability that at a critical point generated a major turbidity current.

2.7.3 Lateral continuity of limestone beds

The continuity of limestone beds or banks adjacent to well recognizable marker beds has been verified, following the approach of, e.g., Brack & Muttoni (2000). In particular, decimetric to metric scale limestone-marl alternations immediately above the Green clay-radiolaritic horizon maintain the same pattern in all localities, and have been thus correlated (Fig. 2.10). This correlation has chronostratigraphic value, as chronostratigraphic markers as ash-fall beds and a distinctive turbidite occur immediately below. The single carbonate beds or banks have the same characteristics or an identical thickness in all the sections studied, and their lateral persistence is thus demonstrated.

On a basin scale, limestone-marl alternations are persistent, though their thickness may vary substantially. This excludes a diagenetic origin of the alternations according to the model of Westphal et alii (2000) and Westphal (2006), also making autocyclic processes highly improbable. On the scale of few km, the thickness of meter scale carbonate banks do not change significantly, further supporting their interpretation as records of external environmental forcing. Summarizing, the limestone-marl alternations constituting the Calcari con Selce in the Lagonegro Basin appear to record some external environmental forcing. It is suggested that forthcoming studies should be focused on the identification of an orbital signal in continuous, well exposed successions of the Calcari con Selce, as the Monte Buccaglione section at Sasso di Castalda or the dismissed quarry front exposed at Monte Cugnone near Marsico Nuovo.

2.8 Conclusions

The Green clay-radiolaritic horizon, representing the Carnian Pluvial Event in a basinal setting, was recognized throughout the Lagonegro Basin. It may be recognized in other basins, and thus serve as a Tethys-wide stratigraphic marker for chronostratigraphic correlation.

A calciturbidite bed is always present immediately above the Green clay-radiolaritic horizon, whit similar characteristics throughout the basin; it is thus a basinal event, probably triggered by a major transgressive during the late Carnian, which generated slope instability.

Limestone beds or banks of the Calcari con Selce formation are correlated at the basinal scale. This implies that the Lagonegro Basin is characterized by laterally continuous sedimentation

of limestone-marl alternations controlled by allocyclic factors. It is suggested that forthcoming studies of the Triassic hemipelagites of the Lagonegro Basin should be focused on the recognition of orbital cycles.

CHAPTER 3
Origin and Composition of Upper Triassic hemipelagic micrite (Sicani Basin, Sicily)

3.1 Introduction

The Upper Triassic Calcari con Selce formation (i.e., Cherty Limestones formation) has been widely studied in the last years, but quantitative and provenance works on hemipelagic micrite are missing. Pizzo Mondello (Sicily) was selected to study the origin and composition of carbonate because it is one of the best preserved, longest (400 m) and most continuous section of the Calcari con Selce fm (Fig. 3.1).

The Triassic is considered a time of "Aragonite Sea" (Stanley & Hardie, 1998), thus the mineralogy of micrite precursor, which is still unknown, should be aragonite or high-Mg calcite. To determine the initial mineralogical composition of the precursor sediment, morphological parameters at Scanning Electron Microscope (average crystal dimension and presence/absence of elongated pits) and chemical analyses (strontium content) were considered. Lasemi & Sandberg (1983, 1984, 1993) recognized two types of micrite-dominated precursors: aragonite-dominated precursor and calcite-dominated precursor. They differ by crystal size, aragonite needles and pitted crystal surface. We have analyzed at SEM several samples (43) of carbonate micrite from Pizzo Mondello section, with the aim to determine the prevailing mineralogy of their precursor.

The possible sources for the carbonate micrite in Triassic hemipelagic settings are: (a) calcareous nannoplankton related to coccolithophores (or pelagic carbonate production from a yet unknown source); (b) autochthonous benthic production, as for Middle Triassic thin-shelled bivalve *Daonella* (Schatz, 2005); (c) allochthonous material from the adjacent carbonate platforms (Bellanca et alii, 1995). Coccolithophores, originated during the Triassic time (Di Nocera & Scandone, 1977), was found so far only in minimal amount in Triassic rocks, and is considered insufficient to build up hundred-meters-thick successions as those of the Calcari con Selce (Bellanca et alii, 1995). Thus, many Authors suggest that this hemipelagic formation is mostly constituted by carbonate from adjacent platforms (e.g., Bellanca et alii, 1995; Rigo et alii, 2007). I evaluated quantitatively the components of the hemipelagic carbonates at Pizzo Mondello via point-counting, to understand the origin of micrite.

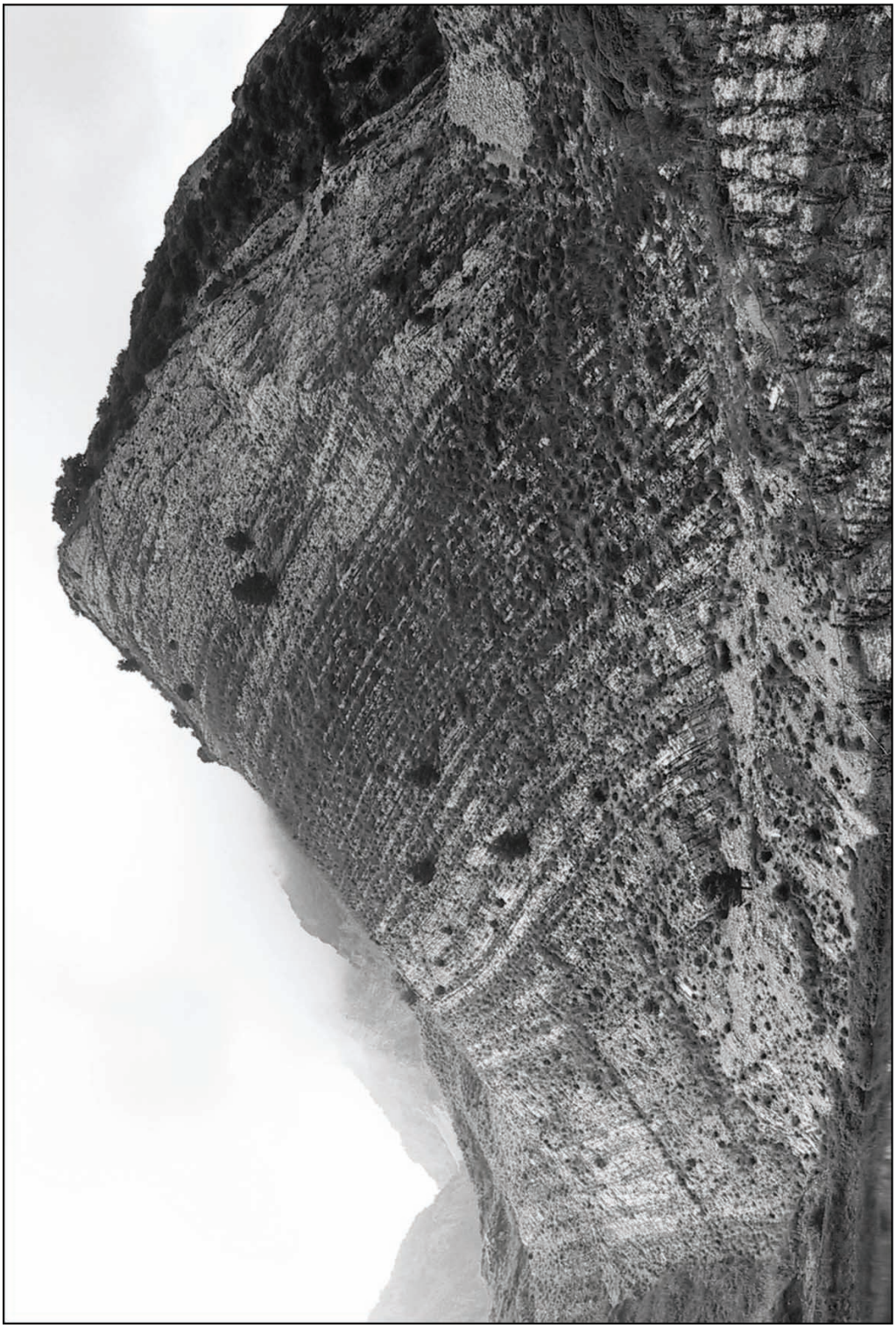

Figure 3.1 – Panoramic view of the Pizzo Mondello section. Based on its good exposure, accessibility, stratigraphic thickness, continuity and multiply chronostratigraphic correlation possibilities, Pizzo Mondello section has been proposed as Global Stratigraphic Section and Point for the base of the Norian (Muttoni et alii, 2004).

3.1.1 Pizzo Mondello, a GSSP candidate for the Norian

Pizzo Mondello is one of the most spectacular pelagic-hemipelagic stratigraphic sections of Late Triassic age, and it has been recently proposed as the GSSP candidate for the base of the Norian stage. During the last decade, several researchers have studied in detail the Pizzo Mondello section in order to better define the bio-, chemo- and magnetostratigraphic events around the proposed boundary (e.g. Muttoni et alii, 2001; Krystyn et alii, 2002; Muttoni et alii, 2004). Recently, the lower part of this section, corresponding to Interval 2 (Fig. 3.2) of Muttoni et alii (2004), has been studied and sampled in detail for conodonts, ammonoids and halobid thin-shelled bivalves. Conodonts were exceptionally abundant; several taxa not yet described in this section were recovered, such as *Zieglericonus* sp. and *Misikella longidentata*. The samples are also very rich in ramiform elements (e.g. >700 in sample NA27). The position of the Carnian/Norian boundary that is now under evaluation is that of Nicora et alii (2006). However, the study on conodont biostratigraphy is in progress and the current base of the Norian is still preliminary. Ammonoids have been found in some levels. Halobids are present either as isolated specimens within the rock matrix or in coquina levels within or intercalated to the cherty limestone beds.

Burial diagenesis has been very weak at Pizzo Mondello, as demonstrated by the CAI (Conodont Alteration Index) value of 1 exhibited by conodonts throughout the section, and indicates maximum burial temperatures <50-80° C. This allowed the preservation of physical signals as the $\delta^{13}C$ and a primary magnetization.

A sequence of 27 magnetozones has been established at Pizzo Mondello, 12 of which are comprised in our section near the boundary interval (Muttoni et alii, 2004). Krystyn et alii, (2002) and later Muttoni et alii (2004) tentatively correlated this sequence of magnetozones with the astronomically tuned magnetic Polarity Time Scale in the Newark Basin (Kent & Olsen, 1999). We here follow the correlation of Muttoni et alii (2004). The oldest astronomically tuned point of the Newark Basin composite section is in the lower part of magnetozone E8r, dated at ca. 226 Ma (Kent & Olsen, 1999). Magnetozone E8r was correlated with the highest part of our studied section at Pizzo Mondello (magnetozone PM6r), well above the boundary interval. Furin et alii (2006, 2007) provided a U/Pb zircon age for a Late Carnian ash-bed (i.e., below the boundary interval) deposited at 230.91 +/- 0.33 Ma. The absolute age of the boundary interval is thus comprised between 230.91 +/- 0.33 and 226 Ma.

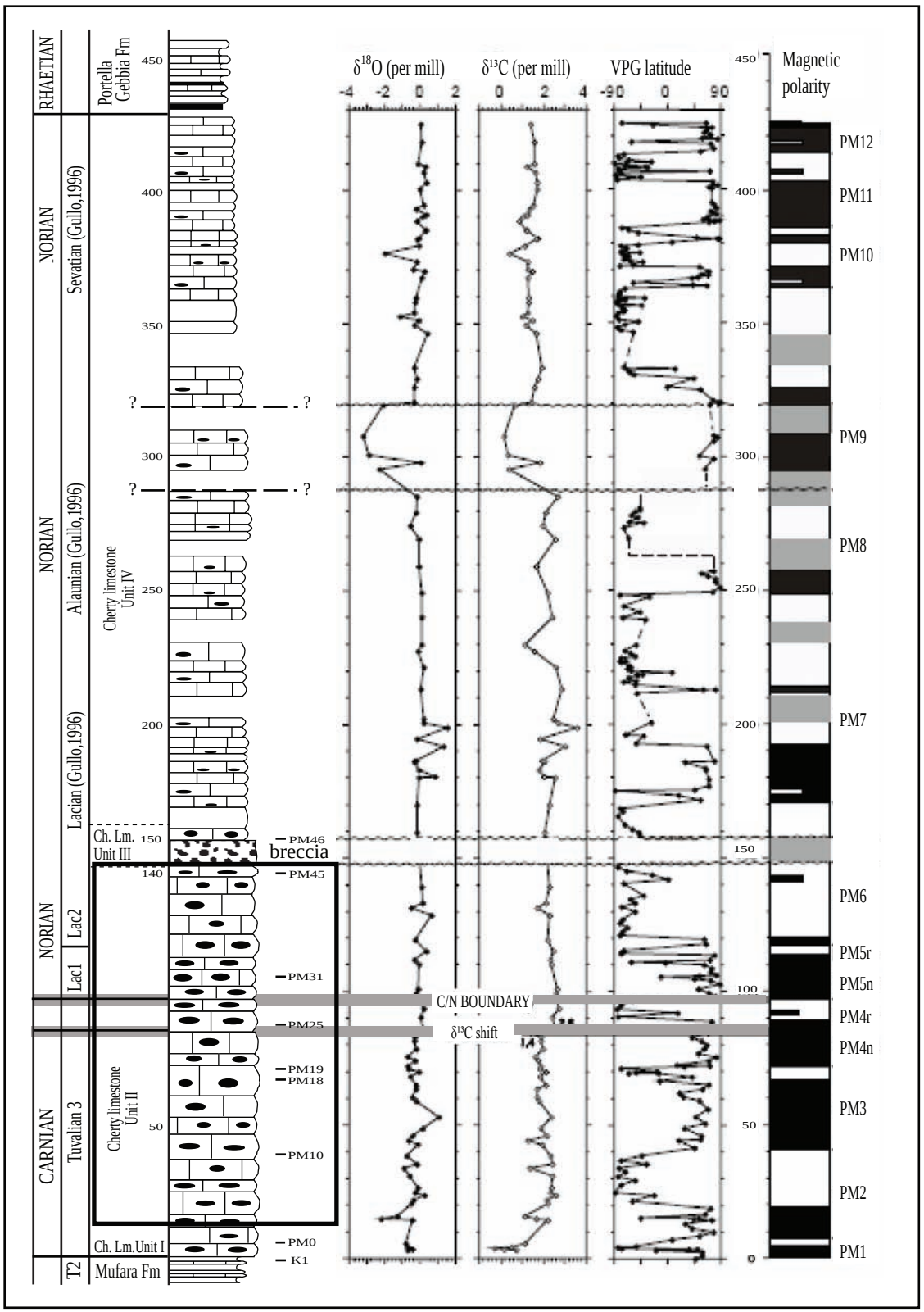

Figure 3.2 - Pizzo Mondello section (after MUTTONI et alii, 2004), with δ13C and δ18O isotope curves and magnetostratigraphy and lithology units.
The lower part of the log, representing the Carnian/Norian boundary interval, is studied in this paper.

3.2 Methods

The lower part of the Pizzo Mondello section (Interval 2 of Muttoni et alii, 2004) has been restudied and sampled in detail (Appendix 4). We have collected 236 samples (marked FNP) of limestone, marl and chert for lithofacies analysis. 100 thin sections were examined at high magnification using a Leica DM-EP petrographic microscope. On some samples a palynological analysis has been also attempted, unfortunately without results.

3.2.1 SEM analyses

Forty-three samples were examined using a CamScan MX 2500 Scanning Electron Microscope (SEM) to observe the microfabric and crystal size of these micritic limestones. Samples were selected among those exhibiting well-preserved fine matrix and minimum presence of non-carbonate elements, allochems, stylolites, veinlets or dolomite. All samples were cut perpendicularly to bedding and polished with corundum powder (borcarbid 500, 800 and 1200). The surfaces were cleaned and etched with 0.3% (0.1 N) hydrochloric acid for 10 to 20 seconds, dried, carbon-coated and observed at the SEM.

3.2.2 Counting Technique

In order to determinate the composition of the Calcari con Selce formation, 77 thin sections from limestone beds were point-counted with optical microscope.

The counting method used for determining the abundance of different grain types is “area counting”. In all the sections the grains have fairly constant dimensions and in the counting analyses the grain size is smaller than the step of the measure. Furthermore, counting was made in lines normal to the bedding plane, in order to minimize the possible effects of grain selection. For each thin section more than 500 points were counted, which is considered to yield statistically significant results. The maximum standard deviation amounts to 4% (Van der Plas & Tobi, 1965).

Typical constituents of thin-sections were summarised in 7 categories: micrite, thin-shelled bivalves and their fragments, calcareous nannofossils, radiolarians, foraminifers, ammonoids and non-identifiable carbonate grains (dolomitized and indeterminate skeletal grains).

3.3 Terminology

Micrite is the abbreviation of microcrystalline calcite with grain-size limit of <4μm (Folk, 1959, 1965).

Microspar is a fine-grained calcite matrix, characterized by rather uniform sized and generally loaf-shaped, calcite crystals ranging from 5 to 30 μm in diameter and mosaic-like microtexture (Folk, 1959).

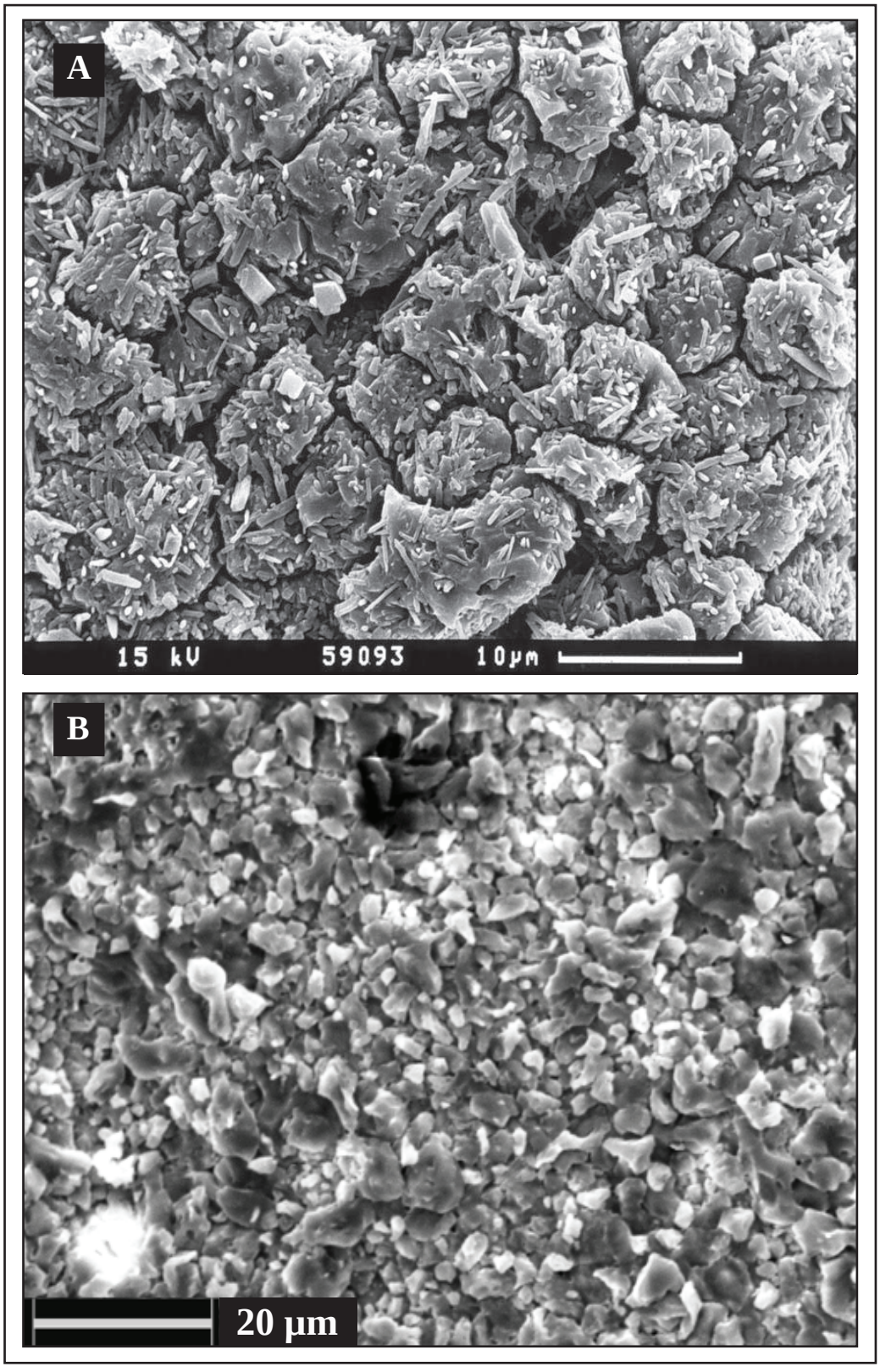

Figure 3.3 - Micrite textural proprieties described by LASEMI & SANDBERG (1993) with Scanning Electron Microscope.
A: Micrite with aragonite-dominated precursor.
B: Micrite with calcite-dominated precursor.

Microsparite is a limestone whose fine-grained matrix is developed as microspar.
The use of SEM permitted high resolution studies of micrite. Lasemi & Sandberg (1993) distinguish between two micrite types (Fig. 3.3):
Micrite with aragonite-dominated precursor (ADP) are characterized by large crystal size (5-15 µm, microspar), aragonite needles relics and pitted crystal surfaces. The strontium content is elevated (ca. 800 ppm or higher).
Micrite with calcite-dominated precursor (CDP) has small crystals (2-5 µm) absence of aragonite needles relics and pitted surfaces. The strontium content is low (ca. 400 ppm or less).

3.4 Calcareous nannofossils

Calcareous nannofossils in the Pizzo Mondello section have been recognized since Di Nocera & Scandone (1977) and Bellanca et alii (1993). The nannofossils are visible in thin section with petrographic microscope and at the SEM. They have a size between 10-40 µm and spherical-rounded forms and they are subdivided in two groups. The first group is characterized by large and rounded forms, with radial arrangement of calcite crystals (Fig. 3.4). Rays have various thicknesses. The ray numbers within the nannofossils varies from 8 to 24. Some forms have a little central area (Fig. 3.4D-E-F). This kind of calcareous nannofossils is that described by Di Nocera & Scandone (1977) and Bellanca et alii (1993, 1995). The second group consists of globular and small forms (Fig. 3.5). Calcareous spherical nannofossils from the Mesozoic with these morphologies are usually named calcispheres. The systematic position of these calcareous nannofossils remains unclear. The nannofossils are observed in all section, but they are more abundant in the facies C (29% of the total volume) (Fig. 3.6). Thus, these calcareous nannofossils provided a significant contribution (18% on average) to carbonate sedimentation.
It is important to stress that these calcareous nannofossils are most probably not related to coccolithophores, and their pelagic habit is only inferred by their prevalent or exclusive occurence within deep-water fine grained carbonate facies as those of the Calcari con Selce.

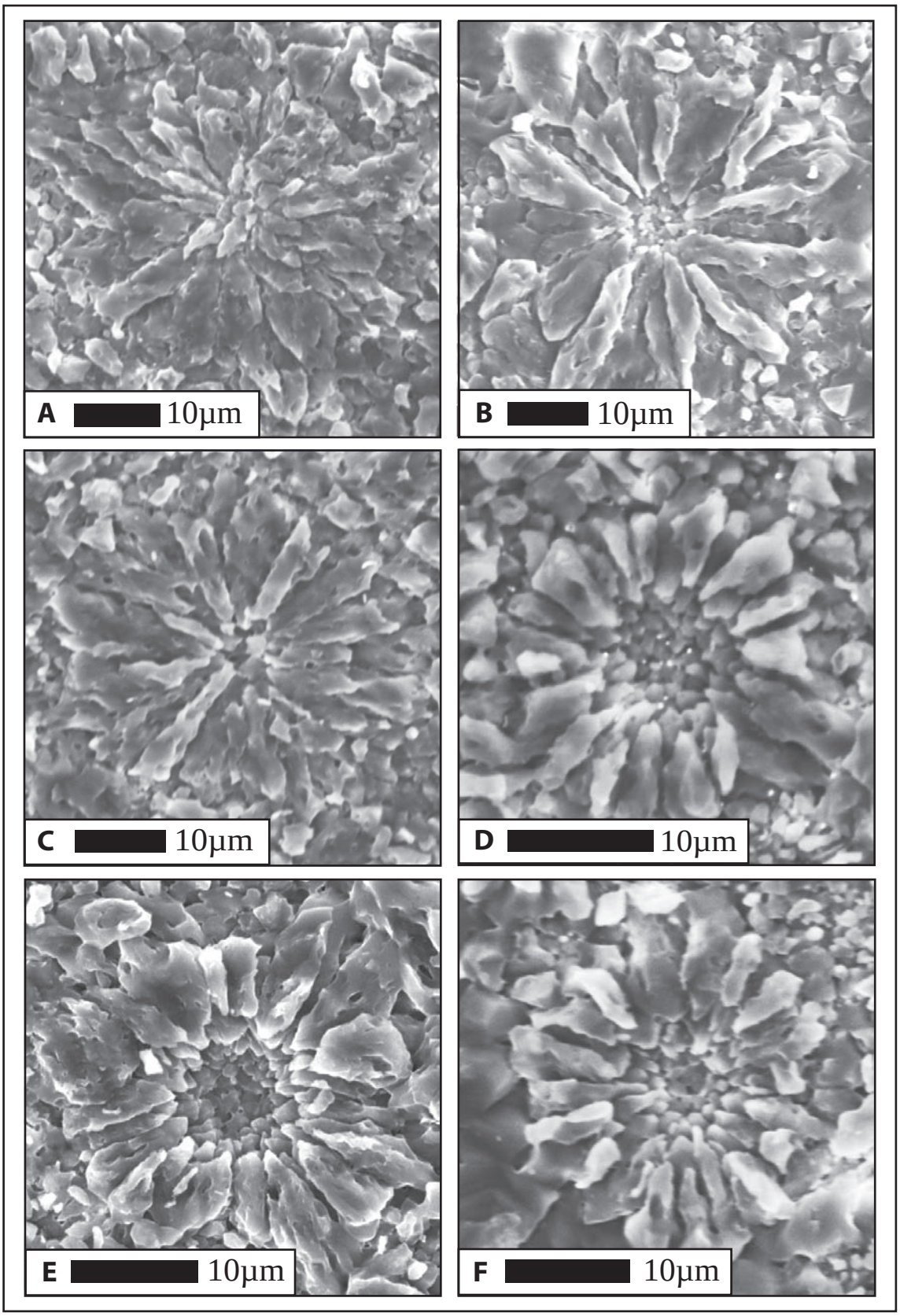

Figure 3.4 – SEM images of large-rounded calcareous nannofossils. These forms have a radial arrangement of calcite crystals.
D, E and F: Radial forms with a little central area.

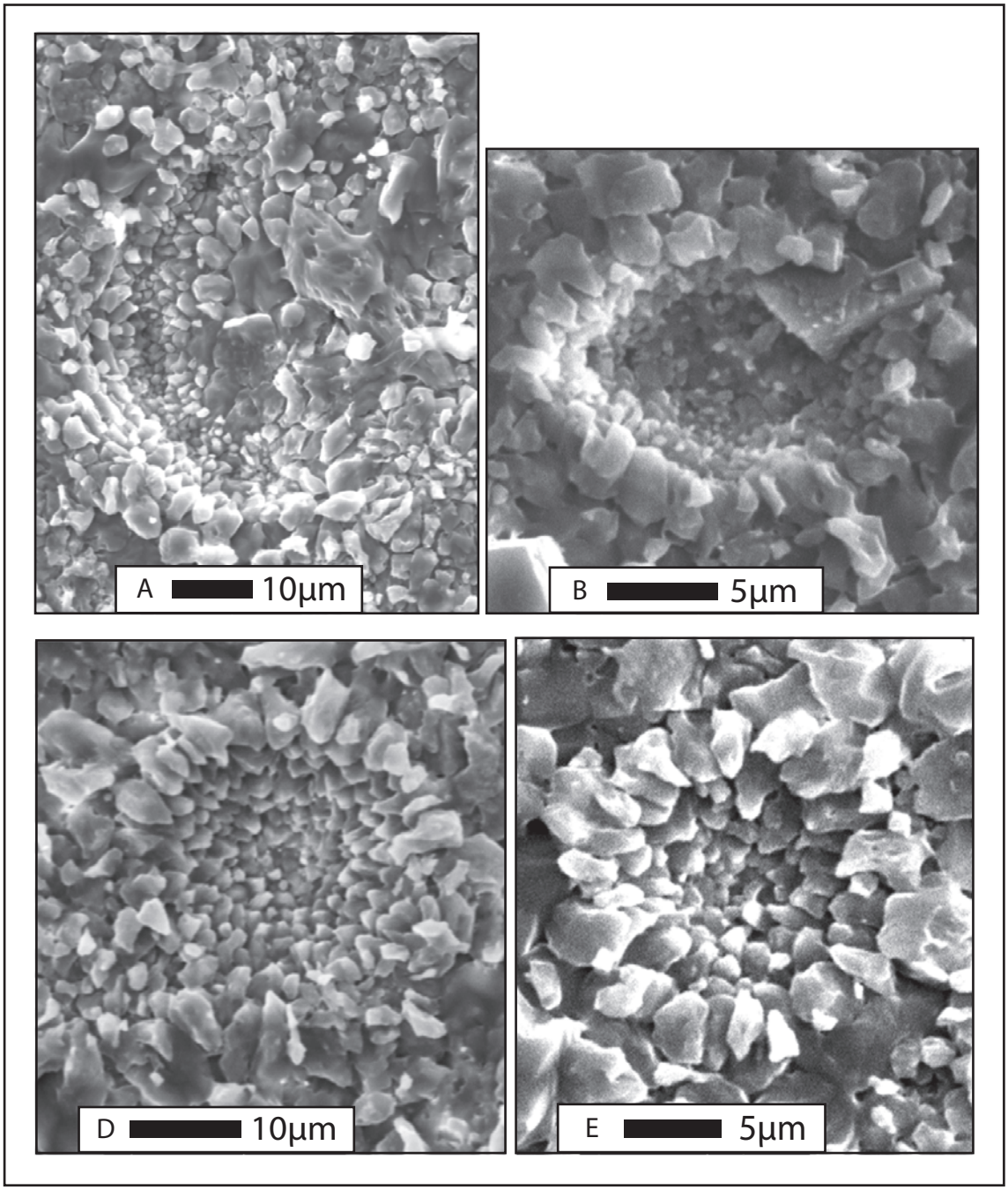

Figure 3.5 – SEM images of calcisphere. These forms are small and globular and they consist of small calcite crystal oriented obliquely respect to the surface.
A: is *Obliquipithonella* (Janofske, 1992).
C: probably belongs to Orthopithonellids (Keupp personal communication, 2008).

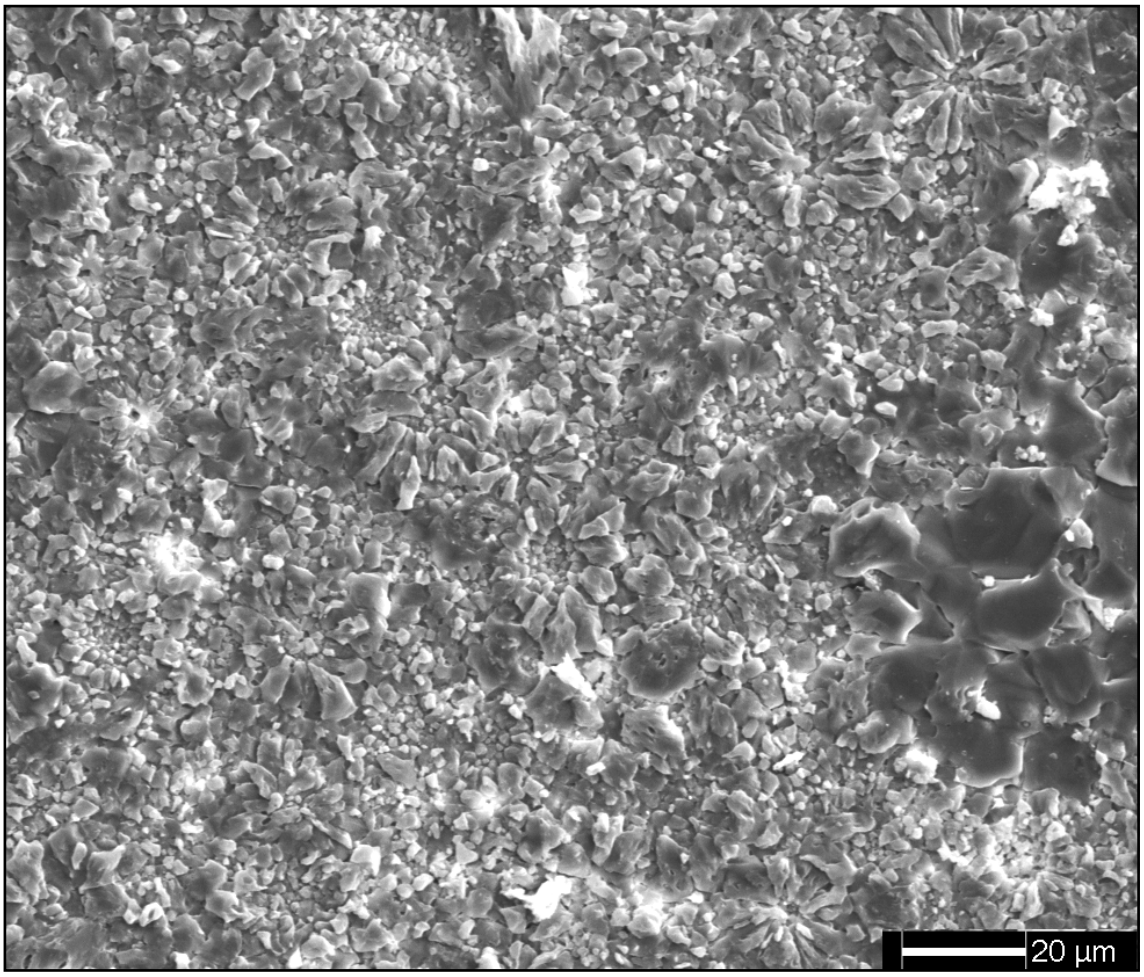

Figure 3.6 – SEM image of calcareous nannofossil-rich facies C. Calcareous nannofossils may reach abundances up to 28.63 % in this part of the section.

3.5 Sedimentology

The Cherty Limestones formation at Pizzo Mondello was divided by Muttoni et alii (2001, 2004) into four lithozones (Fig. 3.2):

1. The basal 3 m are characterized by calcilutites with rare chert nodules;

2. 143.5 m of dm-thick, well-bedded white calcilutites with black chert nodules follow, intercalated with cm-thick marl levels. The calcilutites contain abundant pelagic bivalves (halobids), foraminifers, radiolarians, sponge spicules, sparse ammonoids and ostracods (Gullo, 1996), as well as calcispheres and calcareous nannofossils (Bellanca et alii, 1993, 1995);

3. 11.5 m of brecciated limestones, hereafter referred to as the “breccia” level;

4. The upper 267.5 m are dm- to cm-thick, well-bedded to nodular whitish calcilutites with chert nodules. Chert disappears at meter level 290 ca.

In this study we analyzed the ca. 140 m of sediments belonging to Interval 2 of Muttoni et alii (2004), within the Calcari con Selce formation, which includes the C/N boundary interval (Fig. 3.2).

The high resolution of sedimentological analysis allowed the recognizing of three facies (Fig. 3.7):

Facies A: well-bedded, dm-thick, white calcilutites with black-brown cherty nodules concentrated in the interlayers (Fig. 3.8A1). Calcilutite layers are composed mostly of micrite, with thin-shelled bivalves (halobids), radiolarians, ammonoids, foraminifers and calcispheres; bioturbations and laminations are rare. Bivalve coquinas also occur. The interlayers are composed of mm-thick brownish clays, which are rarely laminated. The typical microfacies is mudstone (Fig. 3.8A2). At SEM, facies A is characterized by small calcite crystals (2-5μm) and few calcareous nannofossils (Fig. 3.8A3).

Facies B: is similar to facies A, but layers are nodular, up to 1 m thick, and characterized by stylolitic joints (Fig. 3.8B1). Thin-shelled bivalves, calcispheres and coquinas are more abundant. Bioturbations and laminations are common. In thin section, limestones of facies B appear as mudstone-wackestone (Fig. 3.8B2). At SEM, facies B is similar to facies A, but calcareous nannofossils increase (Fig. 3.8B3). Several samples are rich in dolomite crystals.

Facies C: calcilutite layers that are even more nodular than in facies B and generally thinner (8-15 cm), and always laminated (Fig. 3.8C1). Thin-shelled bivalves and calcispheres are extremely common. Silicified coquinas are very abundant. Cm- to dm-scale interlayers, composed of brown-black dolomitized clay-marls, are more common than in all other facies. This facies is rich in black chert, occurring in 5-7 cm thick beds. The typical microfacies is wackestone with abundant coquinas (Fig. 3.8C2). At SEM, facies C is characterized by small calcite crystals (2-5 μm) and more abundant calcareous nannofossils (Fig. 3.8C3).

Facies alternate in the studied interval following the scheme A-B-C-B-A (Fig. 3.7).

3.6 Analysis of microfabrics

The study samples are white-grey well cemented limestone from all three facies. Some samples are laminated. Under the optical microscope, all samples consist of very fine carbonate micrite with radiolarians, thin-shelled bivalves and calcareous nannofossils.

The SEM observations show small calcite crystals (2-5 μm) and lack of aragonite needles and pits in all facies (Fig. 3.9). Small, but abundant dolomite crystals homogeneously arranged are recognized in several samples (Fig. 3.10). Some samples are completely dolomitized.

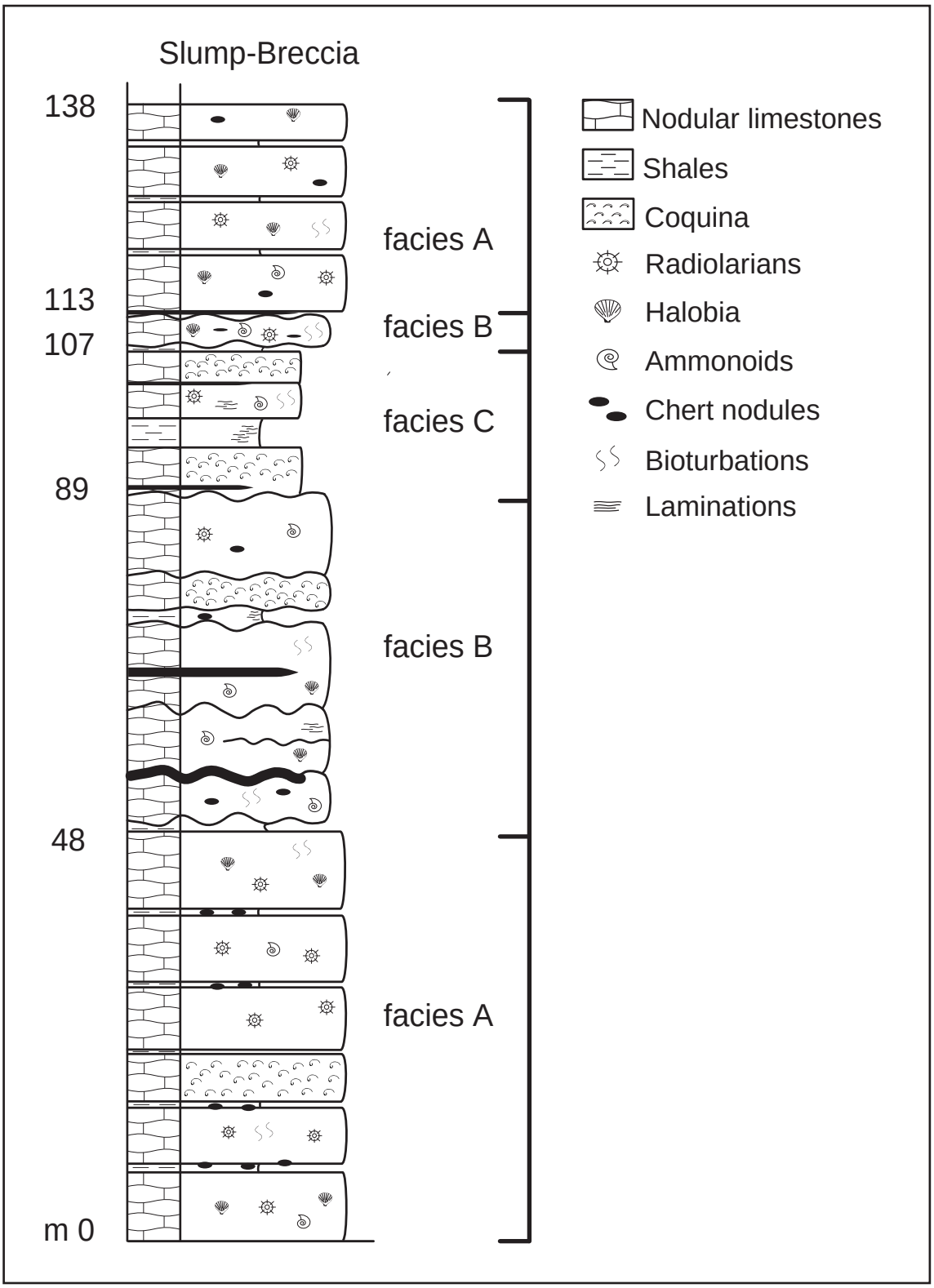

Figure 3.7 – Schematic log of the Pizzo Mondello section. Facies alternations followed the A-B-C-B-A scheme.

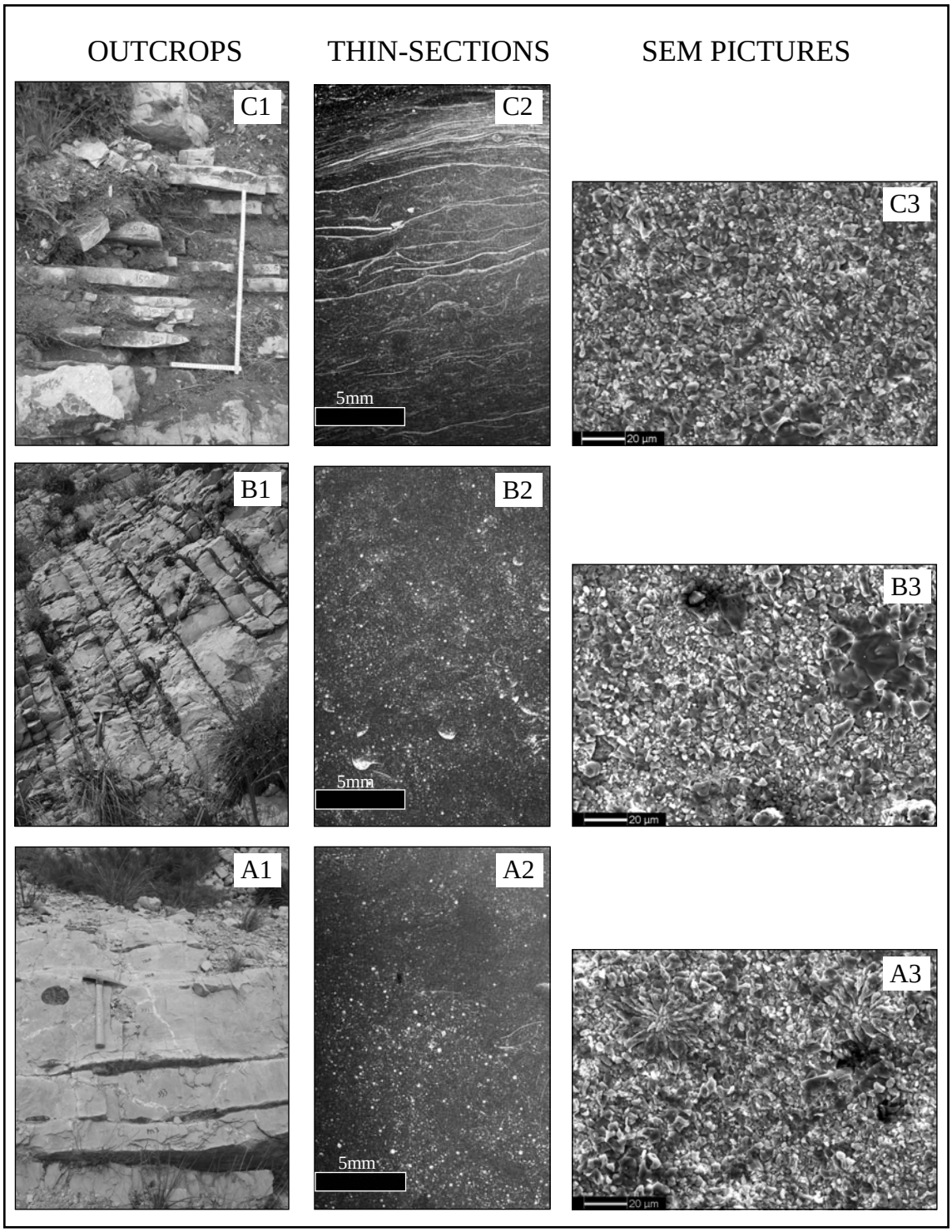

Figure 3.8 - Main facies of the Pizzo Mondello section. C1: thin, plane-bedded layers of limestone and siliceous limestones of facies C in outcrop. C2: concentration of densely packed thin-shelled bivalves (Halobia sp.) of facies C in thin section (Sample fnp 151). C3: abundant calcispheres (sample fnp 145) in the facies C at SEM. B1: dm-scale nodular beds of facies B, outcrop exposure. B2: wackestone with abundant radiolarian moulds and thin-shelled bivalves (sample fnp 110), facies B, thin section. B3: calcispheres in facies B (sample fnp 126) at SEM. A1: dm-scale beds with plane to undulate joints and brown chert nodules, outcrop exposure. A2: wackestone with radiolarian moulds and thin-shelled bivalves (sample fnp 11), facies A in thin section. A3: calcispheres and fine calcite crystals (sample fnp 11), facies A, at SEM.

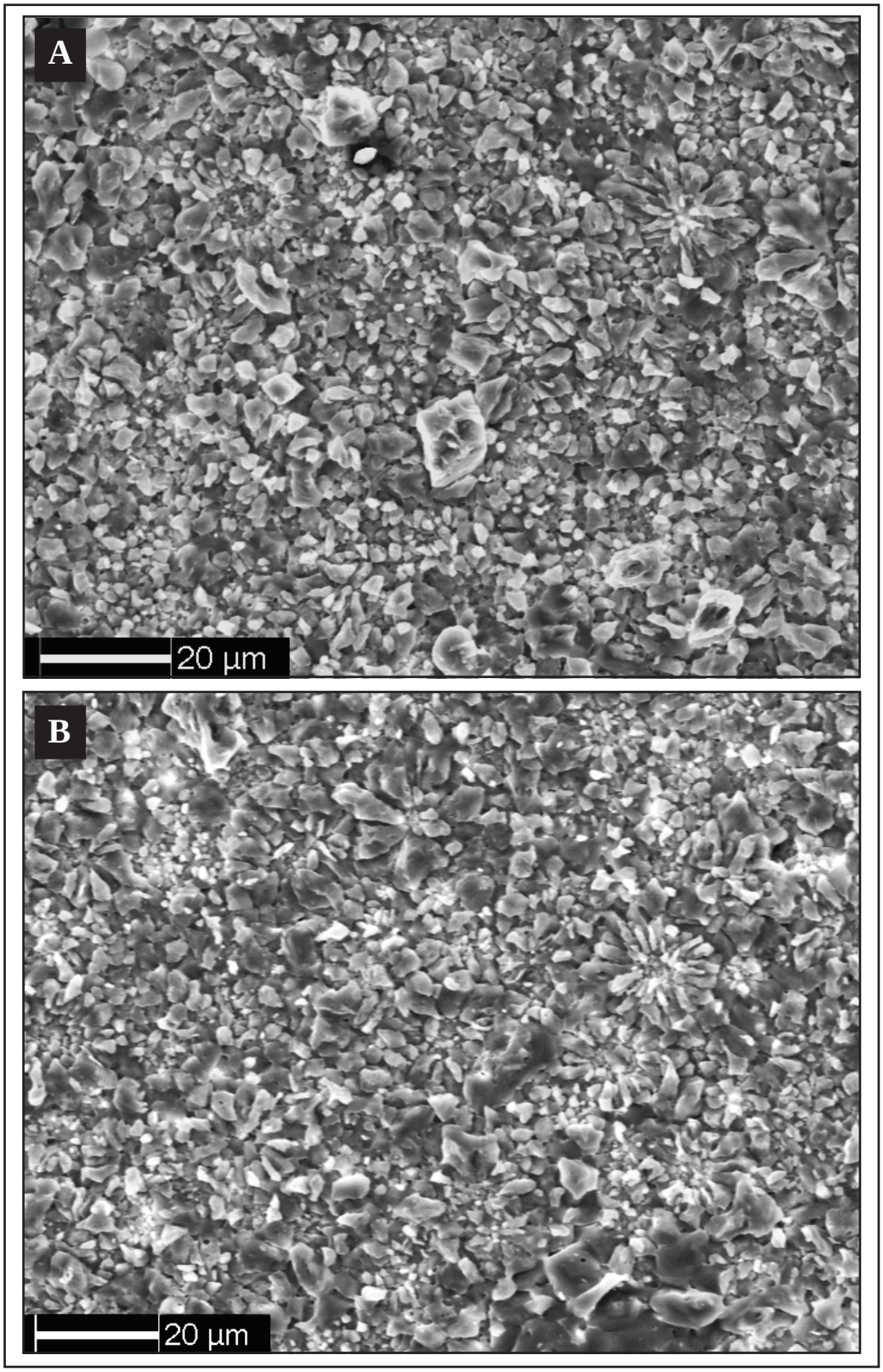

Figure 3.9 – SEM images of the micrite microfabric. Calcite crystals are very small and aragonite needles are absent.
A: sample fnp 126, some crystals pitted are present.
B: sample fnp 145, in the lower part a radiolarian filled by calcite crystals.

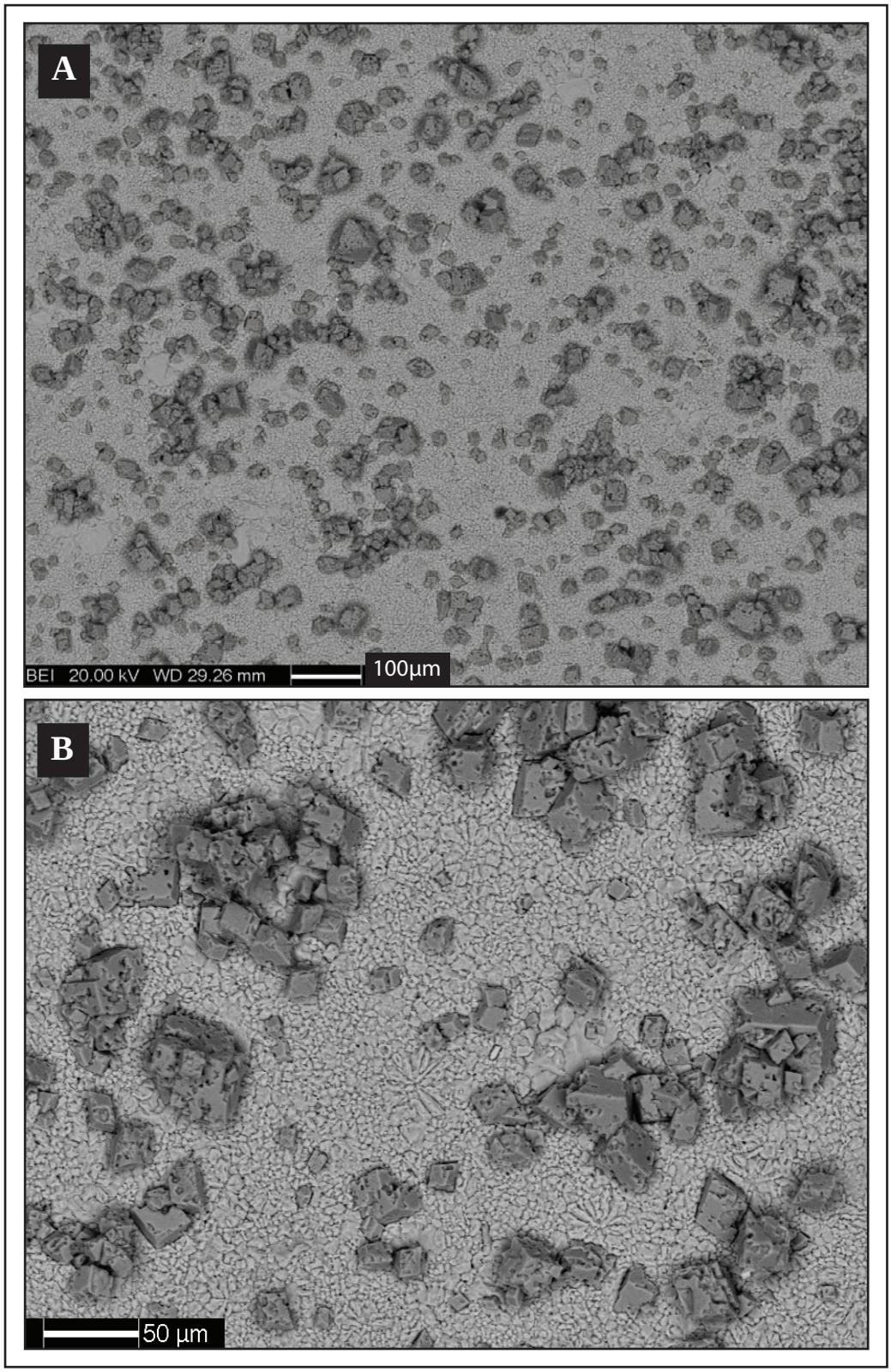

Figure 3.10 – SEM images of the dolomite crystals in the Pizzo Mondello samples.
A: sample fnp 58, typical distribution of dolomite crystals.
B: sample fnp 110, dolomite crystals as seen at higher magnification.

3.7 Point-counting

Seventy-seven thin sections representative of Interval 2 (Muttoni et alii, 2004) were point-counted. The total counting points and percentages for all samples are showed in Appendix 1 and Appendix 2. The average composition of the Calcari con Selce is summarized in Table 3.1.

Micrite is the most common constituent with a mean value of 44.92 %. Radiolarians are the second most common constituent with an average abundance of 25.29 %, followed by calcareous nannofossils with 17.62 % (see description above). The radiolarians are siliceous planktonic organisms and in these samples they are mainly replaced by calcite. Thin-shelled bivalves are also common (6.42 %). They consist of disarticulated valves and small fragments and complete shells are very rare. These bivalves can be determined as cf. *Halobia* sp., and their lifestyle was most probably similar to that of the strictly related genus *Daonella*, i.e., they were deep-water benthonic organisms (Schatz, 2005). They have a shell diameter between 1-1.5 cm to 3-4 centimeters and are commonly recrystallised. Foraminifers have the lowest abundance with 0.17 % and consist of benthic hyaline foraminifers. Ammonoids are 0.02 %. Non-identifiable carbonate grains are 5.5 %.

In the different facies, the average abundance of the main constituents changes (Table 3.1). These differences are well highlight in the Figure 3.11, where separate intervals characterized by facies A and B in the lower and upper part of the section were merged together, because point counting did not highlight any significant differences in composition.

Facies A is characterized by abundant micrite (51.09 %), followed by radiolarians (23.30 %), calcareous nannofossils (13.19 %) and thin-shelled bivalves (6.62 %).

Facies B is composed by micrite (41.95 %), radiolarians (29.27 %), calcareous nannofossils (16.55 %) and thin-shelled bivalves (6.20 %).

In facies C, micrite is even less abundant (38.61 %), but calcareous nannofossils increase (28.63 %). Radiolarians (21.34 %) and thin-shelled bivalves (6.72 %) maintain abundances similar to those of the other facies.

In Figure 3.12 the relative abundances of major components are shown against stratigraphic height. Clear compositional trends are not visible, and component variations are tied to different facies. Micrite progressively decrease from facies A (43.98 %) to facies C (38.61 %), to increase in facies B1 and facies A1 (58.12 %) (Table 3.1). Here, B1 and A1 are used to indicate the intervals characterized by facies B and A in the upper part of the section. The calcareous nannofossils rise from facies A to facies C and drop afterwards. Thin-shelled bivalves do not show any trend throughout the section, but they in correspondence with coquina beds.

POINT COUNT GROUP	MICRITE	CALCAREOUS NANNOFOSSILS	THIN-SHELLED BIVALVES	RADIOLARIANS	FORAMINIFERS	AMMONOIDS	NON DETERM.
FACIES A	43.98	12.13	8.63	28.52	0.2	0.03	6.51
FACIES B	39.75	15.72	7.15	29.72	0.23	0.06	7.37
FACIES C	38.61	28.63	6.72	21.34	0.15	0.02	4.54
FACIES B1	44.14	17.38	5.24	28.81	0.22	0	4.21
FACIES A1	58.12	14.24	4.6	18.08	0.08	0	4.89
AVERAGE	44.92	17.62	6.46	25.29	0.17	0.02	5.5

Table 3.1 – Summary of the seven point-count groups in the different facies. The complete data are summarized in the Appendix 1 and 2.

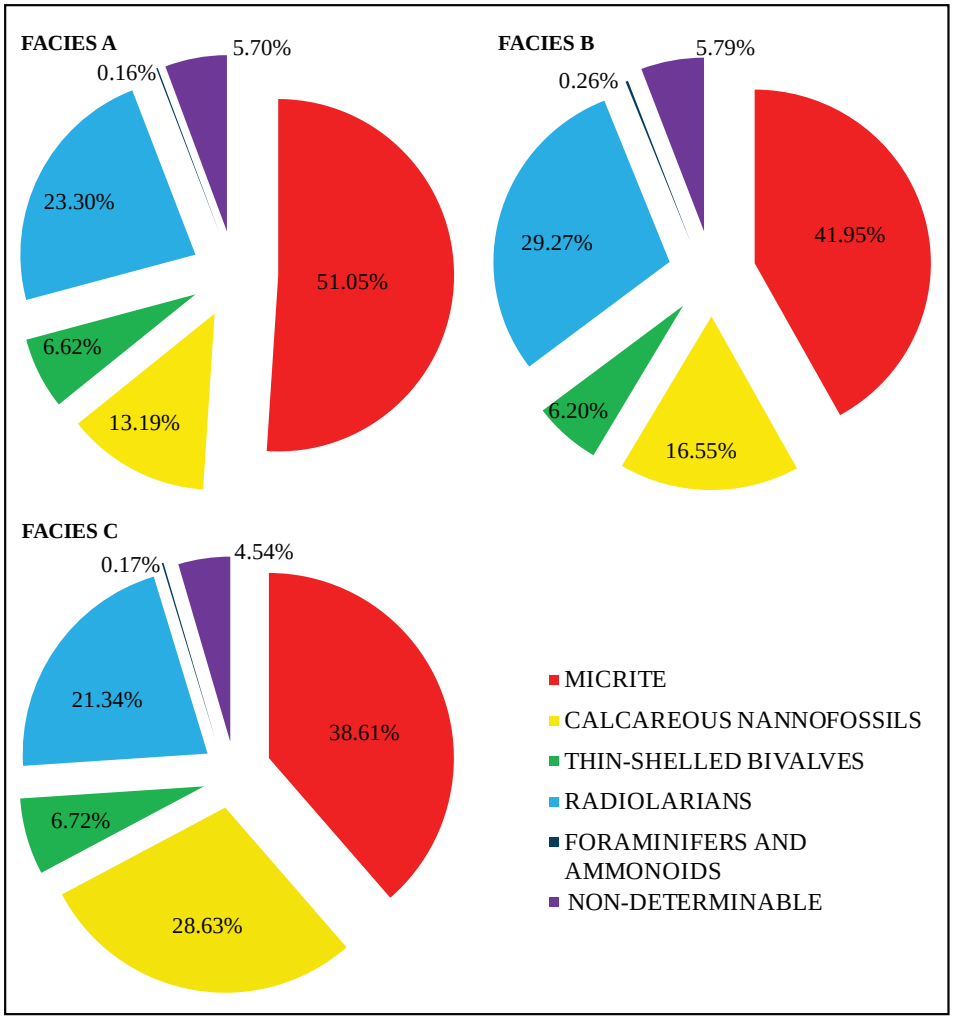

Figure 3.11 – Pie-plots showing the variation in composition of three facies. Foraminifers and ammonoids are lumped together. Facies A includes the mean values between A and A1 and Facies B comprises the mean values between B and B1.

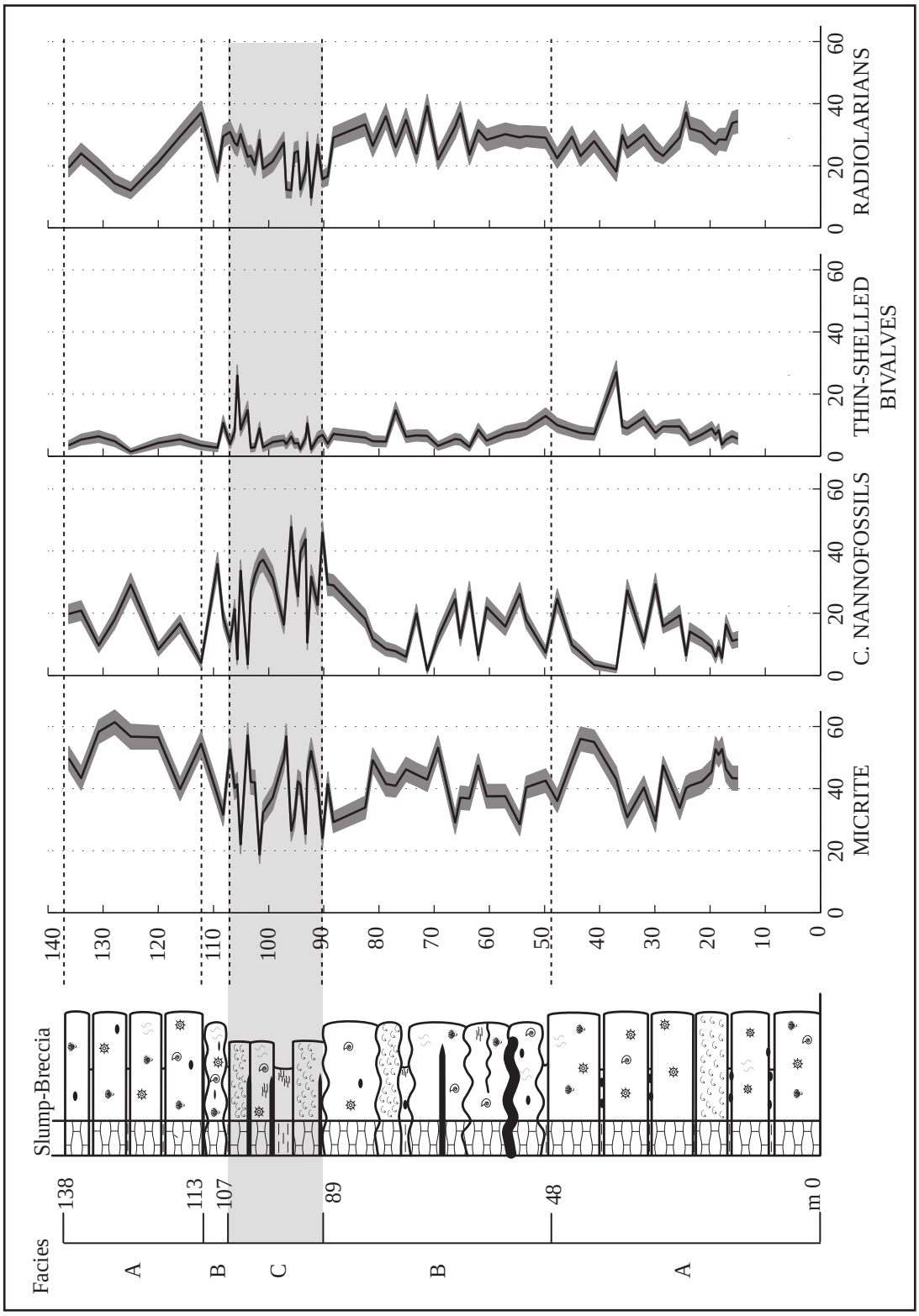

Figure 3.12 – Plot of the total abundance and variations of the main components: micrite, calcareous nannofossils, radiolarians and thin-shelled bivalves. The light grey area marks the facies C. The dark grey band corresponds to 2σ error intervals (see Appendix 3). Facies C is characterized by a abundant calcareous nannofossils and less micrite. Positive spikes, in the thin-shelled bivalve abundances, correspond to coquina beds.

3.8 Discussion

3.8.1 Facies alternation

Limestone-marl alternations in hemipelagic setting are originated and controlled by the interaction of carbonate productivity, terrigenous input and carbonate dissolution (Fig. 3.13) (Einsele, 1982). Variations of carbonate flux exert a major control on limestone-marl alternations, thus, high carbonate input produces an alternation in which limestone beds are much thicker than marls. This seems to be the case of the Upper Triassic Calcari con Selce both in the Lagonegro Basin and at Pizzo Mondello.

The evolution and radiation of calcareous nannofossils (coccolithophores) changed the carbonate pelagic productivity (Erba, 2006). In the pre-Mesozoic time, almost all of the carbonate flux to sediments derived from shallow water carbonate platforms, because the calcareous nannofossils were less abundant. After the Upper Jurassic-Cretaceous radiation of coccolithophores, roughly half of the carbonate sediments are derived from pelagic sources (Ridgwell & Zeebe, 2005). The Upper Triassic represents a time in which the pelagic precipitation of carbonate was at its beginnings.

The terrigenous input is often related to climatic changes, the regular fluctuations in the carbonate-terrigenous rate could thus be interpreted also as climate-driven. Finally, carbonate dissolution in the water column or, more commonly, at the water-sediment interface, can also be a driving factor in limestone-marl alternations. Carbonate dissolution starts at the lysocline, which roughly corresponds, or is slightly deeper than, to the saturation depth, i.e., the depth at which seawater becomes undersaturated with respect to carbonates (Millero, 2007). At the Carbonate Compensation Depth (CCD), all carbonate that reaches the sea floor is dissolved. The depth of the CCD varies mostly as a function of the chemical composition of the seawater (CO_2 concentration and alkalinity) and its temperature (James et alii, 2005).

After the deposition, sediments that ultimately produce limestone-marl alternations are interested by differential diagenetic processes, mainly by cementation, compaction and dissolution. These processes together could emphasize an original facies alternation, or might create it from a uniform sediment. The diagenetic VS primary origin of limestone-marl alternations is subject of debate. Some Authors (Arthur et alii, 1984; Bellanca et alii, 1996) believe that the limestone-marl alternations are primary, and thus record climatic fluctuations, often caused by Milankovitch cycles. Ricken (1987) support that diagenesis enhances the differences in the initial composition of limestones and marls. Munnecke (1997), Munnecke et alii (1997) and Westphal (2006) propose that some alternations are caused solely by selective dissolution of aragonite in marl beds and reprecipitation of calcite cement in limestone beds (Fig. 3.14). This model doesn't require different initial composition and it produces a diagenetic autocyclicity (Fig. 3.15).

The studied part of the Pizzo Mondello section is characterized by changes in the style of limestone-marl alternations, that were identified as facies A, B and C and are stacked following

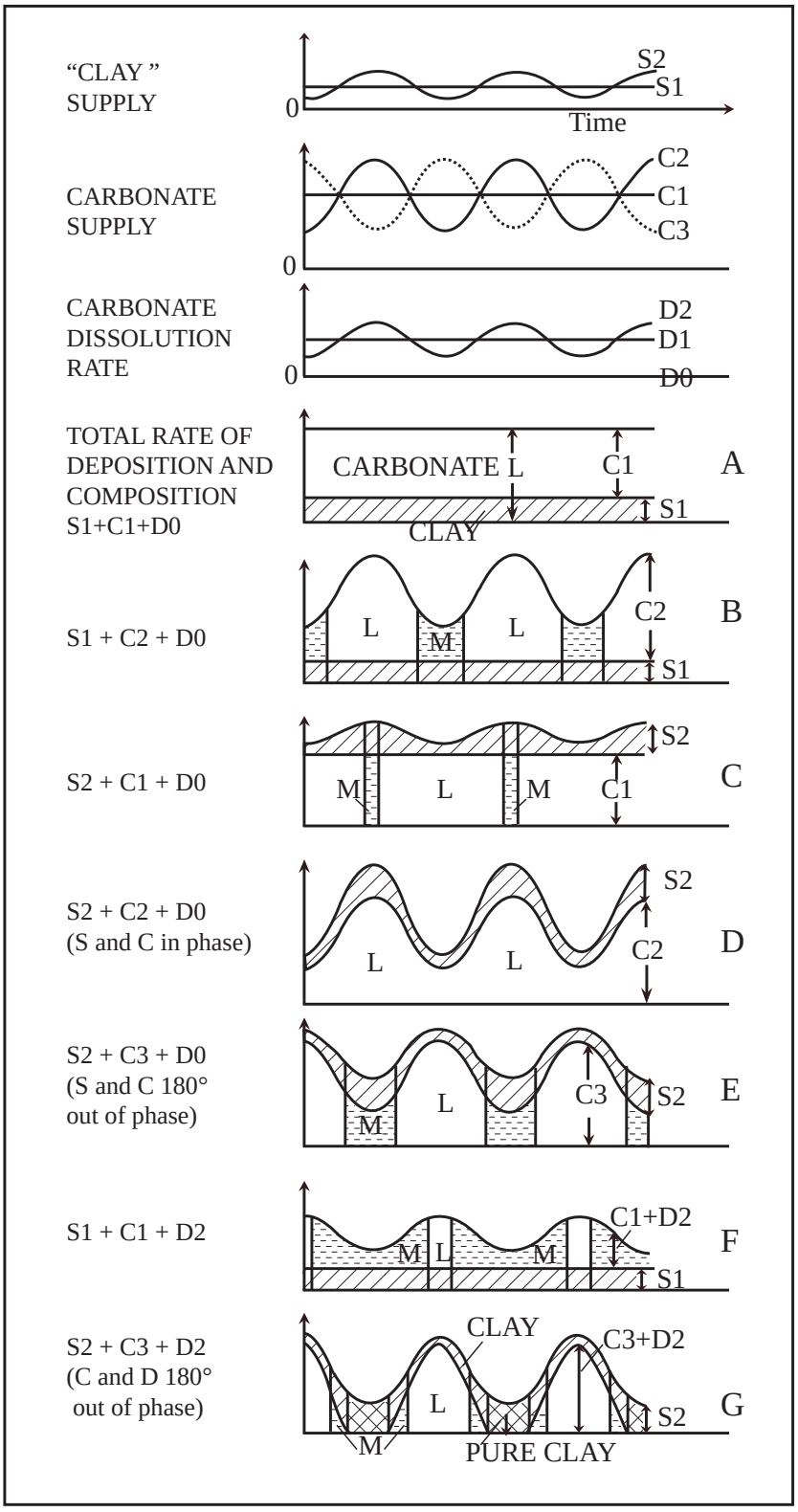

Figure 3.13 – Simplified model for the development of limestone-marl alternations controlled by carbonate productivity, terrigenous input and carbonate dissolution (from EINSELE, 1982).

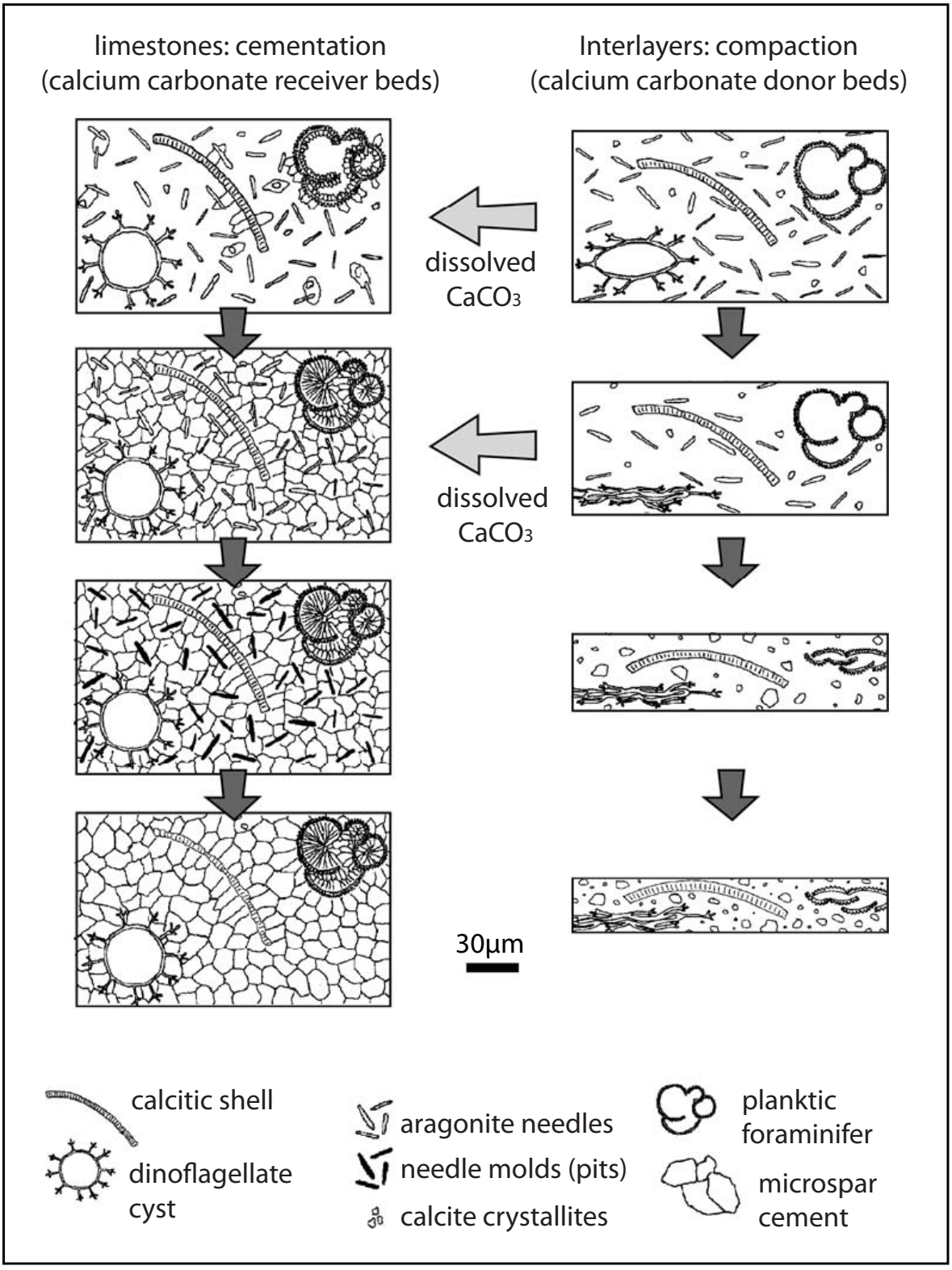

Figure 3.14 – The diagenetic models for origin of limestone-marl alternations (from WESTPHAL, 2006).

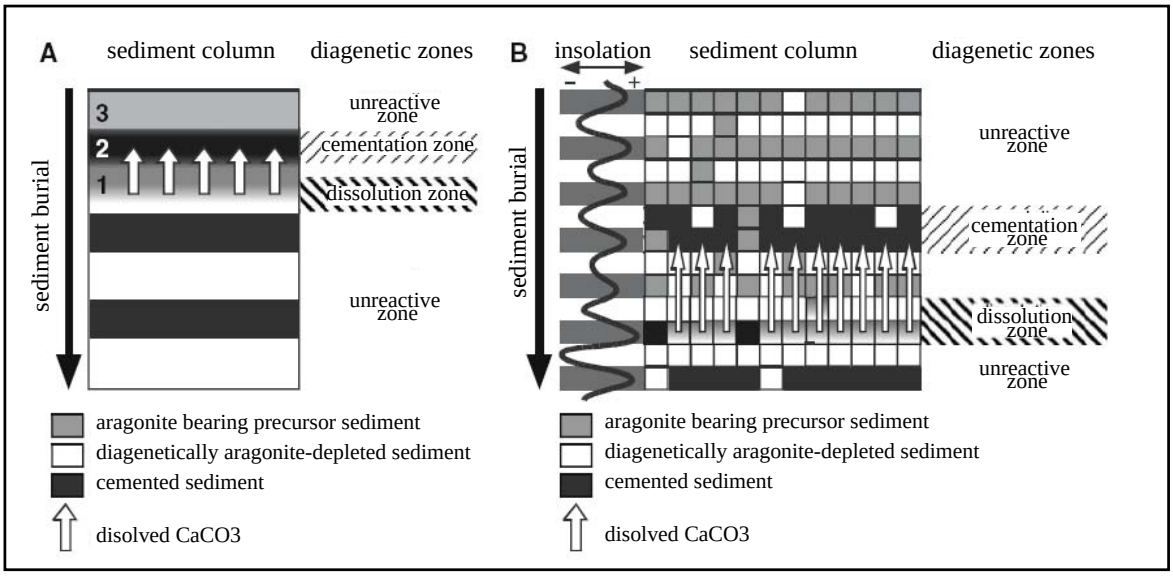

Figure 3.15 – Simplified diagenetic model (from MUNNECKE & SAMTLEBEN, 1996). This model probably explains self-organized diagenetic limestone-marl alternations.

the scheme A-B-C-B-A (see paragraph 3.5). The different facies are easily recognizable in the field, in thin-sections and at SEM. The point-counting highlights quantitatively that the facies recognized in the field are accompanied by a variations in relative abundance of components (Table 3.1, Fig. 3.12).

The main components of the Calcari con Selce are radiolarians, thin-shelled bivalves and calcareous nannofossils. They have different dissolution and preservation rates. Radiolarians preservation is strongly controlled by diagenetic factors. Dissolution of radiolarian tests depends on the degree of silica undersaturation of pore water, the intensity of bioturbation and the accumulation rate. The siliceous radiolarian tests in limestones are often replaced by calcite. In the Pizzo Mondello section, the radiolarians are mainly calcitized; only in the cherty beds they preserved siliceous tests. In the samples, I have recognized two types of radiolarian tests calcitization: in the first case, the test is calcitizied and filled by calcite cement, in the second case, the test is calcitized but filled by fine micrite. This difference is probably linked to dissolution rate. Thin-shelled bivalves, in particular halobids, are a common constituent of the Triassic pelagic limestones. The valves of the halobids are unequal in shape and size and they have two carbonate layers, internal aragonitic and external calcitic. The calcitic external layer is more resistant to dissolution. The shell concentrations (coquinas) can be formed by different processes (KIDWELL, 1991), but in facies C at Pizzo Mondello they are associated with an increase of insoluble sediment (shales and chert) and thinning of carbonate beds, and are thus interpreted as concentration shell beds due to dissolution.

The different facies recognized in the Pizzo Mondello section are probably connected to the differential diagenetic response to carbonate dissolution of their constituents. Calcitic organisms

are more dissolution resistant than those having aragonitic or high-Mg calcitic shells or tests, thus, their abundance fluctuations could be related to different dissolution rates. From facies A to facies C the bivalve coquinas, radiolarians and calcareous nannofossils increase, and after from facies C to facies A, they decrease. The thickness of marl beds relative to carbonate, and thus the proportion of insoluble VS soluble sediment, covaries with the abundance of calcitic fossils. This suggests that the section is characterized by compositional changes that are related to differential dissolution rather than variations of autochthonous carbonate productivity (Fig. 3.12). Probably, facies C was more affected by dissolution than facies A and B.

3.8.2 Significance of facies C

Facies C is characterized by thinner, more nodular and more silicified limestone beds than in the other facies. Thin-shelled bivalves, calcareous nannofossils and bivalve coquina layers are extremely common, and marl interlayers are more abundant and thick. As explained above, the features of facies C are attributed to enhanced dissolution. A similar, though more intense dissolution event, represented there by the "Green clay-radiolaritic horizon", is described in slightly older Calcari con Selce successions of the Lagonegro Basin. This horizon consists of laminated shales and radiolarites completely devoid of carbonate sediment, and represents a temporary rise of the Carbonate Compensation Depth above the sea floor (Rigo et alii, 2007). It is suggested that facies C recorded an event similar to that recorded by the Green clay-radiolaritic horizon in the Lagonegro Basin (Rigo et alii, 2007; see chapter 2 of this thesis), but of minor magnitude. The Green clay-radiolaritic horizon recorded the Carnian Pluvial Event (Simms & Ruffell, 1989) in a basinal setting and was recognized throughout the Lagonegro Basin (chapter 2). Facies C at Pizzo Mondello and the Green clay-radiolaritic horizon have somewhat similar sedimentological characteristics (increase of dissolution and of shale, radiolarite and cherty beds due to enhanced dissolution), but while carbonate is completely dissolved in the Lagonegro Basin during the deposition of the Green clay-radiolaritic, some is preserved in facies C at Pizzo Mondello.

Indeed, in Facies C, limestone are often silicified, but still present and the clay layers are less abundant than in the Julian/Tuvalian Green clay-radiolaritic horizon. Probably, the interval of Pizzo Mondello characterized by facies C also represents a rise of the Carbonate Compensation Depth (CCD), that did not reach the sea floor and was thus less pronounced than that associated to the Green clay-radiolaritic horizon. Alternatively, Pizzo Mondello is significantly shallower than most of the Lagonegro Basin. The picture that can be outlined in this case is perhaps comparable to that of some better studied events associated to a rise of the CCD, e.g., the PETM (Paleocene-Eocene Thermal Maximum) (Zachos et alii, 2005). After the PETM, other similar and smaller events occur, that are characterized by a reduced carbonate flux or preservation, though the prominent rise of the CCD did not repeat (e.g., Lourens et alii, 2005; Nicolo et alii, 2007). Those events followed the PETM by a few million years (between 56 and 53 Ma, thus) (Nicolo et alii, 2007). Facies C at Pizzo Mondello is Lacian in age (Nicora et alii, 2007) and

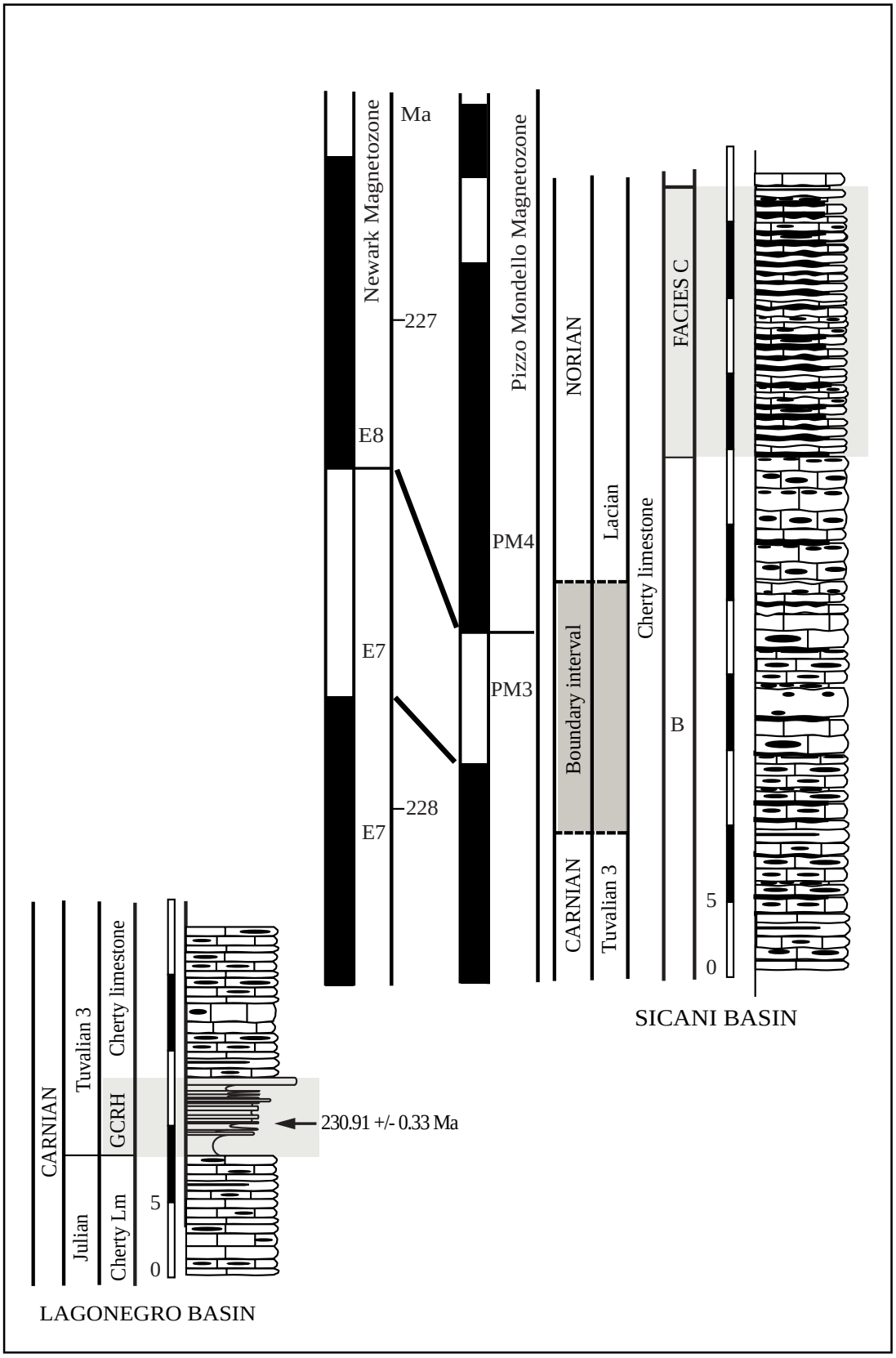

Figure 3.16 – Schematic log of the Carnian Green clay-radiolaritic horizon (GCRH) in the Lagonegro and Lacian facies C of Pizzo Mondello section in the Sicani Basin. The Aglianico volcanic ash-bed within the GCRH has been dated by Furin et alii (2006, 2007). Magnetozonation of the Pizzo Mondello by Muttoni et alii (2004).

thus is certainly younger than the Julian-Tuvalian Green clay-radiolaritic horizon. The Green clay-radiolaritic horizon was dated at 230.91 +/- 0.33 Ma (Furin et alii, 2006, 2007) (Fig. 3.16). Facies C followed the Green clay-radiolaritic horizon by about 4 Ma, and according to Muttoni et alii (2004) its beginning corresponds to magnetozones PM4 which is correlated to magnetozone E8 of the Newark astrochronologic time scale in the ca. 227-228 Ma interval (Muttoni et alii, accepted). This time span is comparable to that between the PETM and, e.g., the H1-Elmo event (3 Ma).

3.8.3 Primary mineralogy

The use of Scanning Electron Microscope permitted the study of micrite at the micron scale. Morphological parameters at SEM (average crystal dimension and presence/absence of elongated pits) and chemical analyses (strontium content) were considered to determine the primary mineralogy of micrites at Pizzo Mondello. Indeed, a distinction is possible between micrites with aragonite-dominated precursor and calcite-dominated precursor on the base of microfabric analysis at SEM and major element chemistry (Lasemi & Sandberg, 1993). All the samples studied have the microfabric characteristics of a micrite with calcite-dominated precursor: small crystals, lack of aragonite needles and pits.

We have used the geochemical data of Pizzo Mondello section from Bellanca et alii, (1995) to confirm our supposition. We have considered only the well preserved and non-dolomitized samples. The Strontium contents are from 162 to 298 ppm, with Manganese going from 83 to 461 ppm, and Iron are from 74 to 712 ppm. The average content of $CaCO_3$ in the limestone beds is 95.77%. The content of $MgCO_3$ is from 1.22 % to 6.64 %. These data support the hypothesis of calcite-dominated precursor for the Pizzo Mondello section. The presence of small and abundant dolomite crystals homogeneously arranged could be the result of the separation of Mg by high-Mg calcite in a closed diagenetic system. High-Mg calcite in fact is metastable in burial diagenetic environments, and is invariably substituted by low-Mg calcite, which is the stable phase. Magnesium is usually lost, but might have been partially retained by the sediment in this case, and stabilized as dolomite, because of early lithification and/or extremely low permeability of the unusually fine carbonate mud. Thus, the primary mineralogy of carbonate mud was probably mainly high-Mg calcite. This is in agreement with the common understanding that the Triassic was a time of "Aragonite Seas" (Stanley & Hardie, 1998) (Fig. 3.17), and thus the precipitation of aragonite and high-Mg calcite was favoured against low-Mg calcite. In our samples, there is no evidence of aragonite crystals. This is in contrast with the behaviour of carbonate producers, that today preferentially precipitate aragonite, but is nevertheless geochemically possible.

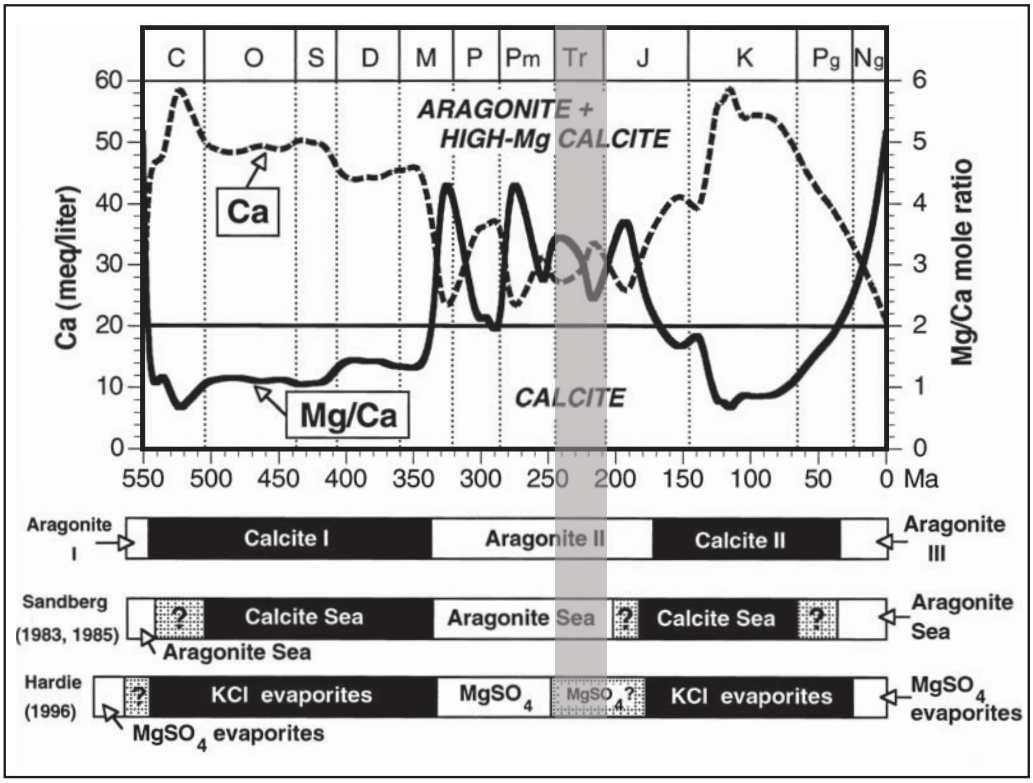

Figure 3.17 – Model of Secular variation in the Mg/Ca ratio and Ca concentration in sea water at 25° that produce calcite or aragonite + high-Mg calcite precipitation (from STANLEY & HARDIE, 1998). The grey area marks the Triassic time.

3.8.4 Origin of micrite

Data on composition of the sediment indicate that the 49.58% of the total volume consists of pelagic components (calcareous nannofossils, thin-shelled bivalves, radiolarians and ammonoids). A 44.90% is represented by fine sediment of unknown provenance (micrite), and the remaining 5.50% is non-determinable grains. As micrite is the major component of sediment, the question arises: what is its origin?

The possible provenances of carbonate mud are: 1) allochthonous material from the adjacent carbonate platforms; 2) autochthonous production in the water column, i.e., a pelagic source which nature is unknown.

Possible transport mechanisms from the adjacent carbonate platforms are turbidity currents or density cascading. If the micrite of Calcari con Selce formation was the result of turbidity currents, the fine part of recognizable turbidites should be similar in composition and fracturation of shells to the micrite of the Calcari con Selce. In such a case, the micrite of the Calcari con Selce may be interpreted as distal turbidites that are no longer recognized because of intense bioturbation. The comparison between the fine fraction of turbidites (Calcari con Selce formation) and fine micrite is exemplified in Figure 3.18. The upper part of turbidites is characterized by parallel laminae within fine-grained sediment, echinoderm and thin-shelled bivalve fragments and non-determinable carbonate grains (Fig. 3.18B-B1). Thin-shelled

bivalves are never represented by complete shells. Instead, micrite commonly consists of fine grained sediment with radiolarians and complete thin-shelled bivalves often of considerable dimensions (1.5-4 cm in diameter). Laminae and echinoderm fragments are completely absent (Fig. 3.18 A-A1). Therefore, the two types of sediments are different and most of the 44.90 % of the Calcari con Selce micrite does not derive from turbidity currents. In the Calcari con Selce formation, some turbidite beds are present, however, their contribution to net sedimentation was only minor.

Wilson & Roberts (1995) proposed the term "Density cascading" to describe the process by which hyperpycnal waters are released from shelf areas and, together with entrained sediments, sink to their compensation level in the adjacent ocean. Thanks to this process, sediment is transported for several kilometres from shelves towards the open ocean and it is then deposited similarly to a pelagic rain (Fig. 3.19) (Wilson & Roberts, 1995). Reijmer & Andresen (2007) have demonstrated that in Pedro Bank (Northern Nicaragua Rise) the neritic fine sediment fraction (>63 μm) transported by density cascading or similar mechanisms is still the most abundant component at a distance up to 40 km from the margin. Thus, this mechanism can explain the sediment transport from platform to basin also in the case of upper Triassic hemipelagic carbonates, that are thought to form far from carbonate shelves.

However, in these ancient limestones, it is difficult to distinguish between sediments accumulated through density cascading and those of pelagic origin, because they are thought to have the same sedimentological characteristics. Thus, deep water micrites as those of Pizzo Mondello are usually interpreted as derived from adjacent platforms, since the known potential pelagic sources, as coccolithophores and planktonic foraminifers, become abundant much later in Earth history (Erba, 2006). Density cascading is the probable transport mechanism for these micrites, including the Triassic micrite at Pizzo Mondello. The problem, in the Sicani area, is the localization of carbonate platforms; indeed, there are sedimentological and stratigraphic evidences that during the Triassic carbonate platforms existed (Catalano et alii, 1995), but their paleogeographic position is not certain because the area suffered of an intense tectonic activity, and platform-basin transitions are not observed, neither they can be reconstructed.

Another potential mechanism of micrite production is abiotic precipitation in the water column. However, inorganic precipitation of $CaCO_3$ (either calcite or aragonite) in sea water is practically impossible, even under extreme supersaturation conditions. Spontaneous nucleation in sea water solution is not experimentally observed until $\Omega_{cal} > 20\text{-}25$ (Morse & He, 1993).

Finally, carbonate could have been produced by some planktonic organisms present in the water column. These hypothetical organisms could be algae, bacteria or protozoa, but they cannot be the same of the present producers. It is probable that during some geological periods, these organisms did not produce carbonate sediment, or they have a different and poor preserved mineralogy. Another possibility is that they are extinct or evolve in other forms. This is a thrilling hypothesis, but at present it appears unlikely with respect to an origin from sedimentary cascading and is, in any case, not demonstrable.

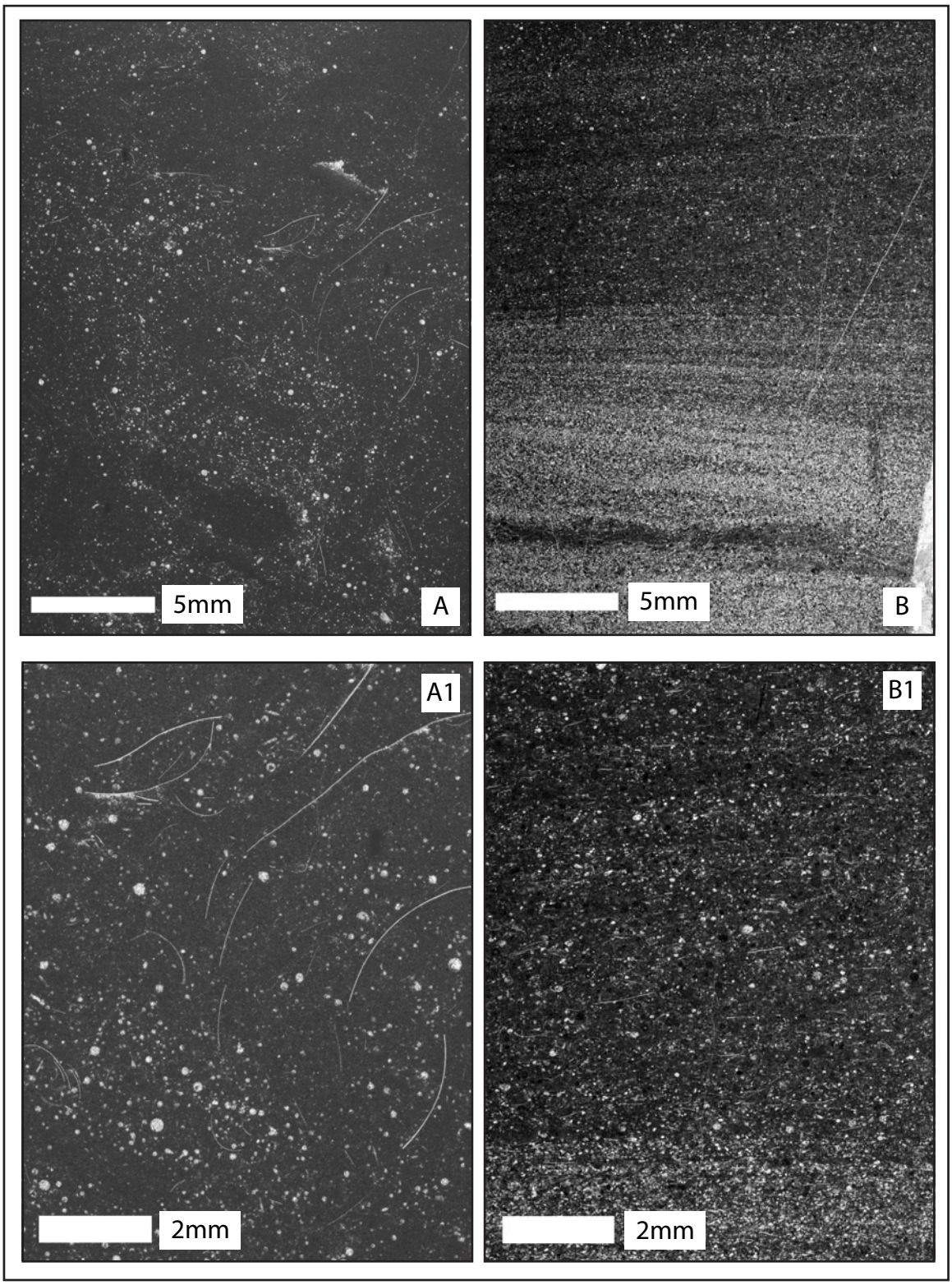

Figure 3.18 – Plate showing the two thin sections of typical fine sediment of the Calcari con Selce (A) and upper part of fine turbidite sediment within the Calcari con Selce (B).
A1: detail of micrite. Bivalves have complete shells, echinoderm fragment and non-determinable carbonate grains are absent.
B1: detail of fine turbidite. Thin-shelled bivalves are never represented by complete shells.

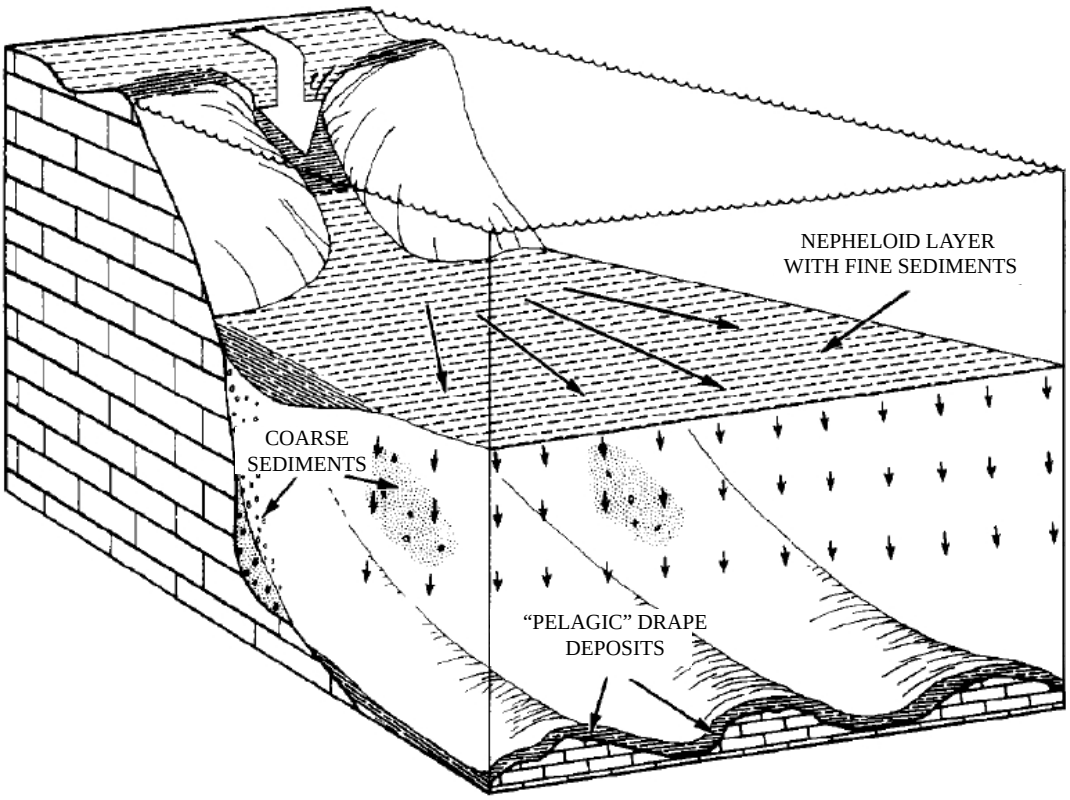

Figure 3.19 – Schematic model of a density cascading event (from WILSON & ROBERTS, 1995). The scheme shows the pelagic-mode of deposition for fine sediments carried by density cascading.

3.9 Conclusions

The facies alternation in the Pizzo Mondello section may represent a combination of oscillations in the carbonate sediment supply from surrounding carbonate platforms, varying dissolution rates at the sea-bottom, and different autochthonous (planktonic or deep-water benthic) carbonate productivity. However, it was demonstrated that carbonate dissolution definitively had a role.

We believe that the facies C is an event similar to that represented by the Green clay-radiolaritic horizon of the Lagonegro Basin, recording the Carnian Pluvial Event, that is expressed as a minor dissolution event.

A relatively wide variety and abundance of calcareous nannofossils of presumably planktonic ecology, though most probably unrelated to coccolithophores, has been observed in the Pizzo Mondello section (Sicani Basin). The systematic classification of these forms is still unclear, but they contribute to carbonate mud production with 18% of the total volume.

The quantitative study of micrite demonstrates that the carbonate sedimentation of the Calcari con Selce is mainly from a pelagic or deep-water benthic source (49.40%). This consists of calcareous nannofossils, thin-shelled bivalves, radiolarians and ammonoids. Micrite (44.92%) probably derived from adjacent carbonate platforms through density cascading.

The fine carbonate fraction of the Calcari con Selce formation consists of small crystals (2-5 μm), without aragonite needles or pits. These morphological parameters, together with geochemical data from literature, indicate that the micrite precursor was calcite-dominated. The abundance of dolomite crystals could indicate a high-Mg calcite-dominated precursor; hence, carbonate platforms adjacent to the Sicani basin were exporting mostly high-Mg calcite. This constitutes a major difference with respect to present carbonate platforms, which export aragonite muds.

CHAPTER 4
Precursor mineralogy of the Middle and Upper Triassic micrites compared

4.1 Introduction

Carbonate samples of micrite of Middle and Upper Triassic age from the Italian western Tethys were studied to determinate the mineralogy of their precursors. Hemipelagic limestone-marl alternations of the Middle Triassic of the Dolomites (northern Italy) and of the Upper Triassic of the Sicani Basin (Sicily), and fine carbonate samples from the carbonate-clastic ramp of the Upper Triassic of the western Julian Alps (northern Italy) were analysed with Scanning Electron Microscopy (SEM). In order to discriminate the dominated mineralogy of micrite precursor, morphological parameters (average crystal dimension and presence/absence of elongated pits) were considered.

4.2 Sections

In the Middle Triassic successions of the Dolomites, the carbonate samples derived from hemipelagic nodular-bedded facies (Bivera Formation and Knollenkalke member) and plane-bedded facies (Ambata Formation) (Preto et alii, in press). The studied Middle Triassic successions of the Dolomites area encompass the Bivera Formation, Ambata Formation and Livinallongo Formation (Plattenkalke, Knollenkalke and Bänderkalke members). The Bivera Formation is a chiefly marly unit with nodular limestone beds and isolated calcareous nodules. The Ambata Formation shows dm-scale plane-bedded limestone-marl alternations. Knollenkalke consists of greenish-grey, bioturbated nodular limestones, with chert nodules and beds.

The carbonate samples of the Sicani Basin derived from Calcari con Selce formation of Pizzo Mondello, described in chapter 3.

The Upper Triassic carbonate samples of western Julian Alps derived from the outer portion of the carbonate-clastic ramp of Dogna (Preto et alii, 2005; Meneguolo, 2008). The Carnian formations of the Dogna area are Schlern Dolomite, Rio di Terrarossa Dolomite (Jadoul et alii, 2002), Rio del Lago Formation (Assereto et alii, 1968), Dogna formation and Tor Formation (Assereto et alii, 1968). The Rio del Lago Formation consists of subtidal clays, marls and bioturbated to nodular wackestone-packstones, with pelecypods and foraminifers. The “Dogna” formation is a mixed carbonate–siliciclastic succession with two main coarse siliciclastic intervals separated by vuggy dolomites. Arenites are decimetric to metric thick,

massive to cross-bedded, with bivalves and intraclasts (Preto et alii, 2005; Meneguolo, 2008). Analysed samples were collected within the Rio del Lago Formation.

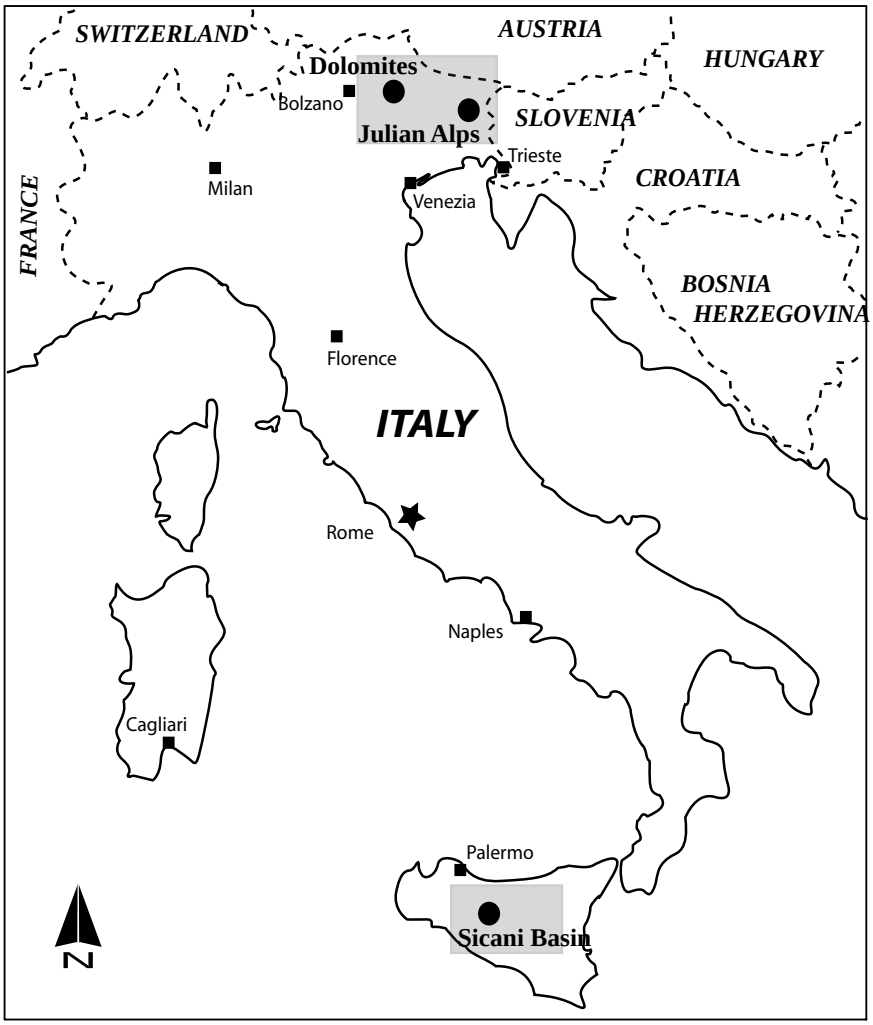

Figure 4.1 - Map of the studied areas. Location of the Dolomites and western Julian Alps and Sicily in Italy.

4.3 Methods

200 thin sections were examined at high magnification using a Leica DM-EP petrographic microscope. Eighty samples were also examined using a CamScan MX 2500 Scanning Electron Microscope (SEM) in order to examine the microfabric and crystal size of these micritic limestones. Samples were selected among those exhibiting well-preserved fine matrix and minimum presence of non-carbonate elements, allochems, stylolites, veinlets or dolomite. All samples were cut perpendicularly to bedding and polished with corundum powder (borcarbid 500, 800 and 1200). The surfaces were cleaned and etched with 0.3% (0.1 N) hydrochloric acid for 20 to 40 seconds, dried, carbon-coated and then observed at the SEM.

4.4 Results

As for the micrites of Pizzo Mondello (chapter 3), Middle Triassic hemipelagites (preserved as limestones) of the Dolomites also exhibit small calcite crystals (2-5 μm) in the nodular facies (Fig. 4.2), but pitted large (10 μm) microspar crystals in the plane-bedded facies (Fig. 4.3). Rare calcispheres are also present.
The lower Carnian of the Julian Alps (Dogna carbonate ramp) shows large (10 μm) pitted microspar crystals (Fig. 4.4) and aragonite needles are also rarely found.
As shown already in chapter 3, the fine carbonate fraction from Sicani Basin (Calcari con Selce formation) shows lack of aragonite needles or pits and small micrite crystals (2-5 μm) (Fig. 4.5). Abundant calcispheres (20-30 μm) are present.

4.5 Discussion and Conclusions

Different hemipelagic facies in the Middle Triassic of the Dolomites indicate different precursors, calcite-dominated in the nodular facies VS aragonite-dominated in plane-bedded facies. Surprisingly, carbonate muds with distinct original mineralogies alternated rapidly within this relatively short time slice. This suggests rapidly alternating precipitation conditions in adjacent carbonate platforms (Preto et alii, in press).
The lower Carnian fine carbonates of Julian Alps clearly had an aragonite-dominated precursor.
On the contrary, the precursor sediment of upper Carnian to Norian Calcari con Selce formation was mainly composed of calcite. The presence of sparse dolomite crystals suggests that the precursor was high-Mg calcite.
On the whole, it appears that the original mineralogy of carbonate muds, and hence the mode of precipitation of carbonate platforms, had a prominent variability during the Triassic, that might reflect the swings of environmental conditions at the basin scale. It is suggested that such variability should be better characterized.
The changes in mineralogy of marine Triassic carbonates are poorly studied, but they are likely linked to seawater chemical or physical parameters (Mg/Ca ratio, pCO_2, temperature and salinity), paleogeography or biota evolution. Further studies are needed to understand the full significance of these oscillations in the mineralogy of fine carbonate precipitates, but they go beyond the aims of this work.

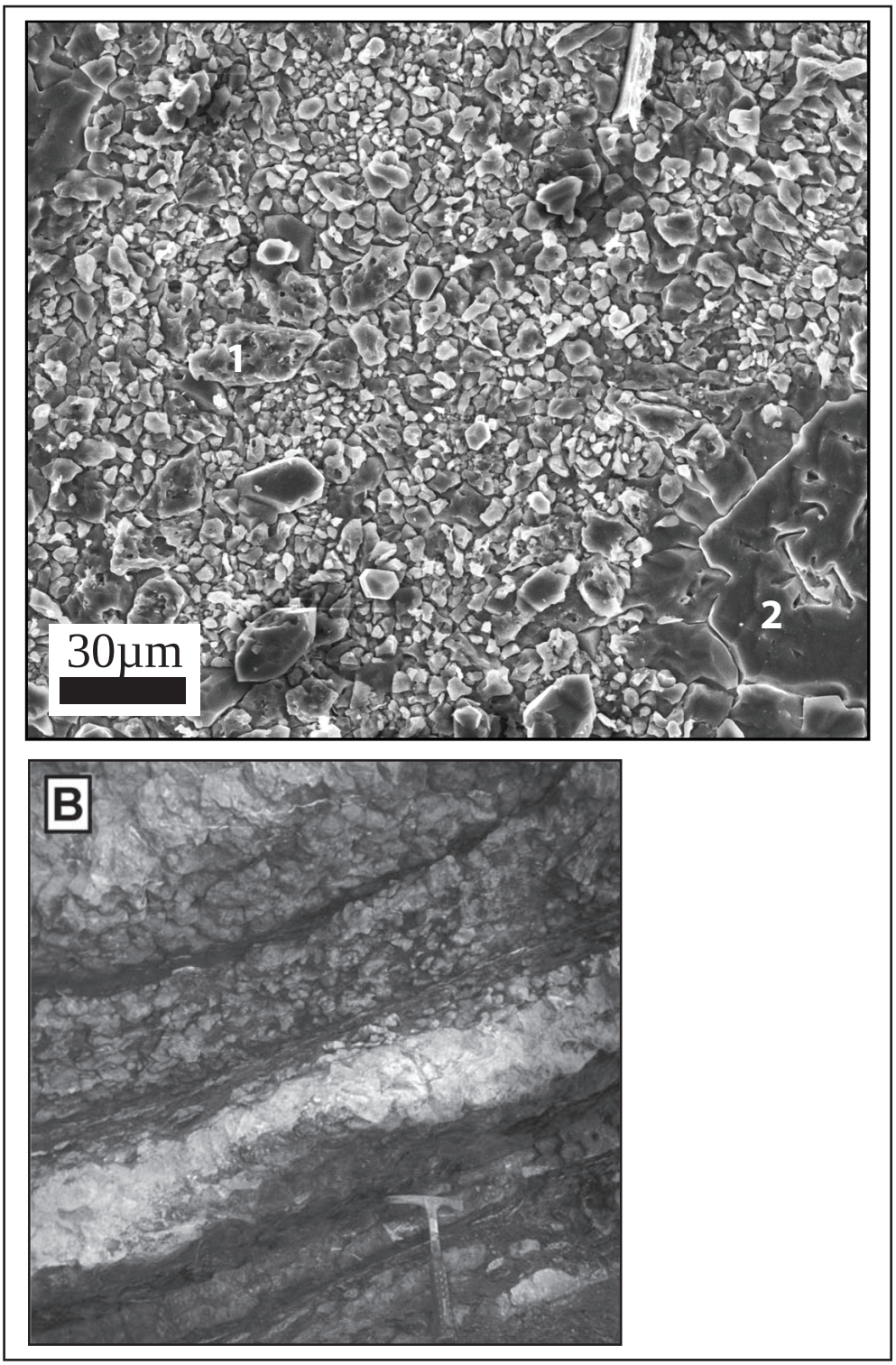

Figure 4.2 - Nodular facies. The microfabric is given mostly by blocky calcite crystals (<5 µm). A few large, pitted calcite crystals (1) and radiolarian moulds filled by sparry calcite (2) are also present. Rio Sacuz section, sample SZ 51 at 65.67 m, Knollenkalke Member.

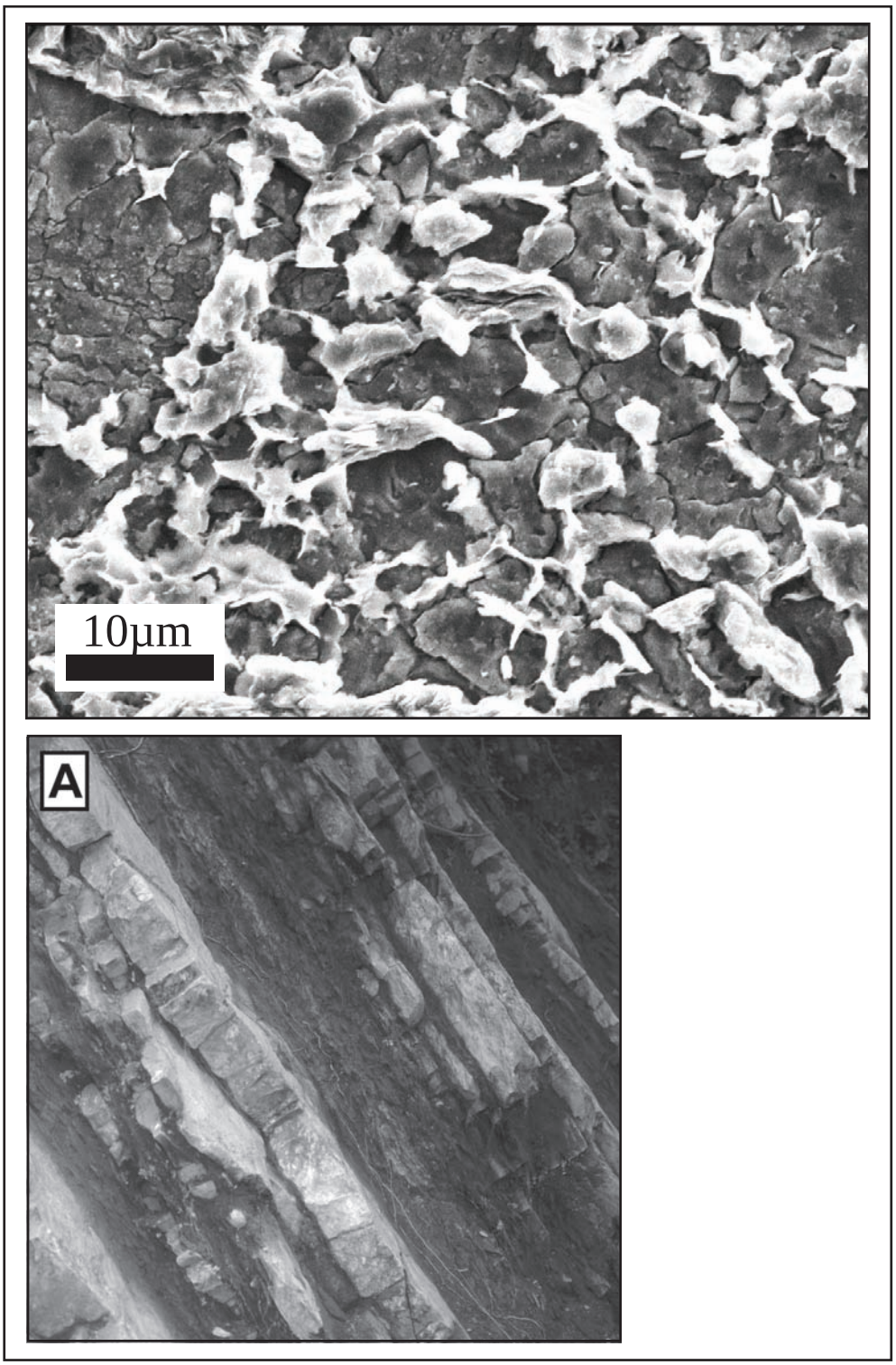

Figure 4.3 - Plane-bedded facies. Pitted calcite crystals with diametre >5 µm. Sample ISA 145, Palus/San Marco section at 14.68 m, upper Ambata Formation.

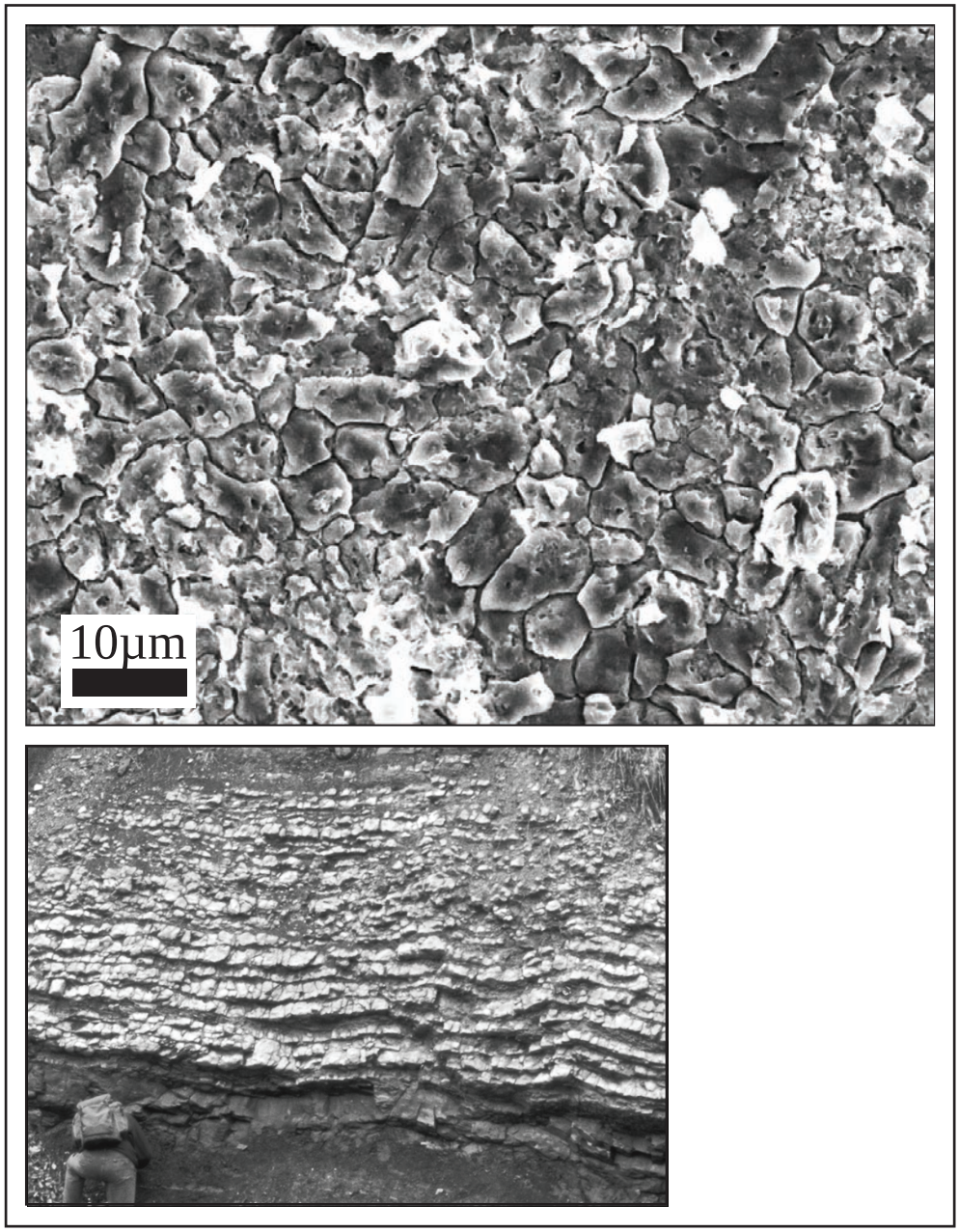

Figure 4.4 - Mosaic of microspar (10 µm). Many crystals are pitted. Gran Colle section, sample GC 37, Rio del Lago Formation.

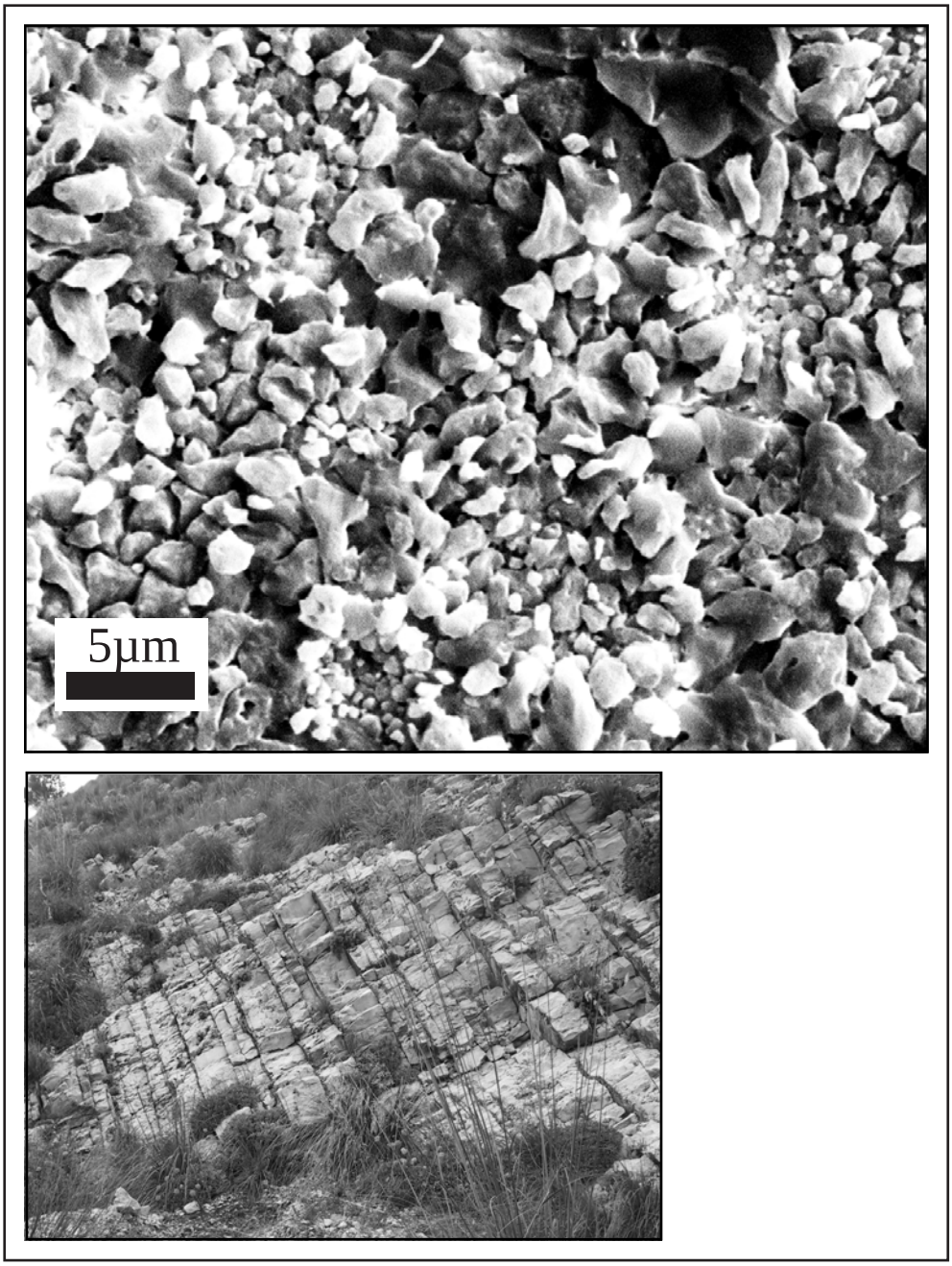

Figure 4.5 - Pizzo Mondello, sample 126 at 62.80 m, Calcari con Selce formation. The microfabric of this facies is mostly given by small calcite crystals (2-5 µm).

REFERENCES

Amodeo F. (1999) - *Il Triassico terminale-Giurassico del Bacino Lagonegrese. Studi stratigrafici sugli Scisti Silicei della Basilicata (Italia meridionale)*. Mémoires de Géologie (Lausanne), **33**, 1-121.

Amodeo F. & Baumgartner P.O. (1994) - *Stratigraphic revision of the «Scisti Silicei» Formation (Upper Triassic-Upper Jurassic), Lagonegro Basin, southern Italy. Preliminary Report.* Paleopelagos, **4**, 35-46.

Arthur M.A., Dean W.E., Bottjer D.J. & Scholle P.A. (1984) - *Rhythmic bedding in Mesozoic-Cenozoic pelagic carbonate sequences: the primary and diagenetic origin of Milankovitch-like cycles.* In: Berger A., Imbrie J., Hays J., Kukla G. & Saltzman B. Eds., Milankovitch and climate. Riedel, Hingham, MA, 191–222.

Assereto R., Desio A., Di Corte Baldo D. & Passeri L.D (1968) - *Note illustrative della Carta Geologica d'Italia. Foglio 14A Tarvisio*. Servizio Geologico Italiano, Roma.

Bellanca A., Di Stefano E., Di Stefano P., Erba E., Neri R. & Pirini Radrizzani C. (1993) - *Ritrovamento di "Calcisfere" e nannofossili calcarei in terreni carnici della Sicilia*. Paleopelagos, **3**, 91-96.

Bellanca A., Di Stefano P. & Neri R. (1995) - *Sedimentology and isotope geochemistry of Carnian deep-water marl/limestone deposits from the Sicani Mountains, Sicily: Environmental implications and evidence for a planktonic source of lime mud.* Palaeogeography, Palaeoclimatology, Palaeoecology, **114**, 111-129.

Bellanca A., Claps M., Erba E., Masetti D., Neri R., Premoli Silva I. & Venezia F. (1996) - *Orbitally induced limestone/marlstone rhythms in the Albian–Cenomanian Cismon section (Venetian region, northern Italy); sedimentology, calcareous and siliceous plankton distribution, elemental and isotope geochemistry*. Palaeogeography, Palaeoclimatology, Palaeoecology, **126**, 227–260.

Bertinelli A. (2003) - *Il Bacino Lagonegrese-Molisano nel contesto della Tetide occidentale durante il Triassico Superiore-Giurassico.* Tesi di Dott. in Scienze della Terra, Università degli Studi di Perugia, 219 pp.

Bertinelli A., Ciarapica G., De Zanche V., Marcucci M., Mietto P., Passeri L., Rigo M. & Roghi G. (2005) - *Stratigraphic evolution of the Triassic–Jurassic Sasso di Castalda succession (Lagonegro Basin, Southern Apennines, Italy)*. Bollettino. Societa Geologica Italiana, **124**, 161–175.

Brack P. & Muttoni G. (2000) - *High-resolution magnetostratigraphic and lithostratigraphic correlations in Middle Triassic pelagic carbonates from the Dolomites (northern Italy).* Palaeogeography, Palaeoclimatology, Palaeoecology, **161**, 361-380.

Breda A., Massari F., Meneguolo R. & Preto N. (2006) - *An alluvial plain - sabkha -*

lagoon system in the Upper Triassic of the Dolomites, northern Italy. In: Atti del congresso: EGU General Asssembly 2006.

Buratti N. & Carrillat A. (2002) - *Palynostratigraphy of the Mufara Formation (Middle-Upper Triassic, Sicily).* Rivista Italiana di Paleontologia e Stratigrafia, **108**, 101–117.

Catalano R., Di Stefano P. & Kozur H. (1991) - *Permian circumpacific deep-water faunas from the western Tethys (Sicily, Italy) - new evidences for the position of the Permian Tethys.* Palaeogeography, Palaeoclimatology, Palaeoecology, **87** (1-4), 75-108.

Catalano R., Di Stefano P., Sulli A. & Vitale F.P. (1995) - *Paleogeography and structure of the central Mediterranean: Sicily and its offshore area.* Tectonophysics, **260**, 291-323.

Ciarapica G. & Passeri L. (1998) - *Evoluzione paleogeografica degli Appennini.* Atti Ticinensi di Scienze della Terra, **40**, 233-290.

Ciarapica G. & Passeri L. (2002) - *The palaeogeographic duplicity of the Apennines.* Bollettino. Societa Geologica Italiana, **1** (Vol. spec.), 67-75.

De Capoa P. (1970) - *Le Daonelle e le Halobie della serie calcareosilico-marnosa della Lucania (Appennino Meridionale). Studio paleontologico e biostratigrafico.* Bollettino. Societa Naturalisti in Napoli, suppl. Boll., **78**, 1-127.

De Capoa Bonardi P. (1984) - *Halobia* zones in the pelagic Late Triassic sequences of the Central Mediterranean area (Greece, Yugoslavia, Southern Apennines, Sicily). Bollettino della Società Paleontologica Italiana, **23**, 91-102.

Di Nocera S. & Scandone P. (1977) - *Triassic nannoplankton limestones of deep basin origin in the Central Mediterranean region*. Palaeogeography, Palaeoclimatology, Palaeoecology, **2l**, 101-111.

Di Stefano P. (1990) - *The Triassic of Sicily and the Southern Apennines*. Bollettino Societa Geologica Italiana, **109**, 21-37.

Di Stefano P. & Gullo M. (1997) - *Late Paleozoic–Early Mesozoic stratigraphy and paleogeography of Sicily, in Catalano, R., ed., Timescales and basin dynamics: Sicily, the adjacent Mediterranean and other natural laboratories*. Palermo, Eurobasin School, June 7–13, 1997, Field Workshop Guide Book, 87–99.

Einsele G. (1982) - *General remarks about the nature, occurence, and recognition of cyclic sequences (periodites)*. In: Einsele G., Ricken W. & Seilacher A. Eds., Cycles and Events in Stratigraphy. Springer-Verlag, Berlin, 3-7.

Epstein A.G., Epstein J.B. & Harris L.D. (1977) - *Conodont color alteration an index to organic metamorphism*. United States Geological Survey. Professional Paper, **27**, 995.

Erba E. (2006) - *The first 150 million years history of calcareous nannoplankton: Biospheregeosphere interactions.* Palaeogeography, Palaeoclimatology, Palaeoecology, **232**, 237–250.

Finetti I. (1982) - *Structure, stratigraphy and evolution of central Mediterranean*. Bollettino di Geofisica Teorica e Applicata, **24**, 247–315.

Finetti I. (1985) - *Structure and evolution of the Central Mediterranean (Pelagian and Ionian Sea).* In: Stanley D.J. & Wezel F.C. Eds., Geological Evolution of the Mediterranean Basin. Springer-Verlag, 215-230.

Folk R.L. (1959) – *Practical petrographic classification of limestones*. American Association Geologists Bulletin, **43**, 1-38.

Folk R.L. (1965) – *Some aspects of recrystallization in ancient limestones*. In: Pray L.C. & Murray R.C. Eds., Dolomitization and limestone diagenesis. Society of Economic Paleontologists and Mineralogists Special Pubblication, **13**, 14-48.

Furin S., Preto N., Rigo M., Roghi G., Gianolla P., Crowley J. & Bowring S.A. (2006) - *A high-precision U/Pb zircon age from the Triassic of Italy – implication for the Carnian origin of calcareous nannoplankton and dinosaurs*. Geology, **34/12**, 1009–1012.

Furin S., Preto N., Rigo M., Roghi G., Gianolla P., Crowley J. & Bowring S.A. (2007) Erratum. - *A high-precision U/Pb zircon age from the Triassic of Italy – Implication for the Carnian origin of calcareous nannoplankton and dinosaurs*. Geology, **35/2**, 146.

Gianolla P. & Jacquin T. (1998) – *Triassic sequence stratigraphic framework of western European Basins*. In: De Graciansky, P. C., Hardenbol, J., Jacquin, T., Vail, P.R. Eds., Mesozoic and Cenozoic sequence stratigraphy of European basins. Special Publication SEPM (Society for Sedimentary Geology), **60**, 644–650.

Gianolla P., Ragazzi E. & Roghi G. (1998) – *Upper Triassic amber from the Dolomites (northern Italy). A paleoclimatic indicator?* Rivista Italiana di Paleontologia e Stratigrafia, **104**, 381–390.

Grippo A., Fischer A. G., Hinnov L. A., Herbert T. D. & Premoli Silva I. (2004) - *Cyclostratigraphy and chronology of the Albian stage (Piobbico core, Italy).* SEPM Special Publication, **81**, 57-81.

Guaiumi C., Nicora A., Preto N., Rigo M., Balini M., Di Stefano P., Gullo M., Levera M., Mazza M. & Muttoni G., (2007) - *New Biostratigraphic data around the Carnian/Norian boundary from the Pizzo Mondello Section, Sicani Mountains, Sicily*. New Mexico Museum of Natural History and Science, Bulletin, **41**, 40-42.

Gullo M. (1996) - *Conodont biostratigraphy of uppermost Triassic deep-water calcilutites from Pizzo Mondello (Sicani Mountains): evidence for Rhaetian pelagites in Sicily*. Palaeogeography, Palaeoclimatology, Palaeoecology, **126**, 309-323.

Hirsch F. (1994) – *Triassic conodonts as ecological and eustatic sensors*. Canadian Society of Petroleum Geologist, Memoir, **17**, 949-959.

Hirsch F. (1994) – *Triassic multielement conodonts versus eustatic cycles*. Mémoires de Géologie (Lausanne), **22**, 35-52.

Hornung T. Krystyn L. & Brandner R. (2007) – *A Tethys-wide mid-Carnian (Upper Triassic) carbonate productivity crisis: Evidence for the Alpine Reingraben event from Spiti (Indian Himalaya)?* Journal of Asian Earth Sciences, **30**, 258–302.

Jadoul F., Nicora A., Ortenzi A. & Pohar C. (2002) - *Ladinian stratigraphy and paleogeography of the Southern Val Canale (Pontebbano-Tarvisiano, Southern Alps, Italy).* Memorie della Società Geologica Italiana, **57**, 29-43.

James R. & the Open University course team (2005) - *Marine biogeochemical cycles (2nd edition)*. The Open University and Elsevier, Milton Keynes (UK), 130 pp.

Janofske D. (1992) – *Kalkiges Nannoplankton, insbesondere kalkige Dinoflagellaten-Zysten*

der alpine Ober-Trias: Taxonomie, Biostratigraphie und Bedeuntung für die Phylogenie der Peridiniales. Berliner Geowissenschaftliche Abhandlungen, (E) **4**, 1-73.

KENT D.V. & OLSEN P.E. (1999) - *Astronomically tuned geomagnetic polarity time scale for the Late Triassic*. Journal of Geophysical Research, **104**, 12831-12841.

KIDWELL S.M. (1991) – *The stratigraphy of shell concentrations.* In: Allison P.A., Briggs D.E.G. Eds., Taphonomy: releasing the data locked in the fossil record. Topics in Geobiology, **9**, 211-290, New York (Plenum).

KRYSTYN L., GALLET Y., BESSE J. & MARCOUX J. (2002) - *Integrated Upper Carnian to Lower Norian biochronology and implications for the Upper Triassic magnetic polarity time scale*. Earth and Planetary Science Letters, **203**, 343–351.

KUTZBACH J. E. & GALLIMORE R. G. (1989) - *Pangaean climates: Megamonsoons of the megacontinent.* Journal of Geophysical Research, **94**, 3341-3357.

LASEMI Z. & SANDBERG P.A. (1983) – *Recognition of original mineralogy in ancient micrites.* American Association of Petroleum Geologists Bulletin, **67**, 499-500.

LASEMI Z. & SANDBERG P.A. (1984) - *Transformation of aragonite-dominated lime muds to microcrystalline limestones*. Geology, **12**, 420-423.

LASEMI Z. & SANDBERG P.A. (1993) - *Microfabric and compositional clues to dominant mud mineralogy of micrite precursors.* In: Rezak R. & Lavoie D.L. Eds., Carbonate Microfabrics. Springer, New York, pp. 173– 185.

LOURENS L.J., SLUIJS A., KROON D., ZACHOS J.C., THOMAS E., RÖHL U., BOWLES J. & RAFFI I. (2005) - *Astronomical pacing of late Palaeocene to early Eocene global warming events*. Nature **435**, 1083–1087.

MARTINI R., ZANINETTI L., VILLENEUVE M., CORNÉE J.J., KRYSTYN L., CIRILLI S., DE WEVER P., DUMITRICA P. & HARSOLUMAKSO A. (2000) - *Triassic pelagic deposits of Timor: palaeogeographic and sea-level implications.* Palaeogeography, Palaeoclimatology, Palaeoecology, **160**,123-151.

MENEGUOLO R. (2008) – *Stratigraphic and compositional study of mixed shallow-water carbonate-siliciclastic units of Carnian age (Late Triassic) in Dolomites and Julian Alps (Italy)*. Unpublished PhD thesis, Università degli Studi di Padova, 120 pp.

MICONNET P. (1983) - *Précisions stratigraphiques et tectoniques dans un secteur du Lagonegro (Italie méridionale)*. Annales. Société Géologique du Nord, **102**, 17-24.

MILLERO F.J. (2007) - *The marine inorganic carbone cycle.* Chemical Review, **107** (2), 308-341.

MORSE J.W. & HE S.L. (1993) - *Influences of T, S and pCO2 on thepseudo-homogeneous precipitation of CaCO3 from seawater-implications for whiting formation*. Marine Chemistry, 41, 291–297.

MULDER T., SAVOYE B. & SYVITSKI J.P.M. (1997) - *Numerical modeling of a mid-sized gravity flow: the 1979 Nice turbidity current (dynamics, processes, sediment budget and seafloor impact)*. Sedimentology, **44**, 305–326.

MUNNECKE A. & SAMTLEBEN C. (1996) - *The formation of micritic limestones and the development of limestone-marl alternations in the Silurian of Gotland, Sweden*. Facies, **34**,

159–176.

Munnecke A. (1997) - *Bildung mikritischer Kalke im Silur auf Gotland*. Courier Forschungsinstitut Senckenberg, **198**, 1–132.

Munnecke A., Westphal H., Reijmer J.J.G. & Samtleben C. (1997) - *Microspar development during early marine burial diagenesis: a comparison of Pliocene carbonates from the Bahamas with Silurian limestones from Gotland (Sweden).* Sedimentology, **44**, 977–990.

Muttoni G., Kent D.V., Di Stefano P., Gullo M., Nicora A., Tait J. & Lowrie W. (2001) - *Magnetostratigraphy and biostratigraphy of the Carnian/Norian boundary interval from the Pizzo Mondello section (Sicani Mountains, Sicily)*. Palaeogeography, Palaeoclimatology, Palaeoecology, **166**, 383-399.

Muttoni G., Kent D.V., Olsen P.E., Di Stefano P., Lowrie W., Bernasconi S.M., & Hernández Fm. (2004) - *Tethyan magnetostratigraphy from Pizzo Mondello (Sicily) and correlation to the Late Triassic Newark astrochronological polarity time scale.* Geological Society of America Bulletin, **116**, 1043-1058.

Muttoni G., Kent D., Jadoul F., Olsen P., Rigo M., Galli M.T. & Nicora A. (2009) - *Rhaetian magnetobiostratigraphy from the Southern Alps (Italy): constraints on Triassic chronology*. Palaeogeography, Palaeoclimatology, Palaeoecology, accepted.

Nakajima T. & Kanai Y. (2000) - *Sedimentary features of seismoturbidites triggered by the 1983 and older historical earthquakes in the eastern margin of the Japan Sea*. Sedimentary Geology, **135**, 1–19.

Neri C., Gianolla P., Furlanis S., Caputo R. & Bosellini A. (2007) - *Carta Geologica d'Italia alla scala 1:50000, foglio 29 Cortina d'Ampezzo, and Note illustrative*. APAT, Roma, 200 pp.

Nicolo M. J., Dickens G.R., Hollis C. J. & Zachos J.C. (2007) - *Multiple early Eocene hyperthermals: Their sedimentary expression on the New Zealand continental margin and in the deep sea*. Geology, **35**, 699–702.

Nicora A., Rigo M. & Gullo M. (2006) - *The Upper Triassic conodont fauna of Pizzo Mondello section (Sicani Mountains, Sicily)*. "ICOS 2006 - First International Conodont Symposium" Leicester, UK, 16-21 July 2006. Programme and Abstracts, 60 pp.

Nicora A., Balini M., Bellanca A., Bertinelli A., Bowring S.A., Di Stefano P., Dumitrica P., Guaiumi C., Gullo M., Hungerbuehler A., Levera M., Mazza M., Mcroberts C.A., Muttoni G., Preto N., & Rigo M. (2007) - *The Carnian/Norian Boundary interval at Pizzo Mondello (Sicani Mountains, Sicily) and its bearing for the definition of the Gssp of the Norian Stage,* Albertiana, **36**, 102-129.

Normark W.R. & Piper D.J.W. (1991) - *Initiation processes and flow evolution of turbidity currents: implications for the depositional record*. In: Osborne R.H. Eds., From Shoreline to Abyss: Contributions in Marine Geology in Honor of Francis Parker Shepard. SEPM Spec. Publ., **46**, 207–230.

Onoue T. & Sano H. (2007) - *Triassic mid-oceanic sedimentation in Panthalassa Ocean: Sambosan accretionary complex, Japan*. Island Arc, **16**, 173-190.

Passeri L., Bertinelli A. & Ciarapica G. (2005) – *Paleogeographic meaning of the Late*

Triassic-Early Jurassic Lagonegro units. Bollettino. Societa Geologica Italiana, **124**, 231-245.

Preto N., Roghi G. & Gianolla P. (2005) - *Carnian stratigraphy of the Dogna area (Julian Alps, northern Italy): tessera of a complex palaeogeography*. Bollettino. Societa Geologica Italiana, **124 (1)**, 269-279.

Preto N., Spötl C. & Guaiumi C. (2008) - *Evaluation of bulk carbonate $d^{13}C$ data from Triassic hemipelagites and the initial composition of carbonate mud*. Sedimentology, in press.

Price G.D. (1999) - *The evidence and implications of polar ice during the Mesozoic*. Earth-Science Reviews, **48** (3), 183–210.

Reggiani L., Bertinelli A., Ciarapica G., Marcucci M., Passeri L., Ricci C. & Rigo M. (2005) - *Triassic-Jurassic stratigraphy of the Madonna del Sirino succession (Lagonegro Basin, Southern Apennines, Italy).* Bollettino Societa Geologica Italiana, **124**, 281-291.

Reijmer J.J.G. & Andresen N. (2007) - *Mineralogy and grain size variations along two carbonate margin-to-basin transects (Pedro Bank, Northern Nicaragua Rise)*. Sedimentary Geology, **198**, 327–350.

Ricken W. (1987) - *The carbonate compaction law: a new tool*. Sedimentology, **34**, 1–14.

Ridgwell A. & Zeebe R. A. (2005) - *The role of the global carbonate cycle in the regulation and the evolution of the Earth system.* Earth Planetary Sciences Letters, **234**, 299-315.

Rigo M., De Zanche V., Mietto P., Preto N. & Roghi G. (2005) - *Correlation of Upper Triassic sections throughout the Lagonegro Basin*. Bollettino Societa Geologica Italiana, **124**, 293-300.

Rigo M., Preto N., Roghi G., Tateo F. & Mietto P. (2007) - *A rise in the Carbonate Compensation Depth of western Tethys in the Carnian (Late Triassic): deep-water evidence for the Carnian pluvial event*. Palaeogeography, Palaeoclimatology, Palaeoecology, **246**, 188-205.

Scandone P. (1967) - *Studi sulla geologia lucana: la serie calcareo-silico-marnosa e i suoi rapporti con l'Appennino calcareo*. Bollettino Societa Naturalisti in Napoli, **76**, 1-175.

Scandone P. (1972) - *Studi di geologia lucana: nota illustrativa della carta dei terreni della serie calcareo-silico-marnosa*. Bollettino Societa Naturalisti in Napoli, **81**, 225-300.

Scandone P. (1975) - *Triassic seaways and the Jurassic Tethys in the central mediterranean area.* Nature, **256**, 117.

Schatz W. (2005) - *Paleoecology of the Triassic black shale bivalves Daonella - new insights into an old controversy*. Palaeogeography, Palaeoclimatology, Palaeoecology, **216**, 189-201.

Sengör A.M.C., Yilmaz Y. & Sungurlu O. (1984) - *Tectonics of the Mediterranean Cimmerides: nature and evolution of the western termination of Palaeo-Tethys.* In: Dixon J.E. & Robertson A.H.F. Eds., The Geological Evolution of the Eastern Mediterranean. Geological Society, London Special Publications, **17**, 77-112.

Simms M.J. & Ruffell A.H. (1989) – *Synchroneity of climatic change and extinctions in the Late Triassic*. Geology, **17**, 265-268.

Simms M.J. & Ruffell A.H. (1990) – *Climatic and biotic change in the Late Triassic*. Journal

of the Geological Society, **147**, 321-327.

Simms M.J., Ruffell A.H. & Johnson A.L.A. (1995) - *Biotic and climatic changes in the Carnian (Triassic) of Europe and adjacent areas*. In: Fraser N.C. & Sues H.D. Eds., In the Shadow of the Dinosaurs. Early Mesozoic Tetrapods. Cambridge Univ. Press, 352–365.

Stampfli G.M, Marcoux J. & Baud A. (1991) - *Tethyan margins in space and time.* Palaeogeography, Palaeoclimatology, Palaeoecology, **87** (1-4), 373-409.

Stampfli G.M. & Marchant R.H. (1995) - *Plate configuration and kinematics in the Alpine region.* In: Polino R. & Sacchi R. Eds., Atti del Convegno «Rapporti Alpi-Appennino». Accademia Nazionale Delle Scienze, Scritti e Documenti, **14**, 147-166.

Stampfli G.M., Mosar J., Marquer D., Marchant R., Baudin T. & Borel G.D. (1998) - *Subduction and obduction processes in the Swiss Alps.* Tectonophysics, **296**, 159-204.

Stampfli G.M., Vavassis I., De Bono A., Rosselet F., Matti B. & Bellini M. (2003) - *Remnants of the Palaeotethys oceanic suture-zone in the western Tethyan area*. Bollettino. Societa Geologica Italiana, **2** (Vol. spec.), 1–23.

Stanley S.M. & Hardie L.A. (1998) – *Secular oscillations in the carbonate mineralogy of reef building and sediment-producing organisms driven by tectonically forced shifts in seawater chemistry*. Palaeogeography, Palaeoclimatology, Palaeoecology, **114** (1-2), 3-19.

Van Der Plas L. & Tobi A.C. (1965) – *A chart for judging the reliability of point-counting results*. American Journal of Science, **263**, 87-90.

Westphal H., Head M.J. & Munnecke A. (2000) - *Differential diagenesis of rhythmic limestone alternations supported by palynological evidence*. Journal of Sedimentary Research, **70**, 715–725.

Westphal H. (2006) - *Limestone-marl alternations as environmental archives and the role of early diagenesis: a critical review*. International Journal of Earth Sciences, **95**, 947-961.

Wilson P.A. & Roberts H.H. (1995) - *Density cascading: off-shelf sediment transport, evidence and implications, Bahama Bank.* Journal of Sedimentary Research **A65**, 45–56.

Zachos J.C., Röhl U., Schellenberg S.A., Sluijs A., Hodell D.A., Kelly D.C., Thomas E., Nicolo M., Raffi I., Lourens L.J., McCarren H. & Kroon D. (2005) - *Rapid Acidification of the Ocean during the Paleocene–Eocene Thermal Maximum*. Science, **308**, 1611–1615.

Ziegler M.A., Parrish J.M., Jiping Y., Gillenhaal E.D., Rowley D.B., Totman Parrish J., Shangyou N., Bekker A. & Hulver M.L. (1994) – *Early Mesozoic phytogeography and climate*. In Allen J.R.L. et alii, Eds., Paleoclimates and their modelling. The Royal Society/ Chapman & Hall, London, 89-97.

APPENDIX 1

This table shows the point-count data of Pizzo Mondello thin sections. For each samples more than 500 points were counted.

	METRI	SAMPLES	MICRITE	CALCAREOUS NANNOFOSSILS	THIN-SHELLED BIVALVES	RADIOLARIANS	FORAMINIFERS	AMMONOIDS	NON-DETERMINABLE	TOTAL
FACIES A	15	335	284	76	37	225	3	1	29	655
	16	333	289	74	43	225			35	666
	17.13	327	277	98	32	170			21	598
	17.85	324	348	37	25	188			61	659
	18.45	322	343	62	56	192			21	674
	19	320	324	37	43	166			45	615
	19.7	316	296	60	58	181	1	1	54	651
	21.45	310	269	75	45	196			51	636
	23.67	305	249	86	31	195			47	608
	24.33	303	267	43	47	247	4	1	55	664
	25.5	1	208	119	59	179			50	615
	28.5	11	525	175	106	257	10	1	32	1,106
	29.9	15	198	196	50	167	1		56	668
	32	21	293	78	91	218	3		42	725
	35	28	214	190	62	179	2		47	694
	35.9	30	237	105	63	198			59	662
	37	34	258	12	162	109			58	599

	41	40	370	23	48	188	3		40	672
	43.5	45	370	49	50	153	3		35	660
	45	48	352	70	60	211	1		23	717
FACIES B	47.7	54	245	167	68	153			47	680
	49.8	58	289	50	88	197	9		45	678
	53.3	65	305	134	67	223	2		23	754
	54.5	68	177	163	52	181			47	620
	57.1	72	244	102	49	196	1	1	56	649
	60.5	80	238	139	32	180			45	634
	62	83	339	47	61	225	5		37	714
	63.6	86	246	179	20	158	1		64	668
	65.25	89	244	79	35	243		1	55	657
	66.2	91	183	154	35	205		1	50	628
	69.3	98	364	84	23	151			62	684
	71.25	102	294	11	45	269	5	1	60	685
	73.2	104	324	145	49	174			35	727
	75.1	107	301	39	41	227			43	651
	77	110	299	57	108	190	6	2	68	730
	78.75	114	264	54	30	229	1	2	56	636
	81.15	117	313	75	31	168			49	636
	82.5	120	226	121	40	222			57	666
	88.25	126	215	213	53	214			40	735
FACIES C	89.3	127	265	187	26	107		1	53	639
	90.25	128	181	345	52	118			55	751
	91.1	130	283	155	41	184	1		20	684
	92.3	131	304	185	13	57	2		22	583
	93	132	330	77	77	201	2		41	728
	93.3	134	183	315	42	132			47	719
	94.25	136	287	274	16	86	1		29	693
	94.7	137	300	180	30	175	1		22	708

FACIES C	95.3	138	202	224	27	159			44	656
	95.9	140	188	339	45	86	1		51	710
	96.8	141	349	162	24	76			3	614
	97.25	142	337	111	35	187	3		7	680
	99.25	145	227	191	28	131	1		32	610
	101	147	217	250	19	128			58	672
	101.65	148	144	278	69	218	2		57	768
	102.5	149	257	197	18	124		1	15	612
	103.25	150	271	173	17	150	1		30	642
	103.8	151	347	22	90	139	1		8	607
	105.1	154	167	255	65	229	3		38	757
	105.7	155	283	35	177	181			6	682
	106.15	156	270	143	54	184	3		17	671
FACIES B	107	158	364	75	27	214	3		9	692
	108.25	160	215	127	73	200			64	679
	109.25	162	247	234	18	116			38	653
	112.25	166	354	27	23	241	3		2	650
FACIES A	116.05	170	284	119	39	210			61	713
	120	174	394	58	30	148			67	697
	125	176c	348	179	9	74			3	613
	127.9	180	380	112	30	89			8	619
	130.8	182	392	65	43	129	1		42	672
	134	186	289	139	36	160			42	666
	136.24	189	337	134	24	132			50	677

APPENDIX 2

This table shows the results of point counts in percentages, of all the samples from Pizzo Mondello. In the table, facies, samples, and meters from the base of section are indicated.

	METERS	SAMPLES	MICRITE	CALCAREOUS NANNOFOSSILS	THIN-SHELLED BIVALVES	RADIOLARIANS	FORAMINIFERS	AMMONOIDS	NON-DETERMINABLE
FACIES A	15	335	43.36	11.6	5.65	34.35	0.46	0.15	4.43
	16	333	43.39	11.11	6.46	33.78	0	0	5.26
	17.13	327	46.32	16.39	5.35	28.43	0	0	3.51
	17.85	324	52.81	5.61	3.79	28.53	0	0	9.26
	18.45	322	50.89	9.2	8.31	28.49	0	0	3.12
	19	320	52.68	6.02	6.99	26.99	0	0	7.32
	19.7	316	45.47	9.22	8.91	27.8	0.15	0.15	8.29
	21.45	310	42.3	11.79	7.08	30.82	0	0	8.02
	23.67	305	40.95	14.14	5.1	32.07	0	0	7.73
	24.33	303	40.21	6.48	7.08	37.2	0.6	0.15	8.28
	25.5	1	33.82	19.35	9.59	29.11	0	0	8.13
	28.5	11	47.47	15.82	9.58	23.24	0.9	0.09	2.89
	29.9	15	29.64	29.34	7.49	25	0.15	0	8.38
	32	21	40.41	10.76	12.55	30.07	0.41	0	5.79
	35	28	30.84	27.38	8.93	25.79	0.29	0	6.77
	35.9	30	35.8	15.86	9.52	29.91	0	0	8.91
	37	34	43.07	2	27.05	18.2	0	0	9.68
	41	40	55.06	3.42	7.14	27.98	0.45	0	5.95

	43.5	45	56.06	7.42	7.58	23.18	0.45	0	5.3
	45	48	49.09	9.76	8.37	29.43	0.14	0	3.21
FACIES B	47.7	54	36.03	24.56	10	22.5	0	0	6.91
	49.8	58	42.63	7.37	12.98	29.06	1.33	0	6.64
	53.3	65	40.45	17.77	8.89	29.58	0.27	0	3.05
	54.5	68	28.55	26.29	8.39	29.19	0	0	7.58
	57.1	72	37.6	15.72	7.55	30.2	0.15	0.15	8.63
	60.5	80	37.54	21.92	5.05	28.39	0	0	7.1
	62	83	47.48	6.58	8.54	31.51	0.7	0	5.18
	63.6	86	36.83	26.8	2.99	23.65	0.15	0	9.58
	65.25	89	37.14	12.02	5.33	36.99	0	0.15	8.37
	66.2	91	29.14	24.52	5.57	32.64	0	0.16	7.96
	69.3	98	53.22	12.28	3.36	22.08	0	0	9.06
	71.25	102	42.92	1.61	6.57	39.27	0.73	0.15	8.76
	73.2	104	44.57	19.94	6.74	23.93	0	0	4.81
	75.1	107	46.24	5.99	6.3	34.87	0	0	6.61
	77	110	40.96	7.81	14.79	26.03	0.82	0.27	9.32
	78.75	114	41.51	8.49	4.72	36.01	0.16	0.31	8.81
	81.15	117	49.21	11.79	4.87	26.42	0	0	7.7
	82.5	120	33.93	18.17	6.01	33.33	0	0	8.56
	88.25	126	29.25	28.98	7.21	29.12	0	0	5.44
FACIES C	89.3	127	41.47	29.26	4.07	16.74	0	0.16	8.29
	90.25	128	24.1	45.94	6.92	15.71	0	0	7.32
	91.1	130	41.37	22.66	5.99	26.9	0.15	0	2.92
	92.3	131	52.14	31.73	2.23	9.78	0.34	0	3.77
	93	132	45.33	10.58	10.58	27.61	0.27	0	5.63
	93.3	134	25.45	43.81	5.84	18.36	0	0	6.54
	94.25	136	41.41	39.54	2.31	12.41	0.14	0	4.18
	94.7	137	42.37	25.42	4.24	24.72	0.14	0	3.11

FACIES C	95.3	138	30.79	34.15	4.12	24.24	0	0	6.71
	95.9	140	26.48	47.75	6.34	12.11	0.14	0	7.18
	96.8	141	56.84	26.38	3.91	12.38	0	0	0.49
	97.25	142	49.56	16.32	5.15	27.5	0.44	0	1.03
	99.25	145	37.21	31.31	4.59	21.48	0.16	0	5.25
	101	147	32.29	37.2	2.83	19.05	0	0	8.63
	101.65	148	18.75	36.2	8.98	28.39	0.26	0	7.42
	102.5	149	41.99	32.19	2.94	20.26	0	0.16	2.45
	103.25	150	42.21	26.95	2.65	23.36	0.16	0	4.67
	103.8	151	57.17	3.62	14.83	22.9	0.16	0	1.32
	105.1	154	22.06	33.69	8.59	30.25	0.4	0	5.02
	105.7	155	41.5	5.13	25.95	26.54	0	0	0.88
	106.15	156	40.24	21.31	8.05	27.42	0.45	0	2.53
FACIES B	107	158	52.6	10.84	3.9	30.92	0.43	0	1.3
	108.25	160	31.66	18.7	10.75	29.46	0	0	9.43
	109.25	162	37.83	35.83	2.76	17.76	0	0	5.82
	112.25	166	54.46	4.15	3.54	37.08	0.46	0	0.31
FACIES A	116.05	170	39.83	16.69	5.47	29.45	0	0	8.56
	120	174	56.53	8.32	4.3	21.23	0	0	9.61
	125	176c	56.77	29.2	1.47	12.07	0	0	0.49
	127.9	180	61.39	18.09	4.85	14.38	0	0	1.29
	130.8	182	58.33	9.67	6.4	19.2	0.15	0	6.25
	134	186	43.39	20.87	5.41	24.02	0	0	6.31
	136.24	189	49.78	19.79	3.55	19.5	0	0	7.39

APPENDIX 3

In this table, standard deviations are calculated for each group in each sample from Pizzo Mondello section. The table reports the value for two standard deviations (2 σ). The real percentage values are expected to fall within +/- 2 σ in 95% of cases.

	METRI	SAMPLES	MICRITE	CALCAREOUS NANNOFOSSILS	THIN-SHELLED BIVALVES	RADIOLARIANS	FORAMINIFERS	AMMONOIDS	NON- DETERMINABLES
FACIES A	15	335	3.87	2.50	1.80	3.71	0.53	0.31	1.61
	16	333	3.84	2.44	1.90	3.67	0.00	0.00	1.73
	17.13	327	4.08	3.03	1.84	3.69	0.00	0.00	1.51
	17.85	324	3.89	1.79	1.49	3.52	0.00	0.00	2.26
	18.45	322	3.85	2.23	2.13	3.48	0.00	0.00	1.34
	19	320	4.03	1.92	2.06	3.58	0.00	0.00	2.10
	19.7	316	3.90	2.27	2.23	3.51	0.31	0.31	2.16
	21.45	310	3.92	2.56	2.03	3.66	0.00	0.00	2.15
	23.67	305	3.99	2.83	1.78	3.79	0.00	0.00	2.17
	24.33	303	3.81	1.91	1.99	3.75	0.60	0.30	2.14
	25.5	1	3.82	3.19	2.38	3.66	0.00	0.00	2.20
	28.5	11	3.00	2.19	1.77	2.54	0.57	0.18	1.01
	29.9	15	3.53	3.52	2.04	3.35	0.30	0.00	2.14
	32	21	3.65	2.30	2.46	3.41	0.48	0.00	1.74
	35	28	3.51	3.39	2.17	3.32	0.41	0.00	1.91
	35.9	30	3.73	2.84	2.28	3.56	0.00	0.00	2.21
	37	34	4.05	1.14	3.63	3.15	0.00	0.00	2.42
	41	40	3.84	1.40	1.99	3.46	0.51	0.00	1.83
	43.5	45	3.86	2.04	2.06	3.29	0.52	0.00	1.74
	45	48	3.73	2.22	2.07	3.40	0.28	0.00	1.32
FACIES B	47.7	54	3.68	3.30	2.30	3.20	0.00	0.00	1.95
	49.8	58	3.80	2.01	2.58	3.49	0.88	0.00	1.91
	53.3	65	3.57	2.78	2.07	3.32	0.37	0.00	1.25
	54.5	68	3.63	3.54	2.23	3.65	0.00	0.00	2.13
	57.1	72	3.80	2.86	2.07	3.60	0.31	0.31	2.20
	60.5	80	3.85	3.29	1.74	3.58	0.00	0.00	2.04

FACIES B	62	83	3.74	1.86	2.09	3.48	0.62	0.00	1.66
	63.6	86	3.73	3.43	1.32	3.29	0.30	0.00	2.28
	65.25	89	3.77	2.54	1.75	3.77	0.00	0.30	2.16
	66.2	91	3.63	3.43	1.83	3.74	0.00	0.32	2.16
	69.3	98	3.82	2.51	1.38	3.17	0.00	0.00	2.20
	71.25	102	3.78	0.96	1.89	3.73	0.65	0.29	2.16
	73.2	104	3.69	2.96	1.86	3.16	0.00	0.00	1.59
	75.1	107	3.91	1.86	1.90	3.74	0.00	0.00	1.95
	77	110	3.64	1.99	2.63	3.25	0.67	0.39	2.15
	78.75	114	3.91	2.21	1.68	3.81	0.31	0.44	2.25
	81.15	117	3.96	2.56	1.71	3.50	0.00	0.00	2.11
	82.5	120	3.67	2.99	1.84	3.65	0.00	0.00	2.17
	88.25	126	3.36	3.35	1.91	3.35	0.00	0.00	1.67
FACIES C	89.3	127	3.90	3.60	1.56	2.95	0.00	0.31	2.18
	90.25	128	3.12	3.64	1.85	2.66	0.00	0.00	1.90
	91.1	130	3.77	3.20	1.82	3.39	0.29	0.00	1.29
	92.3	131	4.14	3.86	1.22	2.46	0.48	0.00	1.58
	93	132	3.69	2.28	2.28	3.31	0.39	0.00	1.71
	93.3	134	3.25	3.70	1.75	2.89	0.00	0.00	1.84
	94.25	136	3.74	3.71	1.14	2.50	0.29	0.00	1.52
	94.7	137	3.71	3.27	1.51	3.24	0.28	0.00	1.30
	95.3	138	3.60	3.70	1.55	3.35	0.00	0.00	1.95
	95.9	140	3.31	3.75	1.83	2.45	0.28	0.00	1.94
	96.8	141	4.00	3.56	1.56	2.66	0.00	0.00	0.56
	97.25	142	3.83	2.83	1.69	3.42	0.51	0.00	0.77
	99.25	145	3.91	3.76	1.69	3.33	0.33	0.00	1.81
	101	147	3.61	3.73	1.28	3.03	0.00	0.00	2.17
	101.65	148	2.82	3.47	2.06	3.25	0.37	0.00	1.89
	102.5	149	3.99	3.78	1.37	3.25	0.00	0.33	1.25
	103.25	150	3.90	3.50	1.27	3.34	0.31	0.00	1.67
	103.8	151	4.02	1.52	2.88	3.41	0.33	0.00	0.93
	105.1	154	3.01	3.44	2.04	3.34	0.46	0.00	1.59
	105.7	155	3.77	1.69	3.36	3.38	0.00	0.00	0.72
	106.15	156	3.79	3.16	2.10	3.44	0.52	0.00	1.21
FACIES B	107	158	3.80	2.36	1.47	3.51	0.50	0.00	0.86
	108.25	160	3.57	2.99	2.38	3.50	0.00	0.00	2.24
	109.25	162	3.80	3.75	1.28	2.99	0.00	0.00	1.83
	112.25	166	3.91	1.57	1.45	3.79	0.53	0.00	0.43
FACIES A	116.05	170	3.67	2.79	1.70	3.41	0.00	0.00	2.10
	120	174	3.76	2.09	1.54	3.10	0.00	0.00	2.23
	125	176c	4.00	3.67	0.97	2.63	0.00	0.00	0.56
	127.9	180	3.91	3.09	1.73	2.82	0.00	0.00	0.91
	130.8	182	3.80	2.28	1.89	3.04	0.30	0.00	1.87
	134	186	3.84	3.15	1.75	3.31	0.00	0.00	1.88
	136.24	189	3.84	3.06	1.42	3.05	0.00	0.00	2.01

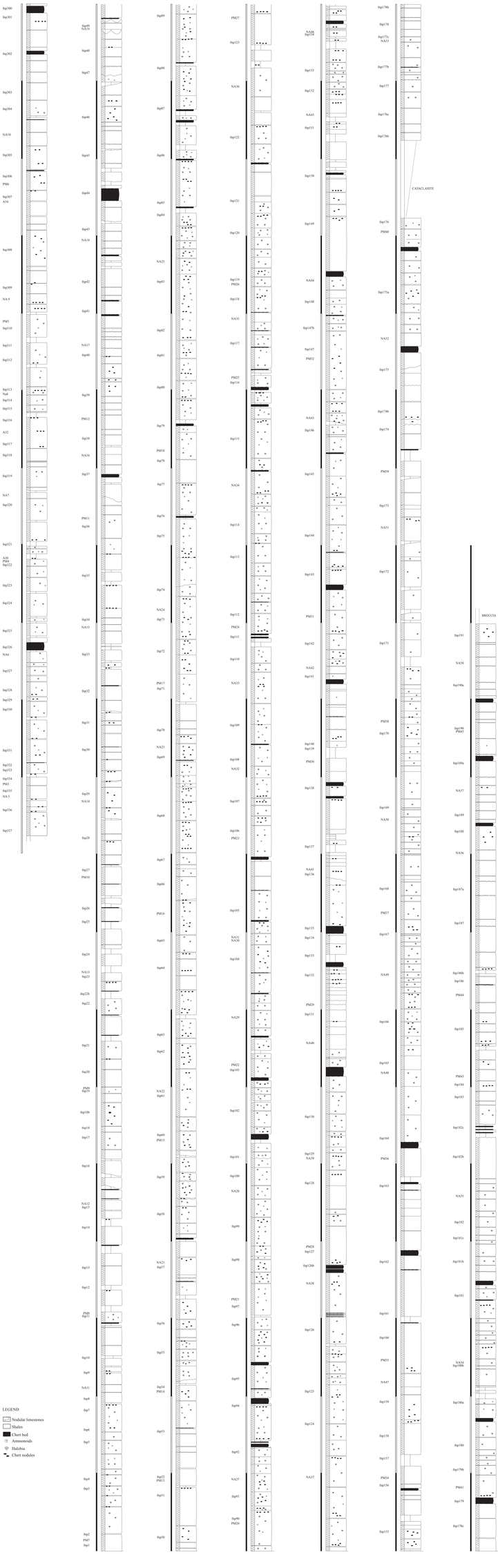
fsp300
fsp301
fsp302
fsp303
fsp304
NA10
fsp305
fsp306
PM6
fsp307
A34
fsp308
fsp309
NA 9
PM5
fsp310
fsp311
fsp312
fsp313
Na8
fsp314
fsp315
fsp316
A32
fsp317
fsp318
fsp319
NA7
fsp320
fsp321
A30
PM4
fsp322
fsp323
fsp324
fsp325
fsp326
NA6
fsp327
fsp328
fsp329
fsp330
fsp331
fsp332
fsp333
fsp334
PM3
fsp335
NA 5
fsp336
fsp337
fsp46
NA39
fsp48
fsp47
fsp46
fsp45
fsp44
fsp43
NA38
fsp42
fsp41
NA37
fsp40
fsp39
PM12
fsp38
NA36
fsp37
PM11
fsp36
fsp35
fsp34
NA35
fsp33
fsp32
fsp31
fsp30
fsp29
NA34
fsp28
fsp27
PM10
fsp26
fsp25
fsp24
NA33
fsp23
fsp22b
fsp22
fsp21
fsp20
PM9
fsp19
fsp18b
fsp18
fsp17
fsp16
NA32
fsp15
fsp14
fsp13
fsp12
PM8
fsp11
fsp10
fsp9
NA31
fsp8
fsp7
fsp6
fsp5
fsp4
fsp3
fsp2
PM7
fsp1
fsp49
fsp48
fsp47
fsp46
fsp45
fsp44
fsp43
NA23
fsp42
fsp41
fsp40
fsp39
fsp38
fsp37
fsp36
fsp35
fsp34
NA24
fsp33
fsp32
fsp31
fsp30
fsp29
fsp68
fsp67
fsp66
PM16
fsp63
fsp64
fsp63
fsp62
NA22
fsp61
fsp60
PM13
fsp59
fsp58
NA21
fsp57
fsp56
fsp55
fsp54
PM14
fsp53
fsp52
PM27
fsp123
NA36
fsp122
fsp121
fsp120
fsp119
PM26
fsp118
NA35
fsp117
PM25
fsp116
fsp115
NA34
fsp114
fsp113
fsp112
PM24
fsp111
fsp110
NA33
fsp109
fsp108
NA32
fsp107
fsp106
PM23
fsp105
NA31
NA30
fsp104
NA29
PM22
fsp103
fsp102
fsp101
fsp100
NA28
fsp99
fsp98
PM21
fsp97
fsp96
fsp95
fsp94
fsp92
NA27
fsp91
fsp90
PM20
NA46
fsp152
fsp153
fsp152
NA45
fsp151
fsp150
fsp149
NA44
fsp148
fsp147b
fsp147
PM32
NA43
fsp146
fsp145
fsp144
fsp143
PM31
fsp142
NA42
fsp141
fsp140
fsp139
PM30
fsp138
fsp137
NA41
fsp136
fsp135
fsp134
fsp133
fsp132
PM29
fsp131
NA40
fsp130
fsp129
NA39
fsp128
PM28
fsp127
fsp126b
NA38
fsp126
fsp125
fsp124
NA37
fsp178b
fsp178
fsp177c
NA53
fsp177b
fsp177
fsp176c
fsp176b
CATACLASITE
fsp176
PM40
fsp175c
NA52
fsp175
fsp174b
fsp174
PM39
fsp173
NA51
fsp172
fsp171
PM38
fsp170
fsp169
NA50
fsp168
PM37
fsp167
NA49
fsp166
fsp165
NA48
fsp164
PM36
fsp163
fsp162
fsp161
fsp160
PM35
NA47
fsp159
fsp158
fsp157
PM34
fsp156
fsp155
BRECCIA
fsp191
NA58
fsp190a
fsp190
PM43
fsp189a
NA57
fsp189
fsp188
NA56
fsp187a
fsp187
fsp186b
fsp186
PM44
fsp185
PM45
fsp184
fsp183
fsp182c
fsp182b
NA55
fsp182
fsp181c
fsp181b
fsp181
NA54
fsp180b
fsp180a
fsp180
fsp179b
PM41
fsp179
fsp178a
LEGEND
Nodular limestones
Shales
Chert bed
Ammonoids
Halobia
Chert nodules